DIPLOMA THESIS

Nanoscale viscoelasticity of hydrated native collagen fibrils: The effect of chemically-induced non-enzymatic glycation and tendon type

carried out at the Institute of Lightweight Design and Structural Biomechanics, Faculty of Mechanical and Industrial Engineering, TU Wien

Under the supervision of

Univ.Prof. Dipl.-Ing. Dr.sc.nat. Philipp THURNER

Orestis ANDRIOTIS, PhD

Projektass. Dipl.-Ing. Manuel RUFIN

by

Mercedes SPANNAGEL

Mat.Nr.: 01122330

September 8, 2022

Statement of authorship

I, Mercedes Spannagel, declare that I completed this thesis on my own and that information which has been directly or indirectly taken from other sources has been noted as such. Neither this nor a similar work has been presented to an examination committee.

Vienna, September 8, 2022   . . . .

Zusammenfassung

Sehnen sind komplexe, multihierarchische biologische Gewebe, deren verschiedene Sublevel unterschiedlich auf mechanische Belastung reagieren. Das kleinste Strukturelement sind Kollagenfibrillen, welche bereits erfolgreich mit Rasterkraftmikroskopie untersucht wurden. In bestehender Literatur werden Kollagenfibrillen mit Hilfe von Indentationsexperimenten im Mikro- oder Nanobereich charakterisiert, allerdings werden sie dabei meist als linear elastisch angenommen, während sie in Realität viskoelastisches Verhalten aufweisen. Um die viskoelastischen Materialkenngrößen (Phasenverschiebung zwischen Kraft und Indentation, dem Verlust-Tangens, dem Speicher- und dem Verlustmodul) zu bestimmen, wurde in dieser Masterarbeit ein Testprotokoll für frequenzabhängige Indentationsexperimente erarbeitet und eine Datenanalyse auf Grundlage der frequenzabhängigen Oliver-Pharr-Gleichungen programmiert. In einem ersten Experiment wurden Kollagenfibrillen von oberflächlicher Beugesehne und Strecksehne eines jungen und eines alten Pferdes (3 vs. 18 Jahre alt) getestet und miteinander verglichen. Das Messprotokoll bestand zunächst aus den vier Frequenzen 10, 1, 0,5 und 0,1 Hz, und wurde im zweiten Experiment zu 10, 5, 1 und 0,5 Hz geändert, da die Daten aufgrund von Störfaktoren bei 0,1 Hz oftmals nicht mit einem Sinus approximiert werden konnten und die Experimentdauer stark verlängerten.

Die Ergebnisse lassen sich bloß vorsichtig formulieren, da aufgrund wenig vorhandener, brauchbarer Daten, keine statistische Analyse durchgeführt wurde: Phasenverschiebungen zwischen Kraft und Indentation um ein paar Grad deuten auf ein viskoelatisches Materialverhalten hin, auch wenn kleine Verlustmodul-Werte im Vergleich zu Speichermodul-Werten auf ein generell recht elastisches Materialverhalten weisen.

In einem zweiten Experiment sollte die These untersucht werden, dass im Alter nichtenzymatische, durch Glykierung entstehende Cross-links zwischen Kollagenmolekülen zunehmen und zu einer Änderung der mechanischen Eigenschaften führen. Dazu wurden die Kollagenfibrillen beider Sehnentypen des jungen Pferdes (3 Jahre alt) einem Glykierungsprozess mit Methylglyoxal (MGO) ausgesetzt. Mit MGO behandelte Kollagenfibrillen beider Sehnentypen weisen höhere Eindrucksmodul Werte auf, d.h. sind steifer als unbehandelte Fibrillen, unabhängig vom Alter.

Dynamische Indentation ist eine in der Literatur aufgrund ihrer Aufwendigkeit bisher wenig verwendete Methode zur Charakterisierung von Kollagenfibrillen, jedoch deuten die Ergebnisse dieser Arbeit darauf hin, dass diese Methode Potential hat, den (viskoelastischen) Charakter von Kollagenfibrillen besser zu bestimmen. Weitere Tests mit modifiziertem

Messprotokoll sollten durchgeführt werden. Der entwickelte MATLAB-Code zur Analyse der Daten kann als guter Grundstein für weitere Forschung dienen.

Abstract

Tendons are complex, multi-hierarchical biological tissues whose different sub-levels react differently to mechanical stimulus. Their smallest structural elements are collagen fibrils, which have already been successfully examined using atomic force microscopy. In the existing literature, collagen fibrils are characterized by indentation experiments in the micro or nano range. However, they are most of the time assumed to be linearly elastic, while in fact they show viscoelastic behaviour. In order to determine the viscoelastic material parameters (phase shift between force and indentation, the loss tangent, the storage and the loss modulus), a test protocol for frequency-dependent indentation experiments was developed and a data analysis based on the frequency-dependent Oliver-Pharr equations was programmed. In a first experiment, collagen fibrils from the superficial digital flexor (SDFT) and common digital extensor (CDET) tendons of a young and an old horse (3 vs. 18 years old) were tested and compared. The measurement protocol initially consisted of four frequencies 10, 1, 0.5 and 0.1 Hz and was changed to 10, 5, 1 and 0.5 Hz in the second experiment, since the data at 0.1 Hz could often not be approximated by a sine and extended the duration of the test considerably.

The results can only be formulated cautiously, since no statistical evaluation was carried out due to a lack of usable data: Phase shifts between force and indentation by a few degrees indicate viscoelastic material behaviour, even if loss modulus values are small compared to storage modulus values, which indicate an overall quite elastic material behaviour.

In a second experiment, the assumption was to be investigated that non-enzymatic cross-linking between collagen fibrils through glycation increases with age and leads to a change in mechanical properties. For this purpose, the collagen fibrils of both tendon types of the young horse (3 years old) were exposed to a glycation process with methylglyoxal (MGO). Collagen fibrils of both tendon types treated with MGO exhibit higher indentation modulus values, i.e. are stiffer than untreated fibrils, independent of age.

Dynamic indentation is a method for characterizing collagen fibrils that has been little discussed in literature due to its complexity. However, the results of this work indicate that this method has the potential to better determine the (viscoelastic) character of collagen fibrils. Further tests with a modified measurement protocol should be carried out. The developed MATLAB code for analyzing the data in this thesis can serve as a good foundation for further research.

Acknowledgements

First of all, I want to thank Prof. Philipp Thurner, who introduced students, including me, to the discussion of scientific work through the seminar on biomechanics of biological tissues, which made me interested in writing my master's thesis in this field. Thanks for motivating students to get involved in the ongoing research at the institute and for the valuable input that helped me a lot during my thesis.

Another extremely big thank goes to Dr. Orestis Andriotis, who accompanied and supported me intensively in the creation of this work from the very beginning. I really appreciated that I felt like I could ask any question and I also valued his motivated and communicative nature.

Another person who was essential for the success of this work was Dipl. Ing. Manuel Rufin. Many thanks for the feedback regarding the developed MATLAB code and also later for the first correction of this thesis.

Thanks of course to everyone else in the institute with whom I was able to exchange ideas. Thanks to Walaa, who had to brood over data similar to mine, for always being able to support each other.

An unbelievable thank you goes to everyone I met during my mechanical engineering studies at TU Wien and who always made it easier to stay motivated and keep going. Also, of course, I want to thank all the other friends who always had to put up with it when I had to cancel fun because of studies. Among them a special thank you to Sophie and Christopher, who always comforted me when the AFM caused problems or calmed me down when MATLAB blocked my computer so much that I wanted to throw it against the wall (thanks too to my computer for the effort, because it looks pretty but is easily overwhelmed with its tasks).

Last but not least, thanks to everyone in my family who always supported me and didn't keep asking me when I would finally finish my studies.

Contents

List of Figures

List of Tables

List of Abbreviations

AFM	Atomic force microscope
AGE	Advanced glycation end-product
CDET	Common digital extensor tendon
DMA	Dynamic mechanical analysis
ECM	Extracellular matrix
EDTA	Ethylenediaminetetraacetic Acid
FACIT	Fibril-associated collagen
GAG	Glycosaminoglycan
IFM	Interfascicular matrix
MACIT	Transmembrane collagens
MGO	Methylglyoxal
MTJ	Myotendinous-junction
OTJ	Osteotendinous junction
PBS	Phosphate buffered saline
PID	Proportional Integral Differential
PMMA	Polymethamethylacrylate
QI	Quantitative imaging
SDFT	Superficial digital flexor tendon
SEM	Scanning electron microscopy
SPM	Scanning probe microscopy
STM	Scanning tunneling microscopy
TEM	Transmission electron microscopy

List of Symbols

A_c — Contact area (m^2)

$b(0)$ — Hydrodynamic drag force (N)

D — Thermal deflection of cantilever (m)
d — Deflection of cantilever (m)

$E^*(\omega)$ — Complex modulus (N/m^2)
E_{dyn} — Dynamic modulus (N/m^2)
$E''(\omega)$ — Viscous (loss) modulus (N/m^2)
$E'(\omega)$ — Elastic (storage) modulus (N/m^2)
E^* — Combined elastic modulus (N/m^2)
E — Elastic modulus (N/m^2)
ϵ — Depth of the local minimum of the potential energy of Lennard-Jones potential
ε — Constant depending on the indenter geometry

F_A — Force amplitude (N)
$F(\omega)$ — Fourier transform of Force (N)
F — Force (N)
F_0 — Operating force (N)
f — Frequency (Hz)

$G^*(\omega)$ — Frequency dependent complex shear modulus (N/m^2)
G — Shear modulus (N/m^2)

h_0 — Operating indentation (m)
h_A — Indentation amplitude (m)
h_{max} — Maximum indentation depth (m)
$h(\omega)$ — Fourier transform of indentation (m)
h_c — Contact depth (m)
h — Indentation depth (m)

k_B — BOLTZMANN's constant (J/K)
k_c — Cantilever spring constant (N/m)

l — Cantilever length (m)

ν — Poisson's ratio

ω — Angular frequency

ϕ — Phase shift (°)

R — Tip radius (m)

r_{eq}	Equilibrium distance (m)
r	Distance between two particles (m)
S	Contact stiffness (N/m)
σ	Distance at which the Lennard-Jones potential becomes zero (m)
T	Temperature (K)
t	Cantilever thickness (m), Time (s)
θ	Half-open angle of pyramidal indenter (°)
V_{LJ}	Lennard-Jones potential
V	Vertical deflection (V)
w	Cantilever width (m)
Z	Piezo Z-displacement (m)
z_0	Location of the contact point (m)
z	Piezo z-displacement (m)

1. Introduction

1.1. State of the art

Biomedical research aims to understand better the behaviour of cells or biological tissues both on micro- and nano-scale levels to be subsequently able to develop artificial tissue that can replace or restore damaged organs or to detect how to treat diseases and injuries effectively. Biological tissues combine solid- and liquidlike behaviour and are therefore called viscoelastic. According to BOLTZMANN's superposition principle, viscoelasticity means that materials can have a mechanical history that influences their future material behaviour.

For probing nanoscale properties of soft biological samples in physiological environments, nanoindentation with atomic force microscopy (AFM) is stated to be a popular method. This complex instrument measures the interactions between a microcantilever probe and the specimen surface. In previous research mechanical properties of biological tissues are mostly extracted by indentation experiments in the time domain and analysed using Hertzian contact mechanics, leading to the (elastic) indentation modulus of a material. Those (quasi-)static experiments are usually performed with an indentation cycle of a loading (approach) and an unloading (retraction) sequence (see fig.1 a and b). The problematic aspect of this kind of experiments and analyzes with the Hertz model is that the material is assumed to be elastic, which is not correct in the case of biological tissue. To consider transient effects, a hold phase is added between approach and retraction, where either the force or indentation is held constant, while the time-dependence of the other is measured and analysed [1]. In dynamic experiments oscillatory deformations with several frequencies and a constant (small) amplitude are performed after an initial hold segment (see fig.1 c and d). Dynamic experiments promise a better resemblance to *in vivo* forces and better consideration of the viscoelastic character of biological tissues, but it needs to be verified in this work whether this testing strategy has future potential in the field of AFM-based nanoindentation of soft materials. Dynamic indentation experiments have been only scarcely applied in literature (i.e. [2], [3], [4], [5]) due to complex loading histories, which make quantitative analysis difficult.

1

Subjects of previous dynamic indentation tests with AFM were lung epithelial cells [2], benign and malignant breast cells [3], astrocytes in white and gray matter brain regions [4] and tunica adventitia of porcine aorta and pulmonary artery [5]. In this work, collagen fibrils of equine tendons are to be examined. Simple indentation tests with AFM were already used successfully to test mechanical properties on the nanoscale and microscale of tendon tissue [6], [7], [8], [9], dynamic tests with AFM were conducted on collagen fibrils by Grant et al. [10].

Collagen, the most abundant protein in mammals, is the smallest structural element of fibrous tissues like tendons. There are two types of tendons, one serves a positional function, one an energy-storing, in their task of transmitting forces from the muscle to the bone. Comparing tendon types, tensile tests show different mechanical properties on the macro-scale at the whole tendon level [11] and also on single fascicles and fibrils [12], [13], [14], while the behaviour on the nano-scale is not so well observed. Thus, it remains of interest if the collagen fibrils of different tendon types show different mechanical behaviour. (Quasi-)static indentation tests have been done on individual collagen fibrils of CDET and SDFT [9], finding differences between tendon types and age.

It is widely assumed in literature that age leads to differences in mechanical properties of tendons, as it is known that the composition of tendon changes with increasing age. In order to form larger structures (e.g. fibrils), the collagen molecules connect to each other through so-called cross-links - some of them are caused by glycation meaning the bonding of a sugar molecule to protein without enzymatic regulation. Those resulting advanced glycation end-products (AGEs) are said to increase with age and change the mechanical properties of the tissue. In a prior study, collagen fibrils were treated with ribose to find altered hydration and mechanical properties in collagen fibrils bearing AGEs [15]. Another study uses methylglyoxal (MGO) to chemically form AGEs resulting in increased strength and stiffness of rat tail and Achilles tendon [16]. Treating the individual equine collagen fibrils with chemically-induced glycation through MGO could help in completing the picture how cross-links effect the mechanical properties, also with respect to age.
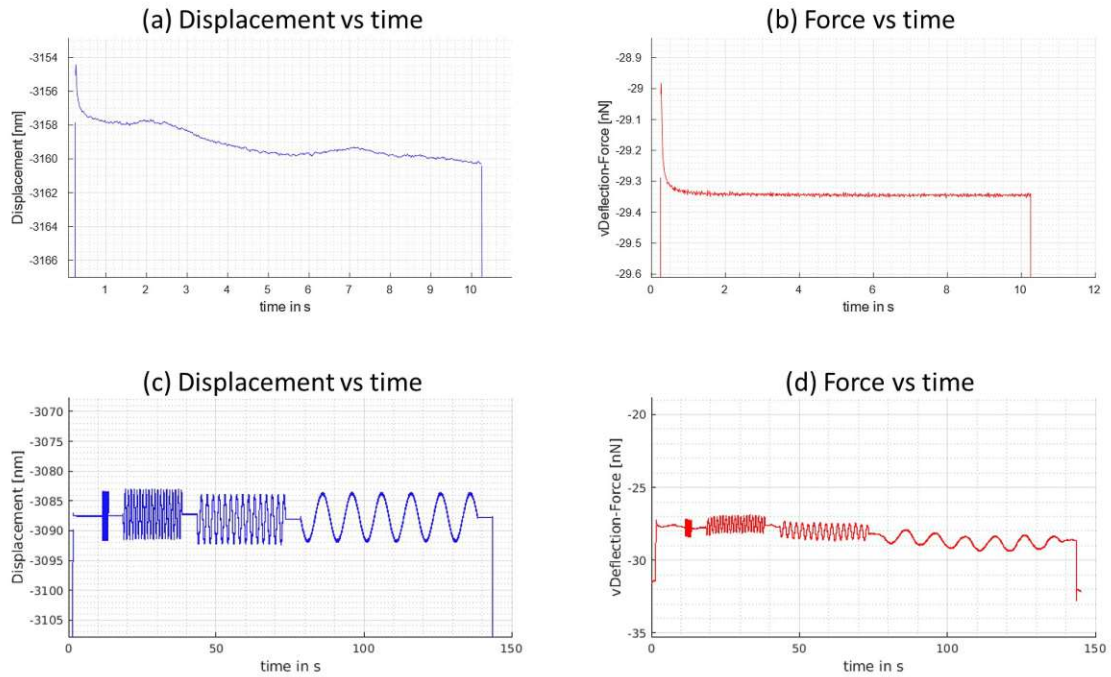
Figure 1: Indentation experiments with AFM to extract the material's viscoelastic properties are usually performed in a (quasi-)static manner (a) and (b) or more seldom in a dynamic manner (c) and (d). The Nanowizard Ultra Speed A (JPK-Bruker, Berlin)) atomic force microscope used in this thesis enables a constant height or constant force hold - (b) displays the force controlled input and (a) is the corresponding displacement response. Although the AFM used allows the creation of a dynamic test protocol, the frequency-dependent segments can only be height-controlled, which leads to a smooth displacement signal (c). The force response is shown in (d).

1.2. Aim of thesis

Aim of this thesis is to define an AFM testing protocol in the frequency domain and an analysis method to extract the viscoelastic properties of collagen fibrils out of indentation experiment data.

The first challenge addresses the choice of the key experimental parameters to conduct a dynamic indentation experiment on collagen fibrils, thus hold time and frequency profile at maximum load [17]. Since input and output signals from dynamic indentation tests have sinusoidal character, the existing literature attempts to fit the force and indentation curves with a simple sine function in MATLAB in order to be able to further calculate the frequency-dependent

3

indentation modulus within the framework of linear viscoelasticity [2], [17], [1]. Due to the fact that frequency-dependent testing protocols are not standardized, programming the analysis environment in MATLAB is a large part of this thesis, with the goal to write bug-free, easy readable code, that offers all necessary information in meaningful plots for future users.

It is of interest to compare the findings of the dynamic indentation experiments with the results from simple indentation tests on collagen fibrils (i.e. [9]), to be able to draw conclusions about the potential of this method to identify the viscoelastic character of biological samples. The viscoelastic properties (particularly the storage and loss modulus) of collagen fibrils are to be studied in relation to the different functions of the tendons from which they are derived, and a possible change in mechanical properties with age are to be evaluated in a first experiment. Ongoing research is attempting to detect changes in mechanical properties at both the macro and micro levels and to infer morphological changes in the tendon structure and chemistry - e.g. on the potential increase of cross-links within individual collagen molecules. Through chemically-induced glycation with MGO the effect of an increase of AGEs between collagen molecules, which are said to be related to age and pathology, are to be examined in the second experiment. To this date, no data about MGO-treated collagen fibrils of equine tendon are known to exist.

1.3. Structure of thesis

Chapter 2 gives an overview of the biological tissue used for experiments in this thesis. Beginning with the smallest structural unit of a tendon, the collagen molecule, a bottom up approach is followed to describe how a tendon is structured. With this knowledge it is possible to go into detail of the two types of equine tendons: The superficial digital flexor tendon (SDFT) and the common digital extensor tendon (CDET). Their differences are laid out such as findings from previous investigations about their mechanical properties and age-related changes.

Chapter 3 explains the atomic force microscope (AFM), used for indentation experiments in this thesis. To obtain mechanical properties from the AFM output data, analysis methods (Hertz and Oliver-Pharr) are presented.

Chapter 4 serves as documentation of the MATLAB code programmed to post-process force vs. displacement data from dynamic AFM indentation experiments. It is explained how the already existing MATLAB program for the analysis of simple indentation experiments works, and, which changes were necessary, to be able to analyze the frequency-dependent data of this thesis. The plots to visualize the results can be found in appendix B.

Chapter 5 gives all details about Experiment 1: First, considerations supported by literature are made that are needed to create a suitable frequency-dependent test protocol. Then, Materials & Methods include sample preparation and the definition of the experimental procedure. At the end, the results are presented and compared with existing literature. Additional results can be found in detail in appendix C.

Chapter 6 covers Experiment 2. The chapter's structure is the same as in 5: Preceded are some practical thoughts on chemically-induced glycation, followed by Materials & Methods, finishing with results.

Chapter 7 summarizes the findings from both experiments conducted in this thesis and will conclude with placing this work into the bigger context of previous studies and evaluate it's future relevance.

2. Biological tissues

Biological tissues are generally highly inhomogeneous and anisotropic (varying in magnitude according to the direction of measurement) complex structures. Like nonbiological materials they posses mechanical properties that can be classified as elastic, plastic, viscous or a mixture of those properties. In this thesis the material responses of two types of equine tendon to external mechanical load shall be analyzed, more precisely the mechanical properties of their collagen fibrils. To be able to interpret the results, an understanding of tendon structure is necessary. Following a bottom up approach, first the smallest unit of a biological tissue, the collagen molecule, will be described, before at the end of this chapter important information about equine tendons will be provided.

2.1. Collagen and Collagen fibrils

Collagen is one of the most common proteins in mammals. In the human body it constitutes about 25% of the total protein mass. It is mainly found in connective tissue - for example in bones, cartilage, tendons, joints and the skin. So far 28 different collagen proteins can be found in human which are given Roman numerals and can be divided into 8 families: Fibril-forming collagens (types I,II,III,V and XI), fibril-associated collagens (FACIT), network-forming collagens, anchoring fibrils, transmembrane collagens (MACIT), basement membrane collagens and others with unique functions [18]. The 28 types of collagen differ primarily in the various segments in the protein organization and the three-dimensional structures they form.
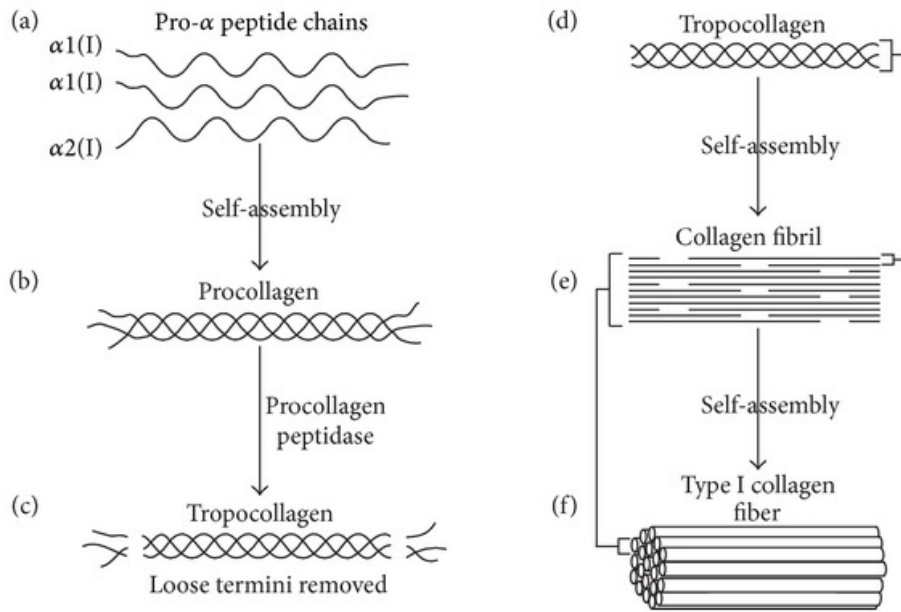
Figure 2: The process of type I collagen synthesis. (a) Two identical $\alpha 1(I)$ and one $\alpha 2(I)$ peptide chains self-assemble to form procollagen (b). (c) Procollagen peptidase removes loose termini to create a type I tropocollagen molecule (d). Tropocollagen molecules self-assemble to form a growing collagen fibril (e). Self-assembly of collagen fibrils forms a type I collagen fiber (f). [19]

Biomechanically of most interest are the collagens assembling into larger fibrillar structure (fibrillar collagens), especially type I collagen which is a major constituent in bone, ligaments, tendon and type II collagen in cartilage. All proteins including collagen are made up of amino acids arranged to alpha chains. Three of those polypeptide chains assemble to a triple helix or superhelix which defines the molecular structure of collagen. The collagen type I procollagen triple helix is usually formed by two identical $\alpha 1(I)$-chains and one $\alpha 2(I)$-chain [18]. Extracellular enzymes then remove the ends of the procollagen peptides. This results in the structure known as tropocollagen molecules, which in the case of type I collagen have a typical size of about 1.5 nm in width and 300 nm in length.

By removing the ends, the molecule can form cross-links (see section 2.2) with other triple helices of type I collagen and thus form larger structures, the so-called collagen fibrils. Collagen fibrils model themselves as an assembly of bundles of five overlapping monomers. Adjacent monomers overlap followed by a gap - those two characteristic zones can be summarized to the so called "D-Period" (after the model of Hodge and Petruska from 1964 [20]) of 67 nm length [21]. Mul-

tiple fibrils together form then collagen fibres.

2.2. Collagen cross-linking

As briefly mentioned in section 2.1, during the process of collagen self-assembly, various types of inter-molecular cross-links stabilize the helical supramolecular structure. These cross-links play a key role in tissue function and matrix remodeling, having either positive or negative effects on age, disease, injury and therapy. Initially they should provide optimum function, but may over-stiffen the fibres when present in excess. Collagen cross-links can be classified as either enzymatic or non-enzymatic [22], [23], [24].

The enzymatic cross-linking process is the initial stabilisation of the fibrils through lysyl oxidase to provide the characteristic functional properties during development and maturation, while the non-enzymatic process is based on the reaction with glucose and other sugars, which plays a central role in aging [24].

Enzymatic cross-linking

Covalent cross-links, which are essential for proper development of fibril structure and mechanical integrity are formed head-to-tail at the overlapping ends of adjacent collagen molecules. The absence of these chemical bonds would lead to a decrease in collagen fibril strength and whole tissue function [22]. This enzymatic cross-linking process is driven by the enzyme lysyl oxidase, which specifically acts on lysine or hydroxylysine in the telopeptide region of the collagen molecule and results in a divalent, immature cross-link. Spontaneously, if hydroxylysine is present, these immature cross-links can convert into more stable trivalent cross-links that increase collagen interconnectivity, fibril stability, and whole tendon mechanical integrity [23]. Following maturation, there is little change in the concentration of the mature cross-links, but there remains a steady increase in the stiffness of the tissue [24].
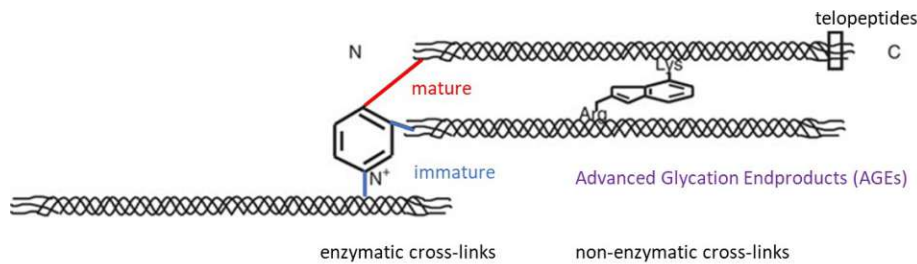
Figure 3: Enzymatic cross-linking through lysyl oxidase resulting in a divalent, immature cross-link. Upon maturation a trivalent cross-link is formed. Non-enzymatic cross-linking happens due to glycation between the helical regions of the collagen molecules. (adapted from [25])

Advanced glycation endproduct cross-linking

While during normal fibrillogenesis the enzymatic cross-linking reaches a plateau at maturation, it has been shown that connective tissue stiffness increases with age and diabetes (which could also be described as "accelerated ageing" [24]). This tissue stiffening has been associated with mechanically disadvantageous covalent bonds between collagens that will form as collagens react with sugars - this process is called glycation. Subsequent oxidation of these reactive products leads to the formation of advanced glycation end-products (AGEs). AGE cross-links have not only been associated with increased fibrillar stiffness, but also with loss of tissue toughness, impaired matrix remodeling, and the chronic inability of tendon to cope with microdamage [23], [22].

2.3. Tendon

Tendons are tough bands of fibrous connective tissue. The basic function of the tendon is to transmit the force created by the muscle to the bone, and, in this way, make joint movement possible. This functionality is enabled by a complex macro- and microstructure of tendons and

tendon fibers [26].
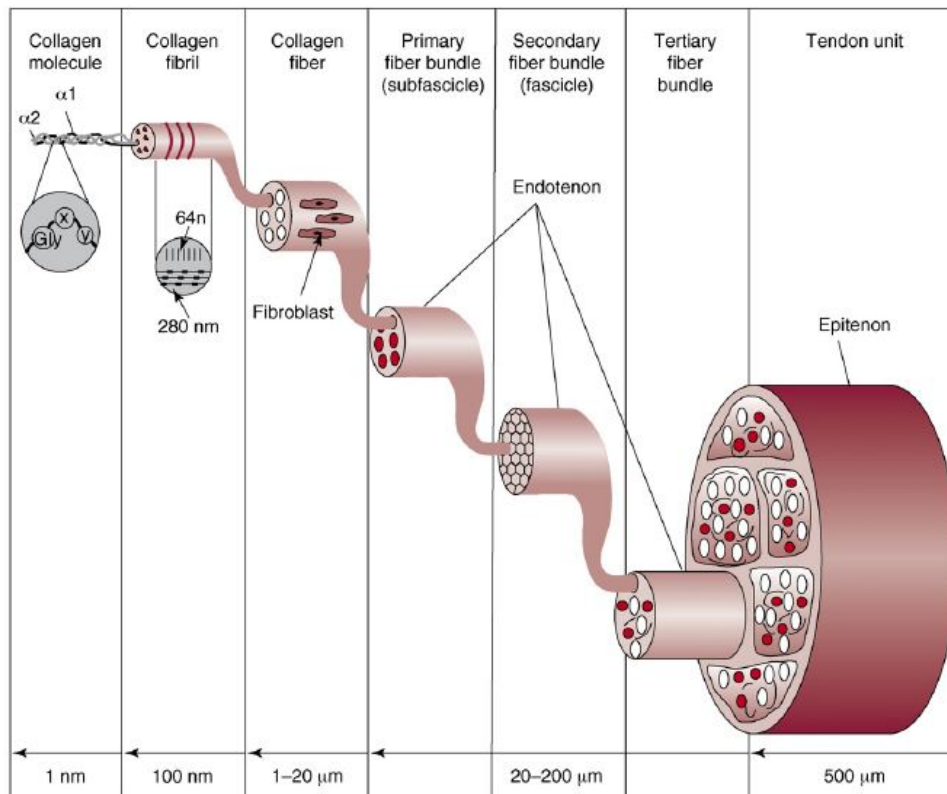
Figure 4: Schematic illustration of the hierarchical structure of a tendon. Longitudinally aligned collagen molecules self-assemble into fibrils. These fibrils are embedded in a proteoglycan-rich matrix and form larger collagen fibers, which in turn form fascicles, and finally, multiple fascicles to compose a whole tendon (adapted from [27])

Micro-structure

Tendons consist of collagens, proteoglycans, glycoproteins, water and cells [28]. Collagen (mostly type I collagen) and elastin are embedded in a proteoglycan-water matrix with collagen accounting for 65-80% and elastin approximately 1-2% of the dry mass of the tendon [26]. Those are the two main groups of which the extracellular matrix (ECM) consists: The shaped components (collagen) that are embedded in the loosely unformed amorphous basic substance, consisting of proteoglycan complexes (consisting of decorin, among others), glucosaminoglycans (such as hyaluronan) and/or glycoproteins. The proteoglycans of the basic substance have the ability to bind water, and are therefore providing hydration and lubrication for the tendon. The ECM lies between the cells of the tissue, surrounds them like a mesh and thus mediates the contact

between them. The extracellular matrix is produced by connective tissue cells called tenoblasts and tenocytes, which are the elongated fibroblasts and fibrocytes that lie between the collagen fibers. Tenoblasts develop into tenocytes upon maturation. Tenocytes form over their numerous spider-like extensions a complex communicating network that reacts to external stimuli and enables the functional adaptation of the proteoglycan and collagen framework to mechanical stress.

Soluble tropocollagen molecules form cross-links to create insoluble collagen molecules which then aggregate progressively into microfibrils and then into microscopically clearly visible units, the collagen fibrils. A bunch of collagen fibrils forms a collagen fiber, which is the basic unit of a tendon. Within one collagen fiber, the fibrils assemble in a wavy pattern called 'crimp' - this structure has a major influence on the mechanical properties of the tendon (see below).

Then, as displayed in fig. 4, a bunch of collagen fibers forms a primary fiber bundle. A group of primary fiber bundles forms a secondary fiber bundle - a fascicle. A group of secondary fiber bundles, in turn, forms a tertiary bundle, and the tertiary bundles make up the tendon.

A fine sheath of connective tissue called endotenon bundles those multiple fibers into subfascicles and fascicles (primary, secondary and tertiary fascicles). The endotenon also called interfascicular matrix (IFM) is there for internal gliding and lubrication. The entire tendon itself is surrounded by a fine connective tissue sheath called epitenon whose characteristic is to reduce friction. In the epitenon there are stem cells as well as blood vessels and nerves. It is situated beneath the paratenon, a loose elastic sleeve or synovial layer (containing interfascicular cells).

Macro-structure

To allow the movement of the muscular and skeletal systems, connective tissues, such as tendons and ligaments, are joined to muscle and bone. Tendons serve different functions in the body: They can be either positional (e.g. tendon tibialis anterior) or energy storage (e.g. achilles) types. The second type works similar to a spring increasing the efficiency of locomotion by recuperating energy - differences in mechanical properties should be further explored in the next subsection.

Mechanical properties

Tendons have unique biomechanical properties that can be attributed to the high degree of organization of the tendon extracellular matrix [27]. While collagen cross-links are fundamental to the mechanical integrity of tendon, with orderly and progressive enzymatic cross-linking being central to healthy development and injury repair [23], collagenous proteins, water, and the interactions between collagens and proteoglycans provide the viscoelasticity of tendons. Viscoelastic means, that the mechanical behaviour depends on the rate of mechanical strain. Precisely, the viscoelasticity of a material is defined by stress-relaxation, creep, and hysteresis [28]. Overall the working manner of tendons can be compared to springs allowing to passively store and recover energy during locomotion. This is enabled through crimped collagen fibers which stretch under load, leading to an increase of stiffness of the whole tendon until reaching a plateau when all it's fibres are completely stretched.
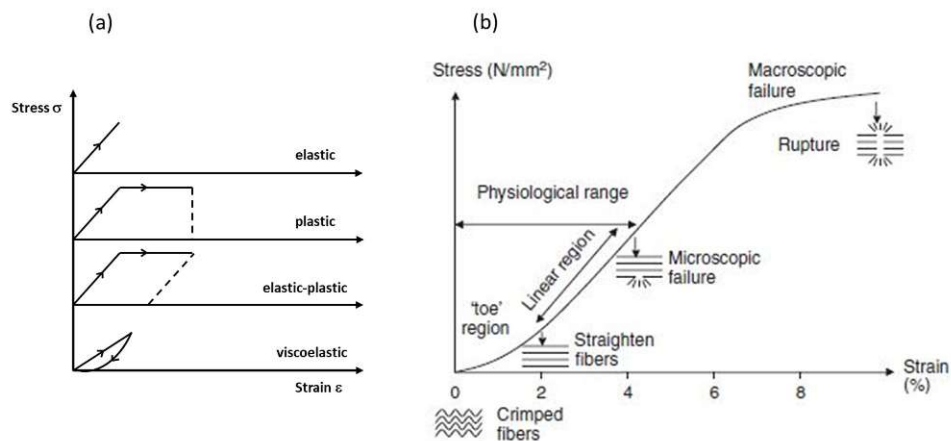
Figure 5: Stress-strain-curves of existing material behaviours (a, reproduced from [9]) versus a typical stress-strain-curve of tendon as a highly complex biological tissue with elastic and viscoelastic characteristics. The four zones of the curve are influenced by the behaviour of the tissue at different strain levels: First the fibers of the tendon show their crimped pattern, which is straighten upon increasing strain until failure starts to begin in the micro-structure, just to end in failure of the whole tendon after a strain threshold is exceeded (b, from [28]).

Tendons as biological tissues have a complex mixture of elastic, plastic and viscous properties inherent in them. A tensile test displays the typical stress-strain curve consisting of four regions [28] (see fig. 5):

I: The initial toe region, where the tendon is strained up to 2%. This toe region represents the stretching-out of the "crimp-pattern" of a tendon. The angle and length of the "crimp pattern" depend on the type of tendon and the sample site within the tendon, where differences in the "crimp pattern" affect the tendon's mechanical properties. For example, fibers with a small crimp angle fail before those with a larger crimp angle.

II: In the "linear" region of the stress–strain curve, where the tendon is stretched less than 4%, collagen fibers lose their crimp pattern. The slope of this linear region is often referred to as the Young's modulus of the tendon, but due to the fact that tendon is not a linear elastic material, it is better to call it 'tensile modulus' (compare to 'indentation modulus' from indentation experiments). All strains/deformations are recoverable.

III: If the tendon is stretched over 4%, microscopic tearing of tendon fibers occurs.

IV: Beyond 8–10% strain, macroscopic failure occurs. Further stretch causes tendon rupture.

2.4. Equine Tendon

Tendons can be divided into two types: the energy-storing tendons used for weight-bearing and locomotion and positional tendons involved in limb placement or manipulative skills [29]. An energy-storing tendon in human is the Achilles tendon which can be compared to the equine superficial digital flexor tendon (SDFT) of the forelimb in the horse (see fig. 2.4). These tendons are stretched during the stance phase, and recoil during swing; returning the stored potential energy to the system [30]. The human anterior tibialis works analogously to the equine common digital extensor tendon (CDET), both positional tendons, which act to directly transmit force to

the bone. Flexor tendons and their anatomically opposing extensor counterparts are commonly compared to each other to investigate tendon structure-function relationships.
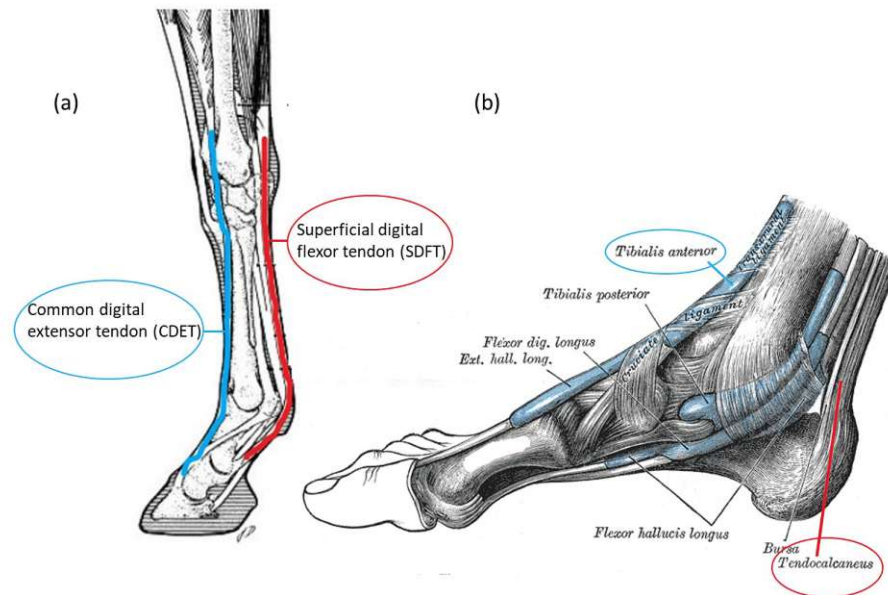
Figure 6: Illustration of the forelimb of the horse showing CDET and SDFT tendon ((a), adapted from [29]) and of the human foot showing the equivalent tibialis anterior and tendo calcaneus (commonly known as Achilles tendon) ((b), adapted from [31]).

Incipient with the biggest difference between both tendon during normal physiological activity: Energy storing tendons are subjected to relatively high strains while positional tendons experience much lower strains. Human Achilles tendon have recorded strains of up to 10.3% during one-legged hopping, while the anterior tibialis tendon have recorded maximum values of only 3.1% [11]. Energy storing tendons are therefore at risk to endure a strain-induced tendinopathy, a common injury in both human and equine athletes, with increasing incidence associated with sport and aging [29].

To simulate the straining/tearing of tendon tissue *in vitro*, tensile testing is used to determine the maximum stress and strain that the tendon can withstand while being stretched before breaking [32]. Birch provides values for the tensile moduli for both tendon types: While the average tensile modulus of the SDFT resulted to 970.8 MPa, the CDET got an tensile modulus of 1236.3 MPa, hence tensile modulus of CDET was significantly higher than the tensile modulus of the SDFT [11]. This leads to the question, where the origins of those different mechanical

properties are located - in the matrix composition and organization of the distinct tendon. Birch suggests that energy storing tendons are composed of a less stiff matrix than positional tendons. It was also detected in previous studies that the SDFT not only has a lower tensile modulus but also a lower failure stress than the CDET, nevertheless the SDFT fails at significantly higher strains [30]. Seemingly contrary to this latter finding, fascicles from SDFT are failing at lower strains than those from CDET (see fig. 7). So, mechanical properties do not only vary between tendon types, but it can also be said, that mechanical properties of the fascicle do not reflect those observed at the whole tendon level.
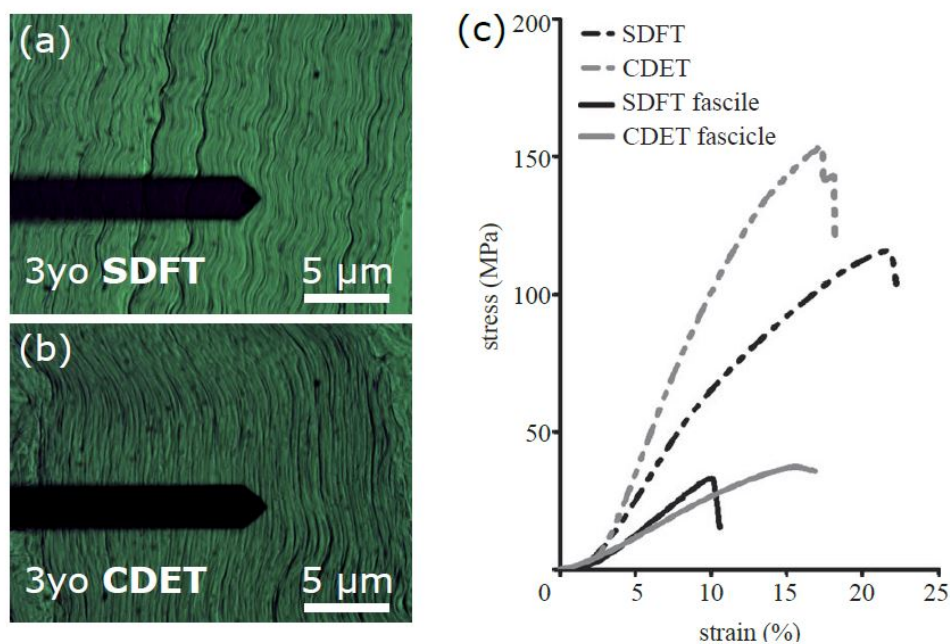
Figure 7: The morphological differences between the SDFT of a young horse (a) and the CDET of a horse of same age (b) can be recognized on the basis of shorter crimp and greater crimp angle in the SDFT in comparison to larger crimp and smaller crimp angle in the CDET ((a),(b) from [9]). These differences may correlate with the differences in the stress-strain behaviour between both tendon types and also on the fascicle level (c) (from [30]). SDFT shows a larger toe region, meaning being able to stretch more at low stresses, which is likely to be possible due to the larger crimp angle. Also visualized is the interesting circumstance, that the failure strain of the SDFT fascicle is much lower than the the failure strain of the CDET fascicle. The fact is not to be overlooked, that whole tendons are able to resist higher stresses and extend further than the tendon fascicles.

The interfascicular matrix (IFM) is responsible for the extensibility of the tendon, allowing

sliding and recoil between fascicles. The IFM in energy-storing tendons (SDFT, Achilles tendon) exhibits low stiffness behaviour and a greater ability to resist and recover from cyclic loading, with less energy loss (hysteresis) and stress relaxation compared with the IFM in positional tendons (CDET, anterior tibialis) - the behaviour from the SDFT compared to the CDET is therefore more elastic and less viscoelastic. It is thought that elastin provides the IFM with efficient recoil, which means that the crimp pattern of the collagen fibres is restored after being strained (see section 2.3). Actually it has been shown that the elastin content is greater in the IFM of the SDFT [33] as well as the GAG content, but the collagen content is lower. SDFT had higher water content and water content showed a significant negative correlation with tensile modulus. All these results to SDFT being a more compliant material. A larger fibril diameter, on the other side, might be responsible for a stiffer matrix in the CDET [11].

While differences in structure and composition between energy-storing and positional tendons were observed at the macroscale, little is known about differences at the microscale [32]. There might be a greater total cross-link density in flexor tendons compared with extensors that cause fibrils from energy-storing tendons to resist molecular disruption while fibrils from positional tendons are able to extend further, but suffer increased damage characterised by formation of kinks. Additionally, shorter crimp and greater crimp angle in the SDFT support the observation that this type of tendon shows more elastic behaviour compared with CDET [34] (also visible in fig. 7).

Effect of Ageing at whole tendon and subunits level

In this thesis the differences in mechanical properties of individual collagen fibrils should be analyzed, but also the change in mechanical properties regarding age. For this reason the SDFT and CDET of a young (3 years old) and an old horse (18 years old) are compared. Previous studies have found that the risk of SDFT injury increases with age, so a lot of effort has been put in understanding how tendon properties alter as a function of age. Object of the studies were mostly mature tendons. Even though the association between increasing age and tendon damage seems obvious, data in the literature deliver conflicting results - studies report variously no alterations or decreasing mechanical properties with aging, both in human and equine tendons

16

[32]. No alterations in modulus, failure stress or failure strain with increasing age are reported to be visible in either the SDFT or the CDET [12]. After looking for changes at the whole tendon level, effects of aging are also investigated in the tendon subunits. Most observed changes occur in subunits of energy storing tendons, with many of them being specific to the IFM. The IFM in the aged SDFT exhibits increased stiffness, decreased fatigue resistance and ability to recover from loading [35], [12]. In contrast, no age-related changes in the mechanical characteristics of the CDET IFM could be identified. The composition of SDFT IFM changed slightly with age: Fibromodulin and elastin are both decreased [33]. The remaining elastin appears disorganised, which may be the reason for decreased recovering ability towards the unstrained crimp pattern. Fascicles of SDFT exhibit increased stress relaxation and decreased fatigue resistance [13], [35]. This behaviour could be explained through a loss of helix structure in these fascicles, leading again to reduced ability to recover from loading [36]. Fascicles of CDET, on the other hand, showed an increase in fascicle failure strain with aging, but only few changes within fascicles [35]. In summary, all those findings suggest that fascicles and interfascicular matrix mainly of SDFT are losing parts of their elastic characteristic and becoming more viscoelastic with age. From this, the hypothesis examined in this thesis is, that the indentation modulus of SDFT collagen fibrils increase with age, while the indentation modulus of CDET collagen fibrils shows no significant changes between young and old sample, but is overall higher than the indentation modulus of the young SDFT collagen fibrils.

3. Atomic force microscopy

3.1. History and Advantage of the atomic force microscope

The atomic force microscope (AFM) is part of the scanning probe microscopy (SPM) branch of microscopy. The common operation of SPMs relies on the interaction of a small tip located on the edge of a sensitive cantilever with the sample surface of interest. The principle and goal of AFM is the tip coming in interaction with the sample surface to measure the interactions like "the old fashion record-player needles in gramophones" as nicely formulated by Kontomaris et al.. They further compare AFM, an instrument that is "feeling" the surface, to optical microscopes, which are "looking" at samples [37].

The AFM was developed by IBM scientists Gerd Binnig, Calvin Quate and Christoph Gerber in 1985 ([38]) to image non-conductive samples (e.g. biological samples or polymers) with the goal to improve imaging resolution over that obtained with optical microscopy. It was created as a solution to the limitations of the scanning tunneling microscope (STM), which required the sample to be conductive [39]. Finally, the structural and mechanical properties of a wide range of materials including biological materials could be investigated. In comparison with other techniques such as scanning electron microscopy (SEM) and transmission electron microscopy (TEM) AFM allows measurements of native biological samples in physiological-like conditions, avoiding complex sample preparation procedures and artefacts connected to them [40]. AFM is a highly diverse and effective tool in material characterization and in particular, nanoindentation with AFM is one of the most popular methods for probing properties of soft biological samples and should be further explored with the potential future goal of more standardization in this field [1].

3.2. Principles of AFM

Commonly the main elements of an atomic force microscope (AFM), also of the one used in this work, are a flexible microcantilever with a sharp tip or bead, a piezoelectric translator, a laser and a photodetector. To enable scanning and indentation experiments in the first place, the probe (=tip) must be moved toward the sample with a predefined vertical speed, this is executed
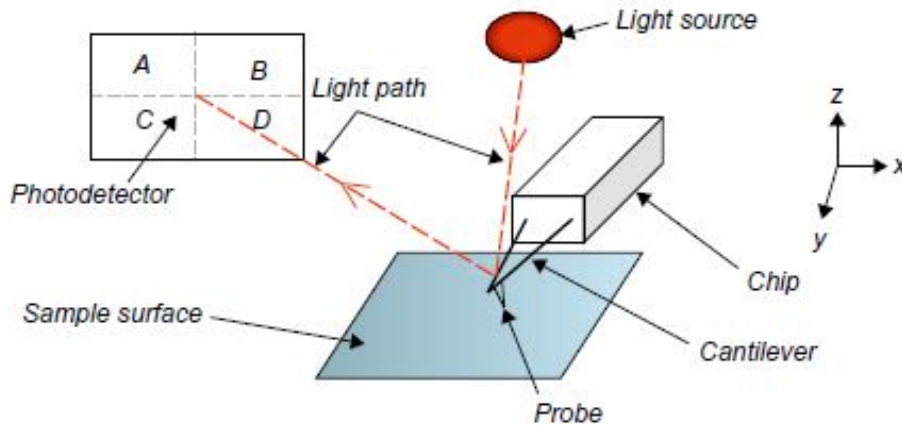
Figure 8: The heart of an AFM instrument is a sharp probe mounted on the end of a flexible micro-cantilever arm. The movement of the cantilever in the z-direction is usually imparted by a piezoelectric transducer. The deflection of the cantilever is translated into an electrical signal by a laser on the cantilever tip, which reflects onto a photodiode (from [41]).

through a piezoelectric translator. At a certain point (the contact point), the microcantilever probe contacts the sample and starts to indent it [1]. During this indentation procedure, the flexible cantilever deflects due to the sample's topographic and mechanical features. The deflection is monitored by a laser beam pointed at the back of the cantilever and then reflected towards a quadrant photodetector using the optical lever method as a detection method. A feedback circuit is responsible for controlling the relative distance between tip and surface and maintaining the interaction at a constant level in the popular imaging variants contact mode and AC-modes. Generally AFM can work in three basic operation modes defined through the forces arising between tip and surface: contact, intermittent and non-contact. Before outlining them in section 3.3, the main mechanical components of an AFM deserve more attention.

Laser and Photodiode

The most popular technique to detect the deflection of the cantilever is the *optical lever* method [42] because of it's simplicity and reliability. This is also the operating way of the AFM used in this thesis. The laser beam is reflected from the apex of the cantilever onto a photodetector. Deflection of the cantilever will therefore result in a change in the position of the laser spot on

the photodetector. The photodetector is commonly a quadrant photodiode divided into four equal parts, labelled from A to D (see fig. 8). A calibration is needed in order to obtain the deflection of the cantilever in nanometers from the change of the photodetector voltage signal (see appendix A).

Piezoelectric translator and feedback control loop

To bring the probe into and out of contact with the sample surface two configurations are possible: The tip-scanning, where during measurement the cantilever moves over the stationary sample, or the surface-scanning process, where the sample stage moves under the stationary cantilever. In both cases, however, a piezo tube scanner controls the relative movement between the cantilever and the sample, which is installed either in the sample stage or in the measuring head. Movement in this direction is conventionally referred to as the z-axis [41]. The piezocrystal of the AFM used in this thesis regulates the movement of the cantilever chip.

During measurements it is necessary to adjust the position of the cantilever to keep the control parameters constant (e.g. vertical deflection, oscillation amplitude, etc.). This is done by changing the height of the piezo, which is desirable to be performed fast and accurate. AFMs use a complex control system for achieving this.

Cantilever and tip

Last but not least, for the AFM measurement most important is the cantilever and its tip. Depending upon the uses required and the forces which may act upon them, different considerations must be made when selecting the cantilever from a large range available. Cantilevers are predominantly out of silicon nitride (e.g. Si_3N_4) or silicon (Si). Typically the upper surface, opposite to the tip, is coated with a thin reflective surface to enhance the reflection of the laser, usually of either gold (Au) or aluminium (Al) [41]. They are commonly either triangular/V-shaped or rectangular/'diving board' shaped. Rectangular cantilevers should be preferred over

V-shaped cantilevers, which seem to be more susceptible to effects of lateral forces during applications [43]. Typical rectangular cantilevers have a length from 90-500 μm and a width from 25-50 μm. Because of this very small geometry, cantilever are typically mounted on a larger chip, making handling and fixation in the AFM holder possible.

The sharp tip, which acts as the probe of interactions, is located at the cantilever's free end. Commonly this probe is in the form of a square-based pyramid, a cylindrical cone or a sphere. The tip's geometry plays an important role in the analysis of the sample's properties, see in section 3.6.
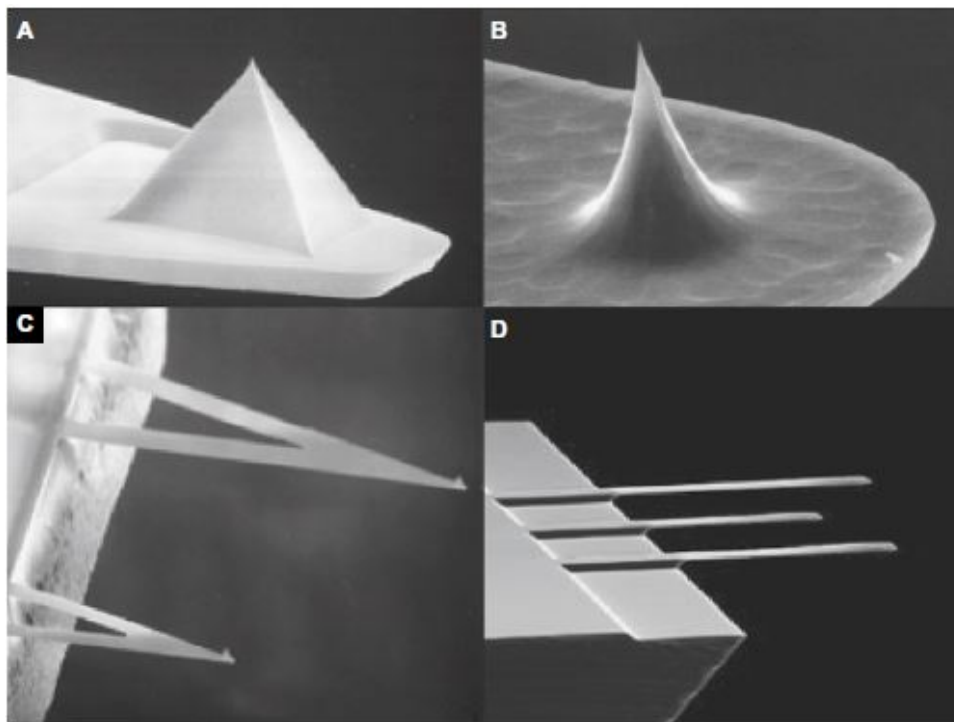
Figure 9: SEM images of different probes, among them a pyramidal (A) and a conical probe (B), and cantilever types like V-shaped cantilevers (C) and rectangular-shaped cantilevers of different lengths, which is also the type used for experiments in this thesis (from [41]).

Cantilevers can be considered physically like springs with spring constants ranging from a few nN/m to several hundreds of N/m. The k_c values given by the manufacturer are nominal values - the specific value for every cantilever first needs to be determined to do quantitative measurements.

The practical method used in this thesis by the AFM software is the *thermal noise method*, based on work of Hutter and Bechhoefer [44]. The experimental way to apply the thermal noise method is described in appendix A.

3.3. Interacting forces

Once the cantilever tip and the sample surface are brought into contact or in close proximity to each other, several forces act that are the basis for data acquisition in atomic force microscopy. At small distances, the force between the AFM tip and the sample surface will be repulsive (electron shell repulsion forces). At large distances attractive Van der Waals forces arise. Both types of forces can be approximated through the Lennard-Jones potential V_{LJ}:

$$V_{LJ}(r) = 4\epsilon \left[\left(\frac{\sigma}{r} \right)^{12} - \left(\frac{\sigma}{r} \right)^{6} \right] \tag{1}$$

with r (m) the distance between two particles, ϵ the depth of the local minimum of the potential energy (a measure of how strongly the two particles attract each other) and σ (m) the distance at which $V_{LJ} = 0$. The term r^{-6} in eq. 1 indicates the attractive interaction and r^{-12} arises from the repulsive forces [45].

In the beginning of a measurement, the cantilever is far away from the sample, meaning no interaction occurs between the cantilever tip and the surface. The tip is then approaching the surface. At some point, long-range attractive Van der Waals forces will start to act. Getting even nearer to the surface will provoke repulsive forces from overlapping of electron orbitals between tip and sample. The three main imaging modes (contact-, intermittent- and non-contact mode) are acting in the attraction, the repulsion or in both zones. The contact mode signifies a continuous contact of tip with sample, which results in exclusively repulsive forces. Conversely, in the non-contact mode solely attractive forces are experienced, because the tip never touches the sample. An additional mode, which is a mixture of the two already mentioned modes, is the
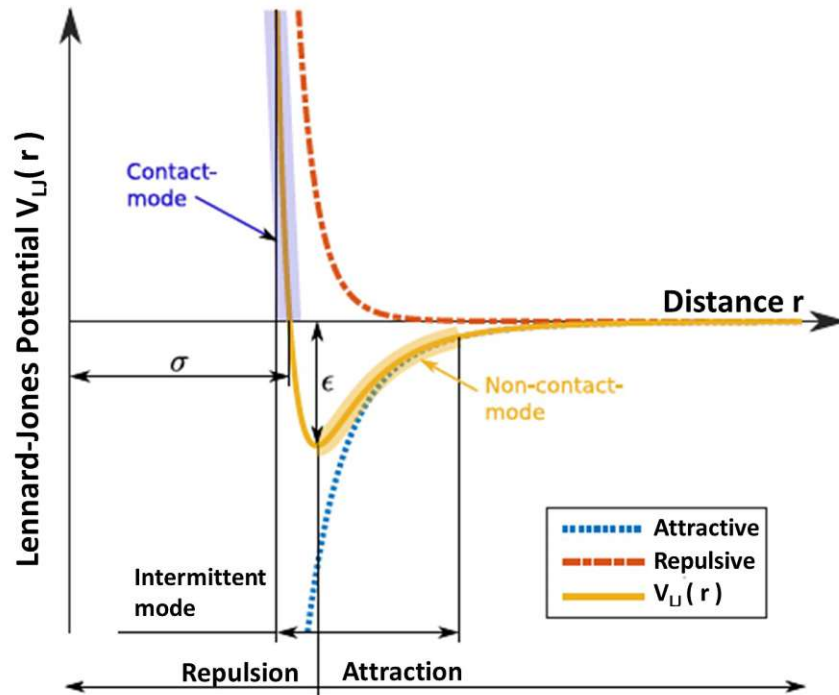
Figure 10: The Lennard-Jones potential curve portrays the forces which occur between tip and sample: The long-range attractive Van der Waals forces (blue) and the short-range electron shell repulsion forces (red). Those combined result in the Lennard-Jones potential (yellow). The common imaging modes (see chapter **??**) are working in the repulsion (contact mode) or attraction (non-contact mode) zone or in both zones (intermittent mode) (adapted from [9]).

intermittent or tapping mode. This mode, where the cantilever is periodically in contact with the surface, operates therefore in the attraction or repulsion zone depending on the tip's position [37].

3.4. Force measurements

The AFM is capable of more than just imaging samples in the micro- and nano-range - its main area of application is the quantitative measurement of the forces exerted between the tip of a cantilever and the sample surface, from which the mechanical properties of the material can be determined. As the tip comes into and out of contact with the surface, a force curve is created that represents the deflection of the cantilever as a function of distance. The raw data is made visible in a diagram: the abscissa shows the displacement of the z-piezo, while the deflection of the cantilever is shown as photodetector signal, usually as voltage in V, on the ordinate. The

sensitivity value of the cantilever (see section 3.2) is now required to convert the raw deflection data into actual deflection distance d. Since a cantilever is assumed to behave like a linear spring, the force acting on the cantilever can be calculated using Hooke's law:

$$F = -k_c d \qquad (2)$$

with F the force generated by the spring (N), d the deflection of the cantilever (m) and k_c the spring constant of the cantilever (N/m), representing the cantilever's stiffness. This enables the transformation of a deflection-displacement curve via simple multiplication of the deflection data with the cantilever's spring constant into a force-displacement curve ($F - z$ curve or just force curve) representing force vs. piezo-displacement. This $F - z$ curve consists of two curves that can be analyzed separately: The loading curve, which describes the movement of the tip towards the sample, and the unloading curve, which conversely is the movement of the tip away from the sample.

First, when the cantilever approaches the surface, there are no forces acting. As it comes closer, long-range forces occur. At some point the probe will touch the surface after overcoming the acting forces in a 'snap-in' or 'jump-to-contact'. Positive forces will be visible due to an upwards deflection of the cantilever due to repulsion between electron shells of atoms. They will act until the deflection reaches a specified value, the maximum applied force. As the cantilever tries to retract adhesive force will drag it downwards, causing hysteresis between trace and retrace. When the separation force becomes large enough, the cantilever will snap back to its original free level position.

The horizontal offset between trace and retrace happens due to scanner hysteresis. If furthermore approach and retraction curve do not coincide as predicted by the ideal elastic Hertz model (see section 3.6) it may be caused by mechanical behaviours of the sample e.g. plasticity, viscoelasticity, etc. The larger the hysteresis area between approach and retraction curve the larger the energy loss and viscoelastic contribution of the material [1]. Nevertheless, the evalu-

(a) r > r_eq   **(b) r = r_eq**   **(c) r < r_eq**
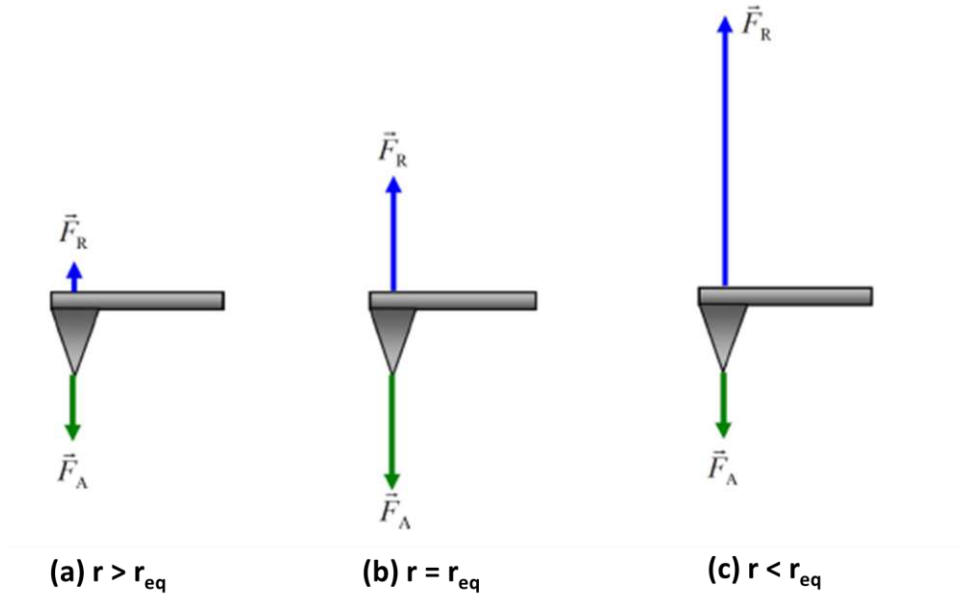
Figure 11: Forces applied on the AFM tip in three different regions of the Lennard-Jones Poten-
tial (see fig. 10). The equilibrium point of the distance r_{eq} is where the Lennard-Jones
Potential curve crosses the x-axis (b). Due to repulsive forces the cantilever will de-
flect upwards, away from the surface (c), whereas attractive forces will cause the
cantilever to deflect downwards, towards the sample (a), (adapted from [37]).

ation of data is often still based on the assumption of a purely elastic material behavior, which

is not the case with biological tissue and is dealt with in section 3.6.

A brief mathematical anticipation of the next section 3.5: In order to enable a mechanical char-

acterization of the samples, the actual indentation is required. Force vs. displacement data are

further processed to obtain the force vs. indentation ($F - h$ curve) dependency. If the cantilever

is brought in contact with a hard surface, as necessary for the calibration of the cantilever's

sensitivity (see section 3.2), no indentation occurs. The situation is different when soft samples

such as biological tissue are tested. Then the scanner displacement z is theoretically made up of

the deflection of the cantilever d and the indentation in the material h ($z = d + h$). However, the

offset from the baseline has yet to be removed from the data. Furthermore, finding the contact

point where the tip penetrates the specimen is essential for correctly determining the depth of

indentation. Finally, the indentation depth can be calculated from $h = z - z_0 - d$, where z_0 is

the location of the contact point (m).

25

3.5. Indentation testing with AFM

The indentation method of the AFM is based on the test methods used in material science (Brinell, Rockwell, Vickers), which measure the hardness of a sample. Standardized test specimen of various geometries (usually spheres or pyramids) are pressed into the sample under specified conditions. The surface or depth of the lasting impression is taken as a measure of the hardness. In practice, this is no longer possible in the micro and nano range, which is why fortunately the AFM provides the force vs. indentation data from which the material characteristics like stiffness, indentation modulus, viscoelastic properties can be extracted with the appropriate analysis methods (see in the next section 3.6).

Although with AFM it is not necessary to measure the indent in the sample, the contact area of the indenter is very important for calculating mechanical properties. Besides spheres, the probe geometry can appear as pyramids (Berkovich and cube corners). Later, for data analysis, probes will be mathematically approximated as solid spheres, cones, paraboloids of revolution or three- and four-sided pyramids [37].

Prior to an indentation experiment, when choosing the indenter, consideration should be given to its geometry, which should correspond to the material properties (and deformation modes) of interest.

In addition to defining the indenter acuity, prior to an indentation test, other decisions must be made regarding the experimental selection, e.g. the time frame of the indentation test and the nature of the total load profile, including the specification of the peak load. Indentation tests are extremely flexible in terms of the displacement-load-time sequence, which is the reason why Efremov et al. lament a lack of standardization in the field of indentation type AFM [1]. Key experimental controllables of a full indentation cycle, which typically consists of at least a loading and unloading sequence, potentially with a hold or dynamic (frequency-sweep) segment at fixed load, are the peak indentation load, the ramp time, and the hold time or other frequency profile at maximum load [17]. These challenges in adjusting the settings for experiments in this thesis will be faced in section 5.

A detailed manual for using the AFM to conduct indentation experiments can be found in appendix A.

Dynamic indentation

The main reason for the origin of this thesis lies in the pursuit of an approach that has only rarely been used in the literature for the mechanical characterization of biological tissue, namely dynamic indentation experiments with AFM. Overall, methods for measuring viscoelastic properties with AFM can be separated in the time domain (sometimes referred to as (quasi-)static experiments) and the frequency domain (referred to as dynamic experiments) [1]. Experiments with AFM in the time domain are performed in a step-hold method, applying a holding phase after the approach and before the withdrawal, during which either the force or the height is held constant, while the time dependence of the other is measured and analyzed. Assuming a viscoelastic material, keeping the height constant leads to a continuous decay in the interaction force (stress relaxation). On the other hand, if the force is kept constant, the indentation depth will increase over time (while head height and tip height decrease), which is called creep. In previous scientific research, viscoelastic properties of biological tissues are mostly extracted through experiments in the time domain, while only a handful of examples of frequency-domain experiments using AFM exist in the published literature (research: [3], [5], [4], [2], review: [17], [1]), where the sample is subjected to oscillatory deformations with a controlled frequency ω (angular frequency, $\omega = 2\pi f$) and a constant small amplitude. The amplitude of the force or the displacement excitation is selected so small that the tip is always in contact with the surface. A dynamic indentation cycle consists of a loading sequence, maybe a few hold and different frequency segments and an unloading sequence.

The AFM used in this thesis performs oscillations in z while being in contact with the surface, probing the frequency-dependent response of the surface [46]. Therefore the input appears as indentation (processed displacement) that can be described as a sine function of time t, $h(t) = h_0 + h_A sin\omega t$, occurring around a primary peak indentation h_0, while the indentation amplitude $h_A \ll h_0$. The output is a straight-forward sinusoidal force curve with an amplitude F_A and a phase shift ϕ such that the force response can be written as $F_0 + F_A sin(\omega t - \phi)$ [1], [17]. The phase shift, that occurs between the force over time and indentation over time curves

27

can have values between 0° and 90° and is calculated as follows:

$$\phi = \phi_F - \phi_H. \tag{3}$$

This phase shift is an indicator for the viscoelasticity of a material. A phase lag of $\phi = 0$ would indicate a pure elastic response, and a phase lag of $\phi = \pi/2$ a pure viscous response [5].

Data processing in this case turns out to be more demanding and will be developed in section 3.6. However, if the handling is much more difficult, why choose this test variant?

Dynamic experiments promise to unravel the true character of biological tissues, while time-domain experiments are said to neglect the material's viscoelastic character. A previously mentioned indicator to better describe certain materials in the context of a time-dependent rheology is the occurrence of a hysteresis between the loading and unloading curve. If the material were perfectly elastic, the two curves would coincide.

Another reason to choose dynamic measurements is that biological entities are often subjected to cyclical forces. Alcaraz et al. explain in their paper that oscillating stresses are of particular interest for lung epithelial cells, since they are subjected to large cyclic forces due to respiration [2]. Tendons also store and dissipate mechanical energy. Even at the micro level, the crimped structure of collagen fibers suggests that their behaviour is dependent on the rate at which force is applied. Dynamic indentation experiments are carried out in this thesis in order to be able to make further statements about this behaviour.

When it comes to choosing an instrument, Alcaraz et al. opt for the AFM thanks to its accuracy compared to dynamic experiments performed with Magnetic Twisting Cytometry (MTC). Another benefit of the AFM is the well-defined shape of the AFM indenter, so only a suitable contact-elastic model is missing to determine the indentation and the contact geometry between tip and sample.

3.6. Data analysis methods

The two commonly used techniques for analysing the force vs. indentation curves are the Hertz and the Oliver-Pharr method, which are discussed separately in the following subsections. As already mentioned, the Hertz method is often used to determine the Young's modulus of a material, although it assumes purely elastic deformations of the material. The Oliver-Pharr method, on the other hand, also takes into account the inelastic properties (like plasticity, damage) of a material, which is why this method is preferable for analyzing biological materials. Subsequently, the frequency-dependent approach of the Oliver-Pharr method, as used in this thesis, is presented.

Hertz method

The basis behind the Hertz method is an analytical description of two elastic spheres in contact. In order to apply the model to process AFM force curves further, a few assumptions need to be validated: The sample must be homogeneous, isotropic, linearly elastic and sufficiently large to be approximated as an infinite half-space, and there are no attractive or adhesive forces between the sample and the probe [1].

In the mathematical Hertz model, the tip is expressed as a sphere. The Sneddon model considers a rigid cone. However, these are only approximations of the actual tip geometry.

The Hertz Model tries to fit the loading curve of force-indentation data linearly. The known force F is a function of the area of a sphere (R is the tip radius (m)), the indentation h and the combined elastic modulus of the contacting bodies E^*:

$$F = \frac{4}{3} E^* R^{1/2} h^{3/2} \quad .$$ (4)

The combined elastic modulus is made up of the elastic modulus and the Poisson's ratio (ν = 0.5 assumed for cells and hydrogels) of the indenter (E, ν) and the sample (E_s, ν_s):

$$\frac{1}{E^*} = \frac{1-\nu^2}{E} + \frac{1-\nu_s^2}{E_s} \quad . \tag{5}$$

Since the probe can be assumed to be infinitely rigid towards soft samples, eq. 7 can be reduced to:

$$\frac{1}{E^*} = \frac{1-\nu_s^2}{E_s} \tag{6}$$

This leads to the equation for the Hertz model, from which the elastic modulus E_{Hertz} of the material can be calculated:

$$F = \frac{4\sqrt{R}}{3}\frac{E_{Hertz}}{1-\nu^2}h^{3/2} \quad . \tag{7}$$

Oliver-Pharr method

A general method that was less dependent on the design of the probe and did not assume linearity of the material was presented in 1992 by Oliver and Pharr, after whom it is also named. They derived a basic formula from Sneddon's model, a geometry independent relation among contact stiffness S (N/m), contact area A_c (m^2) and elastic modulus E (N/m^2) [47]:

$$E = (1-\nu^2)\frac{\sqrt{\pi}}{2\sqrt{A_c}}S \tag{8}$$

with ν the sample's Poisson ratio. The elastic modulus E here is also used in its reduced form from eq. 6.

30

The contact stiffness can be determined by the slope of the upper unloading part of the force-indentation curve at maximum indentation, thus $S = \dfrac{dF}{dh}\Big|_{h_{max}}$.

A_c is the projected area of the indenter at contact depth [48]. Analytical formulas exist for certain tip shapes to calculate the contact area, i.e. the contact area for spherical indenters is $A_{Csphere} = \pi(2Rh_c - h_c^2)$.

The shape of the tip is reconstructed in this thesis by TGT1 grating in order to be able to reproduce the geometry. Thus, none of the equations for calculating the indentation area are used. The TGT1-grating scanning procedure of all probes used during measurements in this thesis is described in appendix A.

Now only the contact depth h_c (m) has to be defined: This is the depth at which contact is
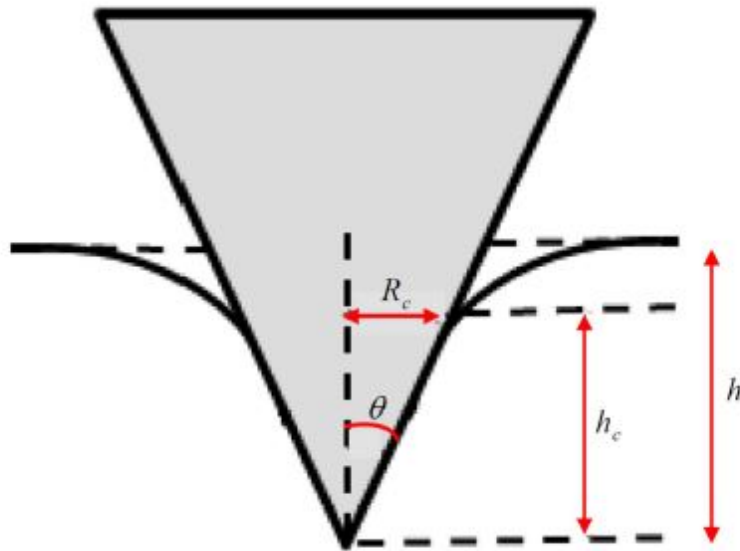
Figure 12: This image visualizes the indentation of a (pyramidal) probe into a sample. As clearly visible, the whole indentation h differs from the contact depth h_c, which is smaller and gives information about the location of the contact radius (or contact area A_c) (from [37]).

made between the indenter and the sample during indentation (see fig. 12) and can be calculated as follows:

$$h_c = h_{max} - \varepsilon \frac{F_{max}}{S} \tag{9}$$

where h_{max} is the maximum indentation depth and ε is a constant that depends on the indenter geometry. For conical geometry ε can be taken as 0.72 and for a paraboloid of revolution geometry $\varepsilon = 0.75$. [37]

Dynamic mechanical analysis

For a linear viscoelastic material under sinusoidal loading, the elastic (storage) modulus, $E'(\omega)$, and the viscous (loss) modulus, $E''(\omega)$, comprise the complex modulus $E^*(\omega)$:

$$E^*(\omega) = E'(\omega) + iE''(\omega) \tag{10}$$

where $i = \sqrt{-1}$.

So far there are two approaches to analyze the sinusoidal force and indentation data for the elastic modulus. For the sake of completeness, the approach of Alcaraz et al. [2], which involves Fourier transformation of force and indentation signals, be presented briefly. The papers by Rother et al. [3], Efremov et al. [1] and the JPK microrheology manual [46] refer to it. Alcaraz et al. state that determining the complex shear modulus of a cell from oscillatory measurements over a wide frequency range is a straightforward and robust approach to characterize microrheology [2]. For the development of the formula, Alcaraz et al. assumed a pyramidal indenter with a half-open angle θ. Including the hydrodynamic drag, Alcaraz et al. present

$$G^*(\omega) = \frac{1 - \nu}{3h_0 tan\theta} \left(\frac{F(\omega)}{h(\omega)} - i\omega b(0) \right) \tag{11}$$

as formula for the frequency dependent complex shear modulus $G^*(\omega)$. $F(\omega)$ and $h(\omega)$ are the Fourier transforms of F and h at ω, the angular frequency ($\omega = 2\pi f$). The term $i\omega b(0)$ considers the hydrodynamic drag force due to viscous friction of the cantilever with the surrounding fluid.

It is the force $b(0)$, which however is independent of the loading force, multiplied by the relative velocity between the surface of the cantilever and the liquid. The factor that stands before the term in brackets in eq. 11 takes into account the tip geometry, the operating indentation h_0 and the Possion's ratio, whereas the term in brackets is the frequency dependent mechanical response of the material [2].

Efremov et al. suggest the complex modulus as more relevant parameter for AFM experiments compared to the shear modulus G (both are related through $2G = E/(1+\nu)$), since the load in AFM experiments is always applied perpendicular to the surface [1].

In this thesis the formulas for the storage and loss modulus that Herbert, Oliver and Pharr published in 2008 should be used [49]. Also Oyen and Cook [17] and Antonovaite et al. [4] use this pair of analytical solvable equations for the real and the imaginary part of the complex indentation modulus as a function of frequency. The extended Oliver-Pharr equations take the phaseshift ϕ (eq. 3) and the amplitude of force F_A and indentation h_A into account:

$$E' = (1 - \nu^2)\frac{\sqrt{\pi}}{2\sqrt{A_c}}\left|\frac{F_A}{h_A}\right|\cos\phi, \quad E'' = (1 - \nu^2)\frac{\sqrt{\pi}}{2\sqrt{A_c}}\left|\frac{F_A}{h_A}\right|\sin\phi \tag{12}$$

Instead of a Fourier transformation, this procedure requires a sine fit of the original force and indentation data in order to be able to read off the amplitude and phase shift - this is dealt with in the next section 4.

Looking at eq. 10 and eq. 12 one also understands easily, that if the material turns out to be an elastic solid, $E''(\omega) = 0$, otherwise, if the material is a viscous liquid, $E'(\omega)$ turns to 0.

The loss tangent $E''(\omega)/E'(\omega)$ can therefore be used as an index of the solid-like or liquid-like behaviour of a material [1].

4. MATLAB code

Several lines of code had to be added to an existing MATLAB program capable of analyzing simple indentation tests to also handle the additional data from dynamic indentation experiments. This object-oriented program called *ForceMapAnalysis* consists of two classes: 'ForceMap.m' and 'Experiments.m'. The force map class contains all necessary functions to process the force curves from indentation experiments, while in the experiment class all functions for the user are listed. Every class is divided into properties and methods. Inside the methods are the functions, by which desired results are calculated, and those results can be assigned a property name and then accessed by any other function in the class. Initially, the user types in 'E=Experiment' in the command window, which will load all data from a '.jpk-force-map'-file in a force map 'E' in MATLAB. The 'Experiment' in this command is a function in the class 'Experiment.m' which uses other functions to be able to save all defined properties (including force vs. displacement curves) in a force map 'E', which is temporarily available in the MATLAB storage.

All added pieces of code in 'ForceMap.m' are first briefly listed and second described in detail. Starting with loading the data from the AFM into MATLAB, through the creation of a sine fit for the data, which enables the analysis of the complex modulus (consisting of storage and loss modulus), to the generation of diagrams to visualize the results. The steps of the procedure are as follows:

1. Reading data properties

2. Loading data

3. Preprocess data (baseline fit and tilt)

4. Calculation of indentation data

5. Sine fit of data

6. Calculation of the storage and loss modulus for microrheology

7. Plots to visualize microrheology data

The plots include the force vs. time, indentation vs. time and force vs. indentation, as well as force and indentation vs. time including sine fit. In addition, the phase shift between the fits is visualized. In further plots, the storage and loss modulus, the phase shift and the loss tangent are plotted against the frequency. The detailed code required for this can be found in appendix B.

4.1. Reading data properties

The first task is to extract the unprocessed data from the AFM experiment from zip files with the file extension '.jpk-force-map'. The unzipped files are in a specific form structured in sub-folders. In addition to the data sets, these folders contain text files from which information about the experiment can be read. For example, the number of deflection-displacement curves can be read out using the 'read_in_header_properties' function and this number then stored under the property 'obj.NCurves'.

In a dynamic indentation experiment, it is also important to find out how many segments a deflection-displacement curve consists of. So, the document is searched for '.settings.force-settings.segments.size='. After the equals sign is the number of segments, which is stored as a property under 'obj.NumSegments' for future reference. Now it remains to find out the duration of each segment and the frequency. Not every segment is an oscillation segment, which is why it is checked first and then the frequency value is saved 'obj.SegFrequency' or set to zero. Important for frequency-dependent measurements is of course the time vector. Since the extraction of the time vector out of the JPK data is not implemented yet in the existing MATLAB code, it is alternatively calculated - the duration of a segment is known, as well as the start and end time. The duration of each further segment is added to this and the result is 'obj.SeriesTime'. However, this still lacks a vector that assigns each deflection or displacement point to a point in time. So the number of points per segment has to be read out, which then divides the duration of each segment into 'obj.SecPerPoint'. These are halved and thus an equidistant time vector 'obj.SegTime' is created. This method applies to given modulation segments, but might need to be revisited for other applications.

```matlab
% NumSegments
clear tline where;
frewind(fileID);
B=strfind(A,strcat(obj.FileType,'.settings.force-settings.
    segments.size='));
if isempty(B)
    clear tline where;
    frewind(fileID);
else
    fseek(fileID,B,'cof');
    tline = fgetl(fileID);
    where=strfind(tline,'=');
    obj.NumSegments = str2double(tline(where+1:end));


    for i=1:obj.NumSegments
        clear tline where;
        frewind(fileID);
        B=strfind(A,strcat(obj.FileType,'.settings.force-
            settings.segment.',string((i-1)),'.duration='));
        fseek(fileID,B,'cof');
        tline = fgetl(fileID);
        where=strfind(tline,'=');
        obj.SegDuration{i} = str2double(tline(where+1:end));


        if i == 1
            obj.SeriesTime{i} = obj.SegDuration{i};
        else
            obj.SeriesTime{i} = obj.SeriesTime{i-1}+obj.
                SegDuration{i};
        end


        clear tline where;
```

```matlab
30                    frewind(fileID);
31                    B=strfind(A,strcat(obj.FileType,'.settings.force-
                          settings.segment.',string((i-1)),'.num-points='));
32                    fseek(fileID,B,'cof');
33                    tline = fgetl(fileID);
34                    where=strfind(tline,'=');
35                    obj.SegNumPoints{i} = str2double(tline(where+1:end));
36
37                    obj.SecPerPoint{i} = obj.SegDuration{i}/obj.
                          SegNumPoints{i};
38
39                    if i == 1
40                        obj.TStart{i} = obj.SecPerPoint{i}/2;
41                    else
42                        obj.TStart{i} = obj.SeriesTime{i-1}+(obj.
                              SecPerPoint{i}/2);
43                    end
44
45                    obj.TEnd{i} = obj.SeriesTime{i};
46                    obj.SegTime{i} = obj.TStart{i}:obj.SecPerPoint{i}:obj.
                          TEnd{i};
47                    obj.InterpTimeF{i} = obj.TStart{i}:0.000001:obj.TEnd{i
                          };
48                    obj.InterpTimeH{i} = obj.TStart{i}:0.000001:obj.TEnd{i
                          };
49                    obj.InterpTimeF{i} = obj.InterpTimeF{i}.';
50                    obj.InterpTimeH{i} = obj.InterpTimeH{i}.';
51                    obj.SegTime{i} = obj.SegTime{i}.';
52
53
54                    clear tline where;
55                    frewind(fileID);
56                    B=strfind(A,strcat(obj.FileType,'.settings.force-
```

37

```matlab
                        settings.segment.',string((i-1)),'.frequency='));
57              if isempty(B)
58                  obj.SegFrequency{i} = 0.0;
59              else
60                  fseek(fileID,B,'cof');
61                  tline = fgetl(fileID);
62                  where=strfind(tline,'=');
63                  obj.SegFrequency{i} = str2double(tline(where+1:end)
                        );
64              end
65          end
66      end
```

Listing 1: MATLAB Code for reading the properties of dynamic indentation experiments from
text files. The number of segments is read out in the first few lines (lines 2-12),
followed by a calculation to determine the time vector (line 14-51), since the JPK
software does not store it with the rest of the data. At the end, it is determined
whether the segment under consideration is one with a frequency or not, and this
frequency is saved or set to zero (line 54-64).

4.2. Loading data

The loading of the force curves happens in the function 'load_force_curves'. When the function
is called, it should first be checked whether this is a dynamic or a simple indentation measure-
ment. If 'obj.NumSegments' is non-zero and also greater than 2, then the function jumps into
an added for-loop that iterates through all segments and stores displacement 'obj.Height' and
deflection data 'obj.Force' in matrices. Since deflection data are no longer needed later, they are
'wrongly' called 'obj.Force' and are, however, in the same step multiplied by the spring constant
of the cantilever, as described in section 3.4 (eq. 2). For the sake of clarity, the approach and
retract data of each force curve are later saved explicitly in vectors ('obj.HHApp'/'obj.App' and
'obj.HHRet'/'obj.Ret').

38

```matlab
if ~isempty(obj.NumSegments)  && (obj.NumSegments > 2)
        obj.HHType = 'capacitiveSensorHeight';
        for i=1:obj.NCurves
            for j=1:obj.NumSegments
                HeaderFileDirectory = fullfile(TempFolder,'shared-data'
                    ,'header.properties');
                SegmentHeaderFileDirectory = fullfile(TempFolder,'index
                    ',string((i-1)),'segments',string((j-1)),'segment-
                    header.properties');
                HeightDataDirectory = fullfile(TempFolder,'index',
                    string((i-1)),'segments',string((j-1)),'channels','
                    capacitiveSensorHeight.dat');
                vDefDataDirectory = fullfile(TempFolder,'index',string
                    ((i-1)),'segments',string((j-1)),'channels','
                    vDeflection.dat');

                if ~isfile(HeightDataDirectory) || isequal(obj.HHType,'
                    measuredHeight')
                    HeightDataDirectory = fullfile(TempFolder,'index',
                        string((i-1)),'segments',string((j-1)),'channels
                        ','measuredHeight.dat');
                    obj.HHType = 'measuredHeight';
                end
                if ~isfile(HeightDataDirectory) || isequal(obj.HHType,'
                    Height')
                    HeightDataDirectory = fullfile(TempFolder,'index',
                        string((i-1)),'segments',string((j-1)),'channels
                        ','Height.dat');
                    obj.HHType = 'Height';
                end
```

39

```matlab
20              [TempHHApp, obj.Force{i,j}, obj.SpringConstant, obj.
                    Sensitivity]=...
21                  obj.writedata(HeaderFileDirectory,
                        SegmentHeaderFileDirectory,...
22                  HeightDataDirectory, vDefDataDirectory, obj.HHType);
23
24              obj.Height{i,j} = -TempHHApp;
25              % force = deflection * spring constant
26              obj.Force{i,j} = obj.Force{i,j}.*obj.SpringConstant;
27              clear TempHHApp
28
29
30          end
31
32          obj.HHApp{i} = obj.Height{i,1};
33          obj.App{i} = obj.Force{i,1};
34
35
36          %lastseg = obj.NumSegments - 1;
37          obj.HHRet{i} = obj.Height{i,obj.NumSegments};
38          obj.Ret{i} = obj.Force{i,obj.NumSegments};
39
40      end
41
42  else
43  [...]
```

Listing 2: MATLAB code for loading the force curves. This is only an excerpt of the function, the upper part of which clarifies whether it is a dynamic or a simple experiment (line 1). After the last 'else' (line 42) comes the part for ordinary indentation measurements. For each segment of each curve, the deflection and displacement data are loaded and saved (line 20-24). Then the deflection data is converted to force data (line 26). The result is two large matrices per curve (line 32-33). Approach and retraction are defined separately in the properties (line 37-38).
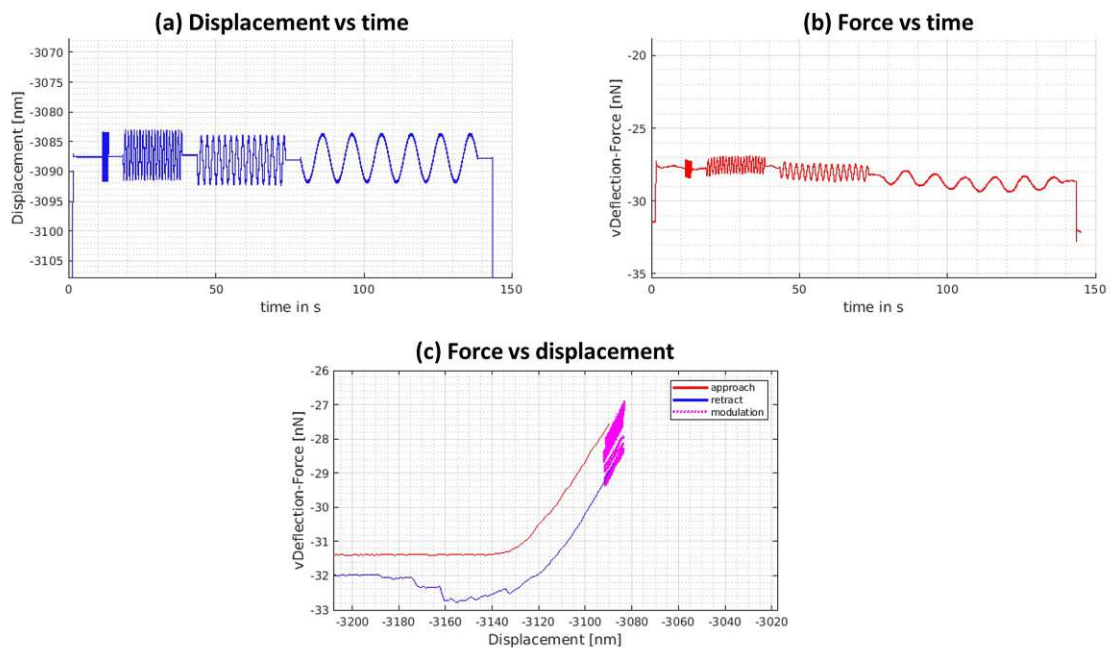
Figure 13: After loading the force maps in MATLAB, displacement and force data can be visualized (a)-(c). Notice: In order to be able to read the actual height and force data from the figures, they must be brought to the zero line in the next step. In addition, the indentation depth is required for the indentation modulus calculation, however only the displacement is given here.

4.3. Preprocess data

In a further step baseline and tilt are subtracted from the force vs. displacement curve with the function 'base_and_tilt'. The purpose of this function is to shift the non-contact part of the force vector to the zero line (displacement data is not changed in this step), which makes it easier to view and edit the data (see fig. 14). For example, it is an necessary step before being able to define the contact point where the cantilever enters the material. The processing of the data is done by fitting a (linear) function to the non-contact zone of the force curve resulting in the so-called 'based' force data, which is stored in 'obj.BasedForce'. The calculation is carried out analogously to the existing calculation of 'obj.BasedApp'/'obj.BasedRet'. In contrast to simple indentation experiments, the baseline-fit must be carried out over all segments. The same applies to the displacement data.

```matlab
[...]
            obj.BasedApp{i} = (obj.App{i}-feval(obj.Basefit{i},obj.
                HHApp{i}));
            obj.BasedRet{i} = (obj.Ret{i}-feval(obj.Basefit{i},obj.
                HHRet{i}));

            if ~isempty(obj.NumSegments)  && (obj.NumSegments > 2)

                %for  i=1:obj.NCurves
                    for  j=1:obj.NumSegments
                        obj.BasedForce{i,j} = (obj.Force{i,j}-feval(obj
                            .Basefit{i},obj.Height{i,j}));
                    end
                %end
                end
            end
        % calculate vertical tip position by subtracting vertical tip
             deflection from head height
        iRange = find(obj.SelectedCurves);
        for  i=iRange'
```

```matlab
17          obj.THApp{i} = obj.HHApp{i} − obj.BasedApp{i}/obj.
                SpringConstant;
18          obj.THRet{i} = obj.HHRet{i} − obj.BasedRet{i}/obj.
                SpringConstant;
19
20          if ~isempty(obj.NumSegments)  && (obj.NumSegments > 2)
21
22              for j=1:obj.NumSegments
23                  obj.THeight{i,j} = obj.Height{i,j} − obj.BasedForce
                        {i,j}./obj.SpringConstant;
24              end
25          end
26      end
27  [...]
```

Listing 3: MATLAB code for preprocessing force curves. Only the part of the code where something was added is shown here. An if-condition is used to check whether a frequency-dependent measurement is present (line 5 and 20). A loop through all segments performs the baseline fit and tilt for force (line 8-10) and displacement data (line 22-24). In comparison, the formulas for simple experiments can be viewed in this code snippet (line 2-3 and 17-18).
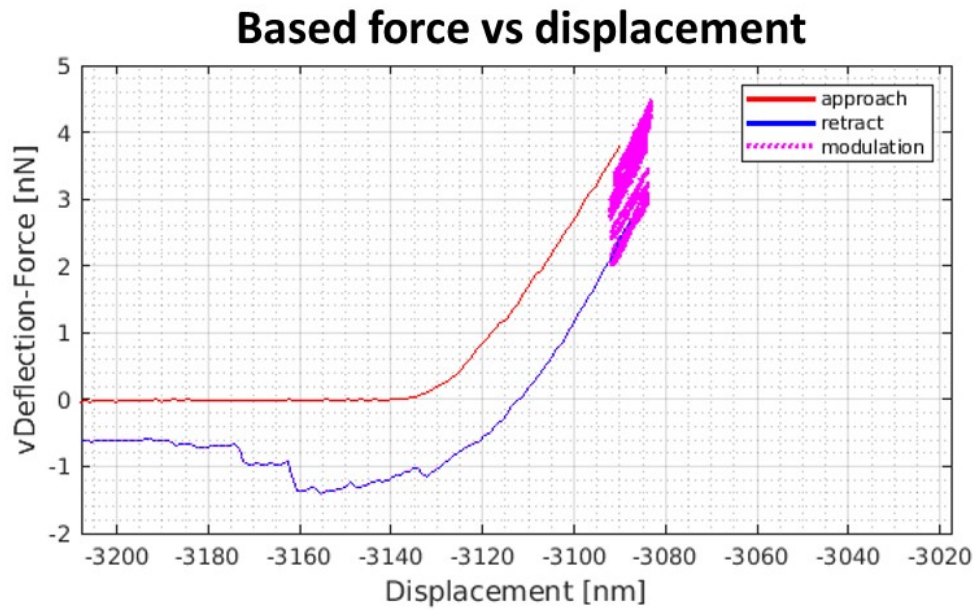
Figure 14: In the preprocessing step, the force data is brought to the zero line. Compared to the last fig. 13 (c), it is easy to see how the approach curve now starts at zero force - however, the point of indentation cannot yet be read from the displacement data on the x-axis.

4.4. Indentation data

As discussed in section 3.4, the indentation is the difference between displacement at contact and the deflection of the cantilever $h = z - z_0 - d$. The indentation is required for the dynamic mechanical analysis (DMA), since the sinusoidal data is to be fitted in order to read the parameters of the sine fit, such as amplitude and phase shift, which are ultimately necessary for the calculation of the complex modulus.

```matlab
1    function indentation(obj)
2
3
4        for i=1:obj.NCurves
5            %lastseg = obj.NumSegments-1;
```

```matlab
for j=1:obj.NumSegments
    Z{i,j} = obj.Height{i,j} - obj.CP(i,1);
    D{i,j} = (obj.BasedForce{i,j} - obj.CP(i,2))./obj.
        SpringConstant;
    obj.Indentation{i,j} = Z{i,j} - D{i,j};
end

    end
end
```

Listing 4: MATLAB code to calculate the indentation. This has to be done for every force curve and will result in a matrix 'obj.Indentation' of the same dimensions as force and displacement. As a first step, the contact point calculated in a separate function is subtracted from the displacement data (line 7). The required deflection is then calculated from the force data after the baseline fit, from which the contact point is also subtracted (line 8). Now the indentation data can easily be calculated by subtracting deflection from displacement data (line 9).
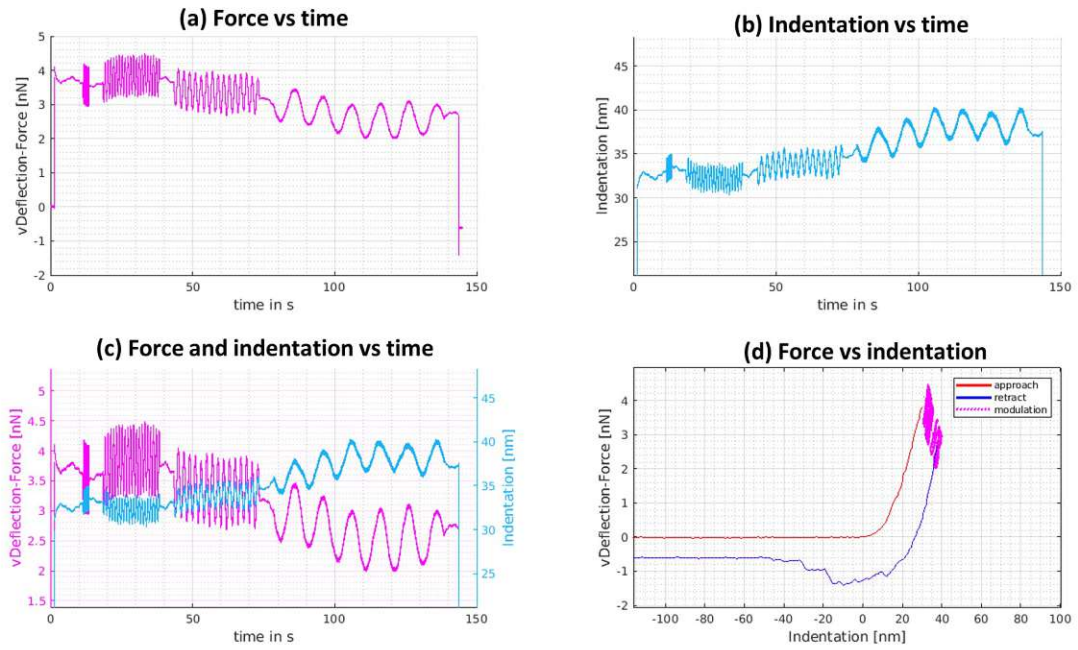
Figure 15: (a) shows base-line fitted force over time and (b) indentation over time. Both are combined in one plot in (c). The contact point of the cantilever tip and the material can now be read from the curves in plot (d): It is located at the intersection of zero force and zero indentation. As the indentation increases, so does the force.

4.5. Sine Fit

The heart of the program is the function 'sine_fit_for_microrheology' that attempts to fit the sinusoidal force over time and indentation over time data (see fig. 15). The underlying analysis approach seems simple at first glance: A sine function is used to fit force and indentation data

$$y = A_1 * sin(A_2x + A_3), \tag{13}$$

where the amplitude of the curve, A_1, must not become negative in the fitting process (line 63-64) and the starting parameter is set by taking half difference of maximum and minimum of the data (line 52-61). The period A_2 is specified by the set frequency. It is clear that the phase A_3 must range between $-\pi$ and π and therefore 0 is simply assumed as the starting parameter (line 73-74).

Because the frequency is preset with 'obj.Frequency', as starting values only two parameters (amplitude and phase shift) are needed for the Least-Squares-Optimization in the MATLAB script seen below (lines 55-70), which was adapted from a code on *mathworks.com* [50].

At the beginning the data are normalized by dividing them by their range (lines 16-18). The signals are initially not perfectly smooth, so first the underlying drift needs to be removed, followed by a zero-phase filtering step, as also suggested in the literature e.g. by Rother et al. [3]. As most curves showed a linear drift, a linear 'polyfit' is used to define the slope and the height shift of the signals (lines 28-33). After the detrending (line 36) follows the filtering (line 39-42). The filter 'filtfilt' is chosen as such that no vertical shifting of the data occurs [51]. The filter slides a window of a certain length, which in this case is depending on the sampling rate and the frequency of a segment, along the data, computing averages of the data contained in each window [52]. However, taking the average compresses the data, which is why the amplitude has to be brought back to its original level using a correction (lines 45-49).

In line 57 the sine function with its variables is defined. In line 58 the least-squares cost function will compare the force vs. time data to the calculated sine function. The input vector is set in line 62 and the lower and upper boundaries follow in lines 63-64. In line 65 a nonlinear minimum search is accomplished, resulting in a vector with amplitude, frequency and phase shift for every

frequency segment of a curve.

The phase shift between force and indentation curve 'obj.DeltaPhi' (°) can be defined directly in this function (line 93), as well as the loss-tangent, which is an important parameter for determining the liquid- or solid-like character of a material (see section 3.6) in line 95.

Finally, the initial normalization must be removed again in order to display the force data, as well as amplitude, slope and height shift, in their normal, undistorted size (line 85 and 98-101).

```matlab
1          function sine_fit_for_microrheology(obj)
2
3
4          obj.slopeF = zeros(obj.NCurves, obj.NumSegments);
5          obj.interceptF = zeros(obj.NCurves, obj.NumSegments);
6
7
8          for i=1:obj.NCurves
9              lastseg = obj.NumSegments-1;
10
11             for j=2:lastseg
12
13                 if obj.SegFrequency{j} > 0
14
15
16                     % Divide data through their range
17                     rangeF = range(obj.BasedForce{i,j});
18
19                     obj.BasedForce{i,j} = obj.BasedForce{i,j}/rangeF;
20
21                     % Calculation of Sampling rate and Invariance to
22                     % be able to subsequently choose the right filter
23                     Samplingrate = 1/obj.SecPerPoint{j};
24                     Invariance = Samplingrate/obj.SegFrequency{j};
25
26                     % Force-Data are only placed horizontally in
```

```matlab
27                              % the zero line with detrend
28                              linearfitF = polyfit(obj.SegTime{j},obj.BasedForce
                                    {i,j},1);
29                              Fvalueslinfit = polyval(linearfitF,obj.SegTime{j})
                                    ;
30
31                              %y =k*x+d;
32                              obj.slopeF(i,j) = linearfitF(1);
33                              obj.interceptF(i,j) = linearfitF(2);
34
35                              %manually detrended data
36                              ForceTrend{i,j} = obj.BasedForce{i,j} -
                                    Fvalueslinfit;
37
38
39                              %1D-digital filter
40                              iN = Invariance/100;
41                              d = ones(1,fix(iN))/iN;
42                              obj.FilterF{i,j} = filtfilt(d,1,ForceTrend{i,j});
43
44
45                              % Amplitude Correction
46                              AmplFiltF = trapz(abs(obj.FilterF{i,j}));
47                              AmplOrigF = trapz(abs(ForceTrend{i,j}));
48                              AmplCorrectionF = AmplOrigF/AmplFiltF;
49                              obj.FilterF{i,j} = obj.FilterF{i,j}*
                                    AmplCorrectionF
50
51                              % Max values of Force and Indentation
52                              maxF = max(obj.FilterF{i,j});
53
54                              % Min values of Force and Indentation
55                              minF = min(obj.FilterF{i,j});
```

49

```matlab
56
57                              % Difference max min
58                              DiffF = maxF - minF;
59
60                              % Amplitude
61                              AmplitudeF=(DiffF/2);
62
63                              x = obj.SegTime{j};
64
65                              % Function to fit force data
66                              %b(1) (max-min)/2 b(2) FFT b(3) first sign change
                                    b(4) mean
67                              fit = @(b,x)   b(1).*(sin(2*pi*x.*obj.SegFrequency{
                                    j} + b(3)));
68                              % Least-Squares cost function:
69                              fcn = @(b) sum((fit(b,x) - obj.FilterF{i,j}).^2);
70                              % Minimise Least-Squares with estimated start
                                    values:
71                              options = optimset('FunValCheck','off');
72                              x0 = [AmplitudeF,obj.SegFrequency{j},0];
73                              lb = [0,-Inf,-pi];
74                              ub = [Inf,Inf,pi];
75                              obj.SineVarsF{i,j} = fmincon(fcn,x0,[],[],[],[],lb
                                    ,ub);
76                              % Spacing of time vector:
77                              %xpF = linspace(min(obj.InterpTimeF{j}),max(obj.
                                    InterpTimeF{j}),100000);
78                              %obj.SineVarsF{i,j}(1)= obj.SineVarsF{i,j}(1)*
                                    rangeF;
79                              obj.SineVarsF{i,j}(2)= obj.SegFrequency{j};
80                              %obj.SineVarsF{i,j}(3)= firstsignchangeF;
81
82
```

```matlab
83
84                        %multiply range back
85                        obj.SineVarsF{i,j}(1) = obj.SineVarsF{i,j}(1)*
                              rangeF;
86
87
88                        % phase shift of force and indentation
89                        obj.psF{i,j} = obj.SineVarsF{i,j}(3);
90
91                        % phase shift between indentation and force in
                              degrees:
92                        obj.DeltaPhi{i,j} = (obj.psF{i,j} - obj.psH{i,j})
                              *(180/pi);
93
94                        % loss tangent:
95                        obj.LossTangent{i,j} = tand(obj.DeltaPhi{i,j});
96
97
98                        % turn range back to normal
99                        obj.interceptF(i,j) = obj.interceptF(i,j)*rangeF;
100                       obj.slopeF(i,j) = obj.slopeF(i,j)*rangeF;
101                       obj.BasedForce{i,j} = obj.BasedForce{i,j}*rangeF;
102
103              end
104          end
105       end
106
107    end
```

Listing 5: MATLAB Code for sine fit. For clarity, only the code for the force data is shown here. The indentation data undergo the same procedure.
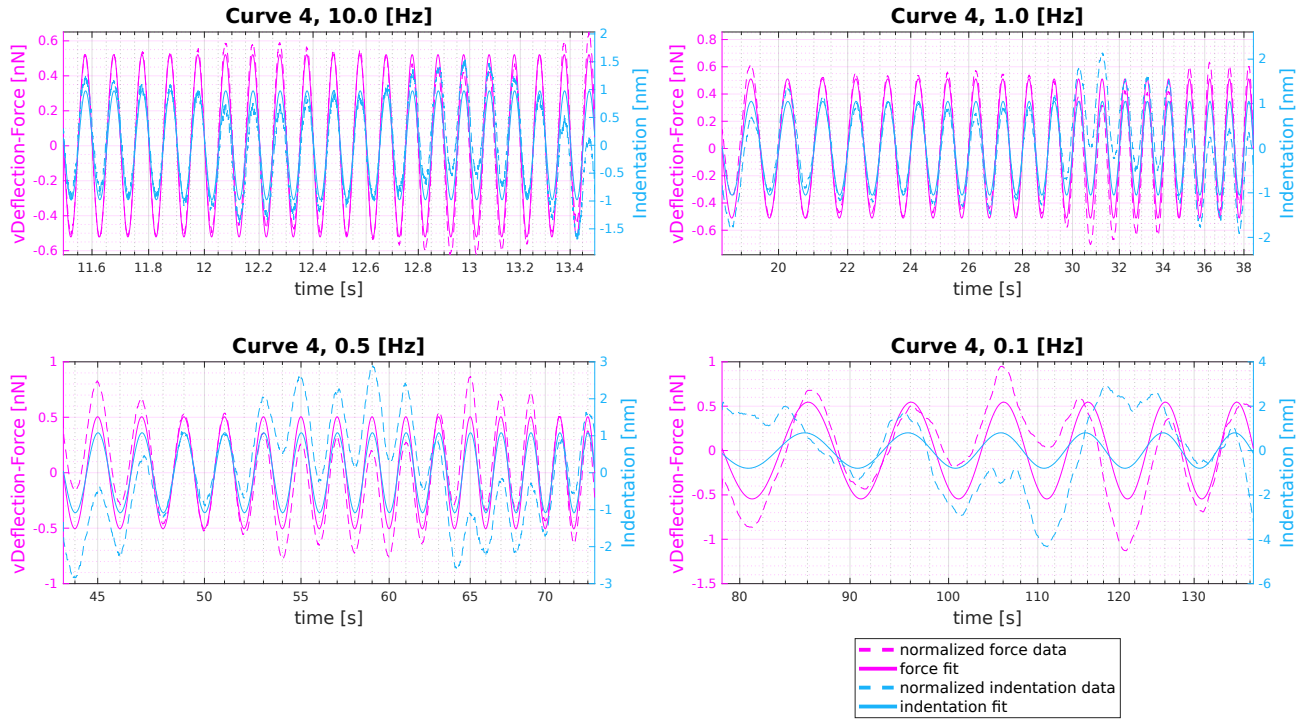
Figure 16: To check whether the fit fits the data well, normalized force and indentation data are shown together with their fits, each frequency of a dynamic indentation cycle in a separate plot. In the figure 17 below the real force and indentation data is displayed with their fits in one plot.
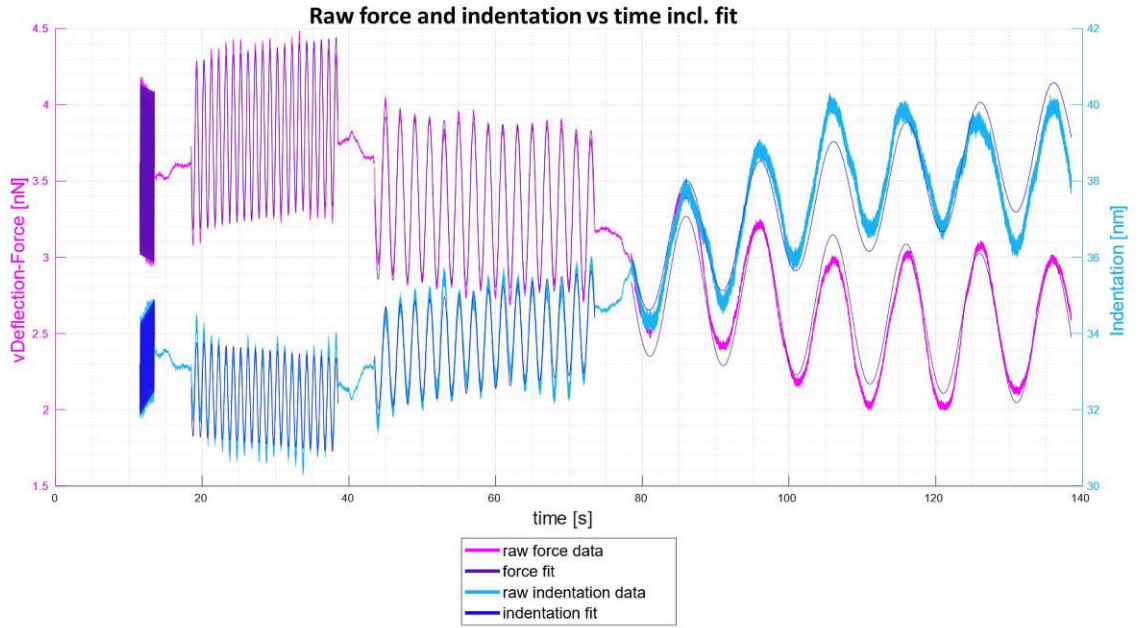
Figure 17: Raw force and indentation data with adapted sine fit.

4.6. E-Modulus

The aim of microrheology measurements is to obtain the elastic (storage) modulus, $E'(\omega)$ and 'obj.EModMicro1' respectively, and the viscous (loss) modulus, $E''(\omega)$ and 'obj.EModMicro2' respectively. For this, the indentation depth must be calculated using the unloading curve (lines 21-35). The formula eq. 9 for the indentation depth is implemented in line 35. With the indentation depth the indentation area can be calculated (lines 46-47). According to Oliver-Pharr, given an analytical function of force-indentation data, the stiffness can be calculated from the first derivative of that function at maximum indentation depth (see section subsec:afmmethods). Lacking such an analytical function, the stiffness is evaluated as follows: The difference of deflection of the upper twenty-five percent of the unloading data is calculated (line 30 in the code), then the difference of indentation is calculated with the knowledge of the slope 'obj.DZslope' corrected by the reference slope on glass 'obj.RefSlope' in case of tip inaccuracies (line 31). The

53

contact stiffness is finally calculated by dividing the difference of force with the difference of indentation (line 33).

Indentation depth and area contribute to the formulas of storage and loss modulus (lines 49-55) (eq. 12). Those values have of course to be positive, which is assured in lines 57-63.

```matlab
function [EModMicro1, EModMicro2] =
    calculate_e_mod_microrheology(obj, TipProjArea, CurvePercent)

if nargin < 3
    CurvePercent = 0.75;
end

Range = find(obj.SelectedCurves);
Epsilon = 0.73; % Correction constant from Oliver Pharr Method
    (1992)
Beta = 1.0226; %Correction constant from Oliver Pharr Method
    (1992)
obj.EModMicro1 = zeros(obj.NCurves,1);
obj.EModMicro2 = zeros(obj.NCurves,1);
EModMicro1 = zeros(obj.NCurves,1);
EModMicro2 = zeros(obj.NCurves,1);
obj.ProjTipArea = TipProjArea;
obj.DZslope = zeros(obj.NCurves,1);
obj.Stiffness = zeros(obj.NCurves,1);
obj.IndDepth = zeros(obj.NCurves,1);
obj.IndentArea = zeros(obj.NCurves,1);
for i=Range'
    for j=1:obj.NumSegments
        Z = obj.HHRet{i} - obj.CP(i,1);
        D = (obj.BasedRet{i} - obj.CP(i,2))/obj.SpringConstant;
        Zmax(i) = max(Z);
        Dmax(i) = max(D);
        DCurvePercent = D(D>=(1-CurvePercent)*Dmax(i));
```

```matlab
26          ZCurvePercent = Z(1:length(DCurvePercent));
27          LineFit = polyfit(ZCurvePercent,DCurvePercent,1);
28          obj.DZslope(i) = LineFit(1);
29          Hmax(i) = Zmax(i) - Dmax(i);
30          dD = Dmax(i) - (1-CurvePercent)*Dmax(i);
31          dh = dD*(1./obj.DZslope(i) - 1/(obj.RefSlope));
32          df = dD*obj.SpringConstant;
33          obj.Stiffness(i) = df/dh;
34          Fmax(i) = Dmax(i).*obj.SpringConstant;
35          obj.IndDepth(i) = Hmax(i) - Epsilon.*Fmax(i)/obj.
                Stiffness(i);
36          % IndentArea is taken as the linear interpolation
                between
37          % the two numeric values of TipProjArea the Hc(i) falls
38          % inbetween
39
40          if obj.SegFrequency{j} > 0
41
42              x = obj.SegTime{j};
43
44
45              try
46                  obj.IndentArea(i) = ((1-(obj.IndDepth(i)*1e9-
                        floor(obj.IndDepth(i)*1e9)))*TipProjArea(
                        floor(obj.IndDepth(i)*1e9))...
47                      + (obj.IndDepth(i)*1e9-floor(obj.IndDepth(i
                        )*1e9))*TipProjArea(ceil(obj.IndDepth(i)
                        *1e9)));
48
49                  EModMicro1(i,j) = sqrt(pi/obj.IndentArea(i))
                        *1/2*...
50                      (1-obj.PoissonR^2)*cosd(obj.DeltaPhi{i,j})
                        *...
```

```matlab
51                              (obj.SineVarsF{i,j}(1)/obj.SineVarsH{i,j
                                    }(1));

52

53                      EModMicro2(i,j) = sqrt(pi/obj.IndentArea(i))
                                *1/2*...
54                              (1-obj.PoissonR^2)*sind(obj.DeltaPhi{i,j})
                                    *...
55                              (obj.SineVarsF{i,j}(1)/obj.SineVarsH{i,j
                                    }(1));

56

57                      if EModMicro1(i,j) <= 0
58                          EModMicro1(i,j) = NaN;
59                      end

60

61                      if EModMicro2(i,j) <= 0
62                          EModMicro2(i,j) = NaN;
63                      end

64

65                  catch
66                      EModMicro1(i,j) = NaN;
67                      EModMicro2(i,j) = NaN;
68                  end
69              end
70          end
71      end

72

73      obj.EModMicro1 = EModMicro1;
74      obj.EModMicro2 = EModMicro2;
75      % Write values into EModMapMicrorheology

76

77      for i=1:obj.NumProfiles
78          for j=1:obj.NumPoints
79              obj.EModMapMicro1(i,j,1) = obj.EModMicro1(obj.Map2List(
```

```matlab
                              i,j));
80                 obj.EModMapMicro2(i,j,1) = obj.EModMicro2(obj.Map2List(
                              i,j));
81             end
82         end
83     end
```

Listing 6: MATLAB Code for E-modulus calculation of microrheology measurements with AFM.

5. Experiment 1

Aim of the first experiment is to determine the viscoelastic properties of individual collagen fibrils from the common digital extensor tendon (CDET) and the superficial digital flexor tendon (SDFT) from 3 years and 18 years old horses, with indentation tests in the frequency domain and evaluation of the data as explained in section 3.6. The macro-scale tendon tissue, from which the individual fibrils were produced, were also used in Kain's master thesis at Vienna University of Technology with the title 'Structural and mechanical evaluation of collagen fibrils from equine tendon: The effect of age, tendon zone and type' and were originally provided by Chavaunne T. Thorpe and Hazel R.C. Screen (Institute of Bioengineering at the Queen Mary University of London). All of the samples are stated to be ethically sourced.

Since there is no standardized testing protocol for frequency dependent indentation with AFM in the literature, it is necessary to look closely at how previous research has performed frequency-dependent measurements to get an idea of building a useful testing protocol before a materials and methods description can be given.

5.1. Practical thoughts on experiments in the frequency domain

The testing protocols from other scientifc studies are summarized below taking into account the different types of biological material tested:

Grant and Twigg [5] used dynamic indentation to examine the viscoelastic properties of two artery types. They opted for a force-controlled testing protocol beginning with a 10 s hold to allow settlement before then undergoing 3 s periods of oscillatory motion at 8, 4, 2, 1, and 0.5 Hz, each separated by a 3 s hold. They had the idea of applying oscillatory frequencies in a decreasing fashion to avoid excessive creep accumulation. They performed a single 10x10 force map over a 32 μm scan size [5]. Before doing dynamic tests they also performed step hold experiments (same to this thesis) with a 3 s hold at maximum load. Elastic modulus was then estimated using a linear elastic Hertzian based theory for a spherical indenter [5].

While Grant and Twigg [5] used an oscillatory force profile as input leading to a corresponding indentation creep as output, Antonovaite et al. applied an indentation-depth controlled profile.

In their experiments they tested treated astrocytes. They kept indentation depth constant for 5 s to allow the material to relax, followed by sinusoidal frequency sweeps that range between 1 Hz and 10 Hz with set amplitude of 0.2 μm [4].

Rother et al., who also controlled their test through indentation, excited the cantilever after a short resting period around the given indentation depth with frequencies ranging from 5 to 200 Hz. They stated that during this procedure, the tip never loses contact with the cell body and noticed that the amplitude of the force response increases considerably with increasing oscillation frequency [3].

Finally, Alcaraz et al. waited 1 min for cell recovery, then they applied low-amplitude (50 nm) sinusoidal oscillations with frequencies ranging from 0.1 to 100 Hz. They pointed out, that cells were probed on the central region of the cell [2].

Although none of the mentioned research examined collagen fibrils, aspects of the collected information about test procedures in the frequency domain are useful for this thesis. First, decision will be made between height- and force-controlled protocol - this is already restricted through the available atomic force microscope, a Nanowizard Ultra Speed A (JPK-Bruker, Berlin), which only allows oscillation segments to be height controlled, while holding segments can be height- or force controlled. This has unsmooth force and indentation signals as a consequence. Force input would be ideal for dynamic testing, to have at least one curve without much noise. To reduce drift, the idea of Grant and Twigg should be adopted, to range the frequencies from high to low and not vice-versa. Also the beginning pause, either force or height controlled, should be held for a few seconds more than the pauses between the segments. The last pause before the retraction turned out to be crucial. The amplitude of the oscillations should be chosen, such that the tip does not loose contact with the material, and on the other hand not to be too small, such that the noise or other effects dominate the signals. The frequencies for collagen fibrils are chosen in a comparable low Hertz range, from 0.1 Hz to 0.5 Hz, because higher frequencies might not leave time for the material to react to the stimulus, thus resembling more simple indentation tests. It is often pointed out in literature that indentation is supposed to hit the central region of the cell. However, in the case of testing fibrils, hitting the fibril turns into a challenge, because of cantilever drift. Therefore it has to be thought about a workaround or a proper way to conduct experiments to receive useful data in the end.

5.2. Materials and Methods

5.2.1. Tissue Samples

In the first indentation experiment, individual collagen fibrils of two types of tendon, of the common digital extensor tendon (CDET) and the superficial digital flexor tendon (SDFT) from a 3-year and a 18-year old horse are tested. These tendons were already characterized regarding structural and mechanical properties in another master thesis at the Institute of Lightweight Design and Structural Biomechanics at Vienna University of Technology [9]. The results of the experiments conducted during this master thesis will be compared to those gathered by Kain in 2017 [9], or more precisely: His results should serve as primary reference to draw conclusions about the viscoelastic properties found with the methods applied in this master thesis.

The equine tendons were stored in a freezer at -80° for about 5 years since Kain [9] used them for his research. Similar to his way of preparing individual collagen fibrils, sections with a thickness of only a few millimeters were cut transversely from the SDFT and CDET tendons using a scalpel. While Kain cut the samples in completely frozen state, they were defrosted nearly fully for this thesis because the paper tissue covering the harvested cross-sections with the former intention of keeping them hydrated by being water soaked ([9]) sticked now to the biological tissue. Afterwards the tendons were put into plastic tubes and back into the freezer, whereas the small tissue sections were directly put into plastic tissue culture dishes filled with distilled water as Kain did in 2017. Collagen fibres were pulled out of the fascicular region of the cross section with the help of sharp tweezers and little amount was put on a glass slide, that was previously rinsed with ethanol and distilled water. Under a microscope the wet collagen fibres could easily be pulled over the glass slide with aforementioned tweezers. When they started to dry, the tissue began to smear on the glass and the collagen fibre package was uncoiled resulting in regions consisting of several single collagen fibrils for nanoindentation analysis. If this uncoiling procedure did not work properly the sharp tweezers were also used to push fascicle tissue apart. Samples were stored in a box at room temperature to the day the experiments were done.

For measuring viscoelastic properties of these collagen fibrils, experiments have to take place in liquid condition at pH 7.4 which is achieved using phosphate buffered saline (PBS). For this reason a PMMA (Polymethamethylacrylate) ring was glued on the glass slide using dental silicon with the tissue sample in the center of it. Now samples are ready for indentation testing.

5.2.2. AFM Nanomechanics

Measurements were carried out at room temperature with a Nanowizard Ultra Speed A (JPK-Bruker, Berlin)) atomic force microscope. The glass slide with the prepared tissue sample was placed under the AFM's optical microscope ($\times$10). A PNP-DB-50 cantilever with a nominal spring constant of 0.48 N/m and tip radius of 10 nm was mounted on the chip holder. This relatively soft cantilever, made for experiments in liquid, was moved to a location on the sample with high fibril density. Following laser alignment, the cantilever was calibrated for laser sensitivity and spring constant ($k \approx 0.2 N/m$) using the contact free method. Then, phosphate buffered saline (PBS) with a pH value of 7.4 was gently added in the PMMA ring around the sample. The sensitivity was calibrated again with the contact-based method after around 20 minutes equilibration time. Before adding the PBS, fibrils were imaged in contact mode, afterwards, to find their present location, another image was taken in QI mode. From this image, vertical areas were chosen for force mapping with enough space left and right to the apparent location of the fibril in case of drift to be sure to receive at least one point on the fibril. (All steps in detail can be found in appendix A.)

Only 10x1 indentations per force map were carried out, a number that seems rather low in comparison to literature were e.g. 32x32 indentations are made [5]. Through force maps, force-displacement curves are measured providing information about the local mechanical response of the fibrils on the previously imaged area, so from this point of view, collecting larger amounts of data make sense. The problem between experiments in time vs. frequency domain are the different duration of one indentation cycle: While it takes approximately 15 s for a simple step hold indentation, an indentation cycle with a reasonable amount of periods per oscillation needs around two minutes. These two minutes summed up will give the cantilever enough time to drift away or allow some other uncontrolled movement. Before and after every modulation force

map, a simple indentation force map was run to verify the location of the fibril. After remaining a longer time period with the cantilever at the same position the drift seemed to decrease. Each indentation had a maximum load of $F_{max} = 1.5$ nN and a tip velocity of 6.5 μm/s. Five individual collagen fibrils were tested from one sample of each tendon type.

The protocol in the **time domain** consisted of an approach of 1.5 s (force-controlled), a force-controlled hold of 10 s and a retraction of 1.5 s (height-controlled). Creep is then to be observed when the indentation increases with time while the force is held constant.

During experiments in the **frequency domain**, the microcantilever is oscillated relative to the sample with a small fixed amplitude (4 nm) at several frequencies, in the case of this experiment at 10 Hz, 1 Hz, 0.5 Hz and 0.1 Hz. After changing the order of frequencies from high to low (compare to [5]) and varying force- and height-controlled pauses (while oscillations could only be height-controlled, compare to 5.1), also assuming the existence of a pause after the last modulation as necessary, the final chosen protocol that gave the best (smoothest) data displays as follows:

1. approach, 1.5 s, force controlled

2. pause, 10 s, height controlled

3. modulation with 10 Hz, 20 periods, height controlled

4. pause, 5 s, height controlled

5. modulation with 1 Hz, 20 periods, height controlled

6. pause, 5 s, height controlled

7. modulation with 0.5 Hz, 10 periods, height controlled

8. pause, 5 s, height controlled

9. modulation with 0.1 Hz, 6 periods, height controlled

10. pause, 5 s, height controlled

11. retract, 1.5 s, height controlled

5.3. Results

The results of the dynamic indentation tests of individual collagen fibrils with AFM are presented and discussed below. Data were collected for 5 fibrils per sample. The 10 indentation points go vertically over the fibril - a circumstance that is due to the duration of the experiment and the occurrence of interference effects that appear during longer measurements. The test window was chosen, such that the fibril occupied as much space as possible to measure many points on the fibril. An already integrated function in the MATLAB program tries to find the apex of a fibril by analyzing the height data. For an precise determination of the apex, however, more data points than recorded in the present measurements would be required. In a first step the mean value and standard deviation were formed from the data at the calculated apex and presented in associated box plots. However, the automatic search for the apex chose points with large phase shifts over 100 °, which are likely to be points not located on the fibril. Because the cantilever does not indent in the glass slide, a phase shift of 180 ° between force and indentation signal and equal amplitudes of force and indentation can be interpreted as a measurement on glass. This leads to the next step, a manual assessment of each fibril. The point that is most likely to be on the fibril and has the most plausible results should be identified. On the one hand, the slope of the retraction curve is used as a parameter: the closer it approaches 1, the more likely it is that glass is measured instead of fibril. A further check is provided by looking at the visualization of force and indentation data together with their associated fit. Signals that were difficult to fit do not provide meaningful results as a consequence. Since the AFM is a very sensitive instrument, collecting the frequency-dependent data proved difficult. A problem with the AFM used in this thesis is decisive for the poor data quality, which unfortunately has a negative impact on the results of this work. The error could not be precisely localized or fixed by the time this thesis was completed. It was observed in the deflection channel and influenced the low-frequency measurements of the experiment through a characteristic frequency band. Already the deflection signal often meandered strongly, which led to indentation signals that were difficult to fit. Discrepancies between data signals and sine fits were particularly evident at the lowest frequencies (0.5 Hz and 0.1 Hz). Measures such as extinguishing the microscope light were used to try to reduce the disruptive influences on the quality of the data, although they could not be fully prevented.

Even though in the end only plausible data are included in the calculation of phase shift, loss tangent, storage and loss modulus (and dynamic modulus E_{dyn}, as measure of material stiffness, which is calculated from storage and loss modulus with $E_{dyn} = \sqrt{E'^2 + E''^2}$), they are scattered widely due to only a few data points being considered. This is why the changes in values within a fibril require attention (see detailed results in appendix C). In order to be able to classify the results even better, some data from the quasi-static experiment preceding the dynamic experiment are also discussed (indentation modulus, slopes from approach and retraction curves and indentation depth, see appendix C) - these can individually be compared with results in the literature.

In the literature, as already depicted in section 2.4, the mechanical properties of horse tendons were mostly determined by tensile tests [32], while Kain tested individual collagen fibrils by nano-indentation with AFM in his master's thesis at the Institute of Lightweight Design and Structural Biomechanics, TU Wien, 2017 [9]. Derived from their function *in vivo*, SDFT can be described as more elastic than CDET. Looking at the results from Kain in fig. 18 this assumption is only reflected by comparing the indentation modulus of the collagen fibrils of old CDET and old SDFT - the lower indentation modulus indicates the more elastically behaviour of the old SDFT fibrils. Findings about age-related changes in equine tendons have been controversial, but suggested that fascicles and interfascicular matrix mainly of SDFT are losing parts of their elastic characteristic and becoming more viscoelastic with age due to changes in composition (see 2.4). From this, the following hypothesis was set up in section 2.4: The indentation (or storage) modulus of SDFT collagen fibrils should be higher in the old sample, while the indentation (or storage) modulus of the CDET collagen fibrils, with a higher value from the beginning, should not show significant changes in the old sample - exactly the opposite can be read from Kain's data (fig. 18). One reason for this is that horse tendons have not yet been tested with AFM for their mechanical properties at the level of individual fibrils. In addition, the mechanical properties vary across the different sublevels of a tendon. Kain explains the difference between the indentation modulus values of a couple hundred MPa (see section 2.4) measured before him and the few MPa indentation modulus measured with the AFM (see fig. 18) by the type of hydration of the sample: while the sample in his and also in this thesis was placed in a PBS bath, the sample in the reference literature was stored in tissues soaked in PBS only before and

after measurement [13]. Perhaps by looking at the frequency-dependent moduli, conclusions can be drawn about the behaviour of horse tendons at higher levels. The first focus, however, is to compare the trend in the data with the results of Kain.
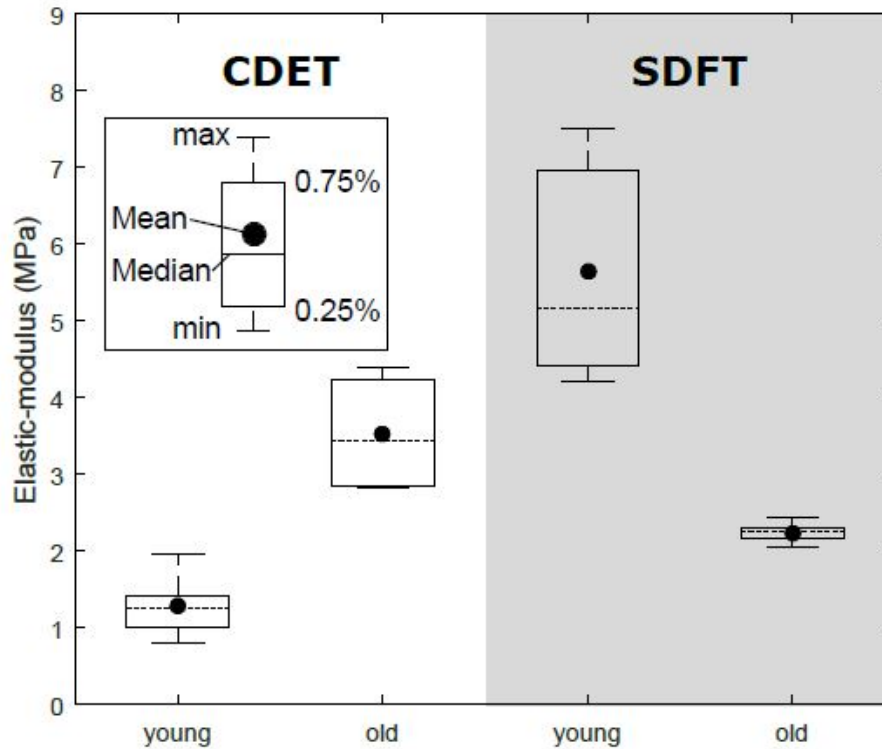
Figure 18: This plot shows the results from Kain which serve as reference for this master thesis (he tested at least six individual collagen fibrils from one sample of each tendon type with force maps over a length of 2.5 μm on the fibril consisting of 16 pixels in this direction [9]). From his nano-indentation experiments on individual collagen fibrils he found fibrils from CDET becoming stiffer with age (increasing indentation modulus) and those from SDFT becoming softer (decreasing indentation modulus). Kain further noticed that fibrils from the young and the old SDFT are both stiffer than fibrils from the young CDET. The mean of the indentation modulus of the young CDET can be found at 1.28 $\pm$ 0.4 MPa. The mean of the young SDFT's indentation modulus is much higher: 5.65 $\pm$ 1.35 MPa. This contrasts with the old samples with 3.53 $\pm$ 0.7 MPa for the mean indentation modulus of the CDET and 2.24 $\pm$ 0.13 MPa for the mean indentation modulus of the SDFT. ([9])

As already mentioned, prior to every dynamic measurement a quasi-static measurement on the same fibril was conducted. The protocol for this quasi-static measurement consisted of the approach, a force controlled hold of 10 s and then the retraction. This measurement was

performed before the dynamic one because it takes much less time and after the dynamic measurement it is even less certain that the same points are being tested due to cantilever drift. The same 10 points were measured, i.e. it was checked that the test window was not shifted and the image on the monitor showed the fibril clearly visible in the center of the window. Too few data points were collected to give an accurate picture of the data, or even to get close to Kain's values (see fig. 18). However, it is helpful if the values of the quasi-static experiment are at least consistent with those of the dynamic measurement - which they are. The values for the indentation modulus and the later calculated storage modulus are of similar magnitude (4-5 MPa). Furthermore, the four different samples do not show clear differences in indentation modulus between them as Kain's data do. Whether the trend, which is very faintly apparent (see fig. 19), corresponds to the trend in Kain's data is not clearly ascertainable. A possible reason for this may just be the manual selection of the point used for the mean calculation. Some fibrils only provide disproportionately high values for indentation or storage modulus (tens of MPa), which were then excluded from the calculation in order not to distort the already sparse picture that the few data provide (see appendix C for all results per fibril for quasi-static and dynamic measurements).

After looking at the results from the quasi-static experiment 1 in table 1 and fig. 19, the results from the frequency-dependent measurement will be discussed in the following order: H169 CDET (young horse), H170 CDET (old horse), H169 SDFT (young horse) and H170 SDFT (old horse).

Quasi-static results				
sample	H169 CDET (young)	H170 CDET (old)	H169 SDFT (young)	H170 SDFT (old)
indentation modulus (MPa)	4.4 ± 1	4.5 ± 0.7	5.4 ± 1.4	4.9 ± 0.7

Table 1: Visible in this table is the mean value with corresponding standard deviation of the indentation modulus of the 4 different samples tested in a quasi-static experiment 1.
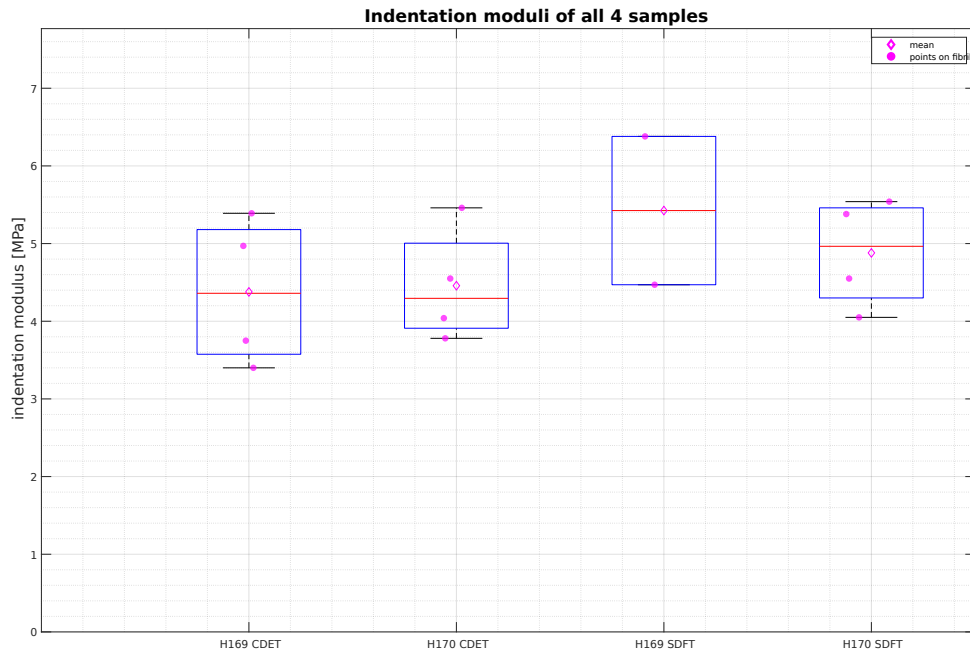
Figure 19: This box plot shows the distribution of the indentation modulus including the calculated mean per 4 samples: H169 CDET, H170 CDET, H169 SDFT, H170 SDFT. Since only a few points are available to create this and the following box plots, the chosen data points are made visible for better understanding. The trend in Kain's results (fig. 18 can be seen in this representation of the data, although this may be skewed by the few biased data points. Overall the differences between the tested specimens of different ages and tendons are small.

H169 CDET (young horse)

According to Kain, young CDET fibrils exhibit the lowest indentation modulus with 1.28 ± 0.4 MPa, are therefore showing the lowest stiffness compared to old CDET and young and old SDFT. This cannot be reproduced with the data from the dynamic experiment. Overall values of storage modulus appear to be lower, compared to the energy-storing tendon type (H169 SDFT), but this can also be due to the fact that only two fibrils (fibril 1 and 3) were used for the mean value calculation, due to bad data quality (for further details see appendix C). Low data quality is also responsible, that from the curves with 0.1 Hz no mean values could be calculated.

H169 CDET (young)				
frequency	0.1 Hz	0.5 Hz	1 Hz	10 Hz
phase shift ϕ (°)	NaN $\pm$ NaN	3.27 ± 0.05	2.6 ± 1	3.66 ± 1.08
loss tangent	NaN $\pm$ NaN	0.0573 ± 0.0011	0.045 ± 0.018	0.064 ± 0.019
storage modulus E' (MPa)	NaN $\pm$ NaN	4.36 ± 0.16	4.63 ± 0.028	5.3 ± 0.3
loss modulus E'' (MPa)	NaN $\pm$ NaN	0.25 ± 0.014	0.21 ± 0.09	0.34 ± 0.08
dynamic modulus E_{dyn} (MPa)	NaN $\pm$ NaN	4.37 ± 0.12	4.64 ± 0.02	5.34 ± 0.23

Table 2: In this table the mean value of the chosen points with the corresponding standard deviation of the 5 tested H169 CDET fibrils are shown.

Figure 20: The four plots show the results of the 5 tested H169 CDET fibrils in the form of box plots. Additionally the mean of the chosen points is displayed. Only 2 of the 5 fibrils are included in the calculation of the mean value and are shown here and connected by lines. The very narrow box at 0.5 Hz shows that these two points almost coincide. With a look at the sine fit plots 30 and 33 this circumstance can be explained: Both indentation signals at 0.5 Hz do meander. In comparison to the signal at 0.5 Hz the signals at 1 Hz and 10 Hz are quite smooth, leading to a decreasing phase shift from 0.5 Hz to 1 Hz. It also makes sense that the difference in the results is smaller between 0.5 Hz and 1 Hz than between 1 Hz and 10 Hz. With increasing frequency, the storage modulus also increases. The blue line connecting the points of fibril 1 indicates less variation in data quality between points of different frequencies.

H170 CDET (old horse)

Kain finds that the indentation modulus values for the old CDET sample are higher than the ones from the young sample (see fig. 18). H170 CDET is the only sample where the storage modulus results seems to decrease with increasing frequency - however, due to the lack of statistics, no reliable statement can be made. The mean values shown in table 3 are calculated from the fibril 2 (orange line) and fibril 3 (yellow line) data sets, whereas the only plausible data for 0.1 Hz came from fibril 3. In this special case the signal can approximately be fitted by a sine - this is visible in the sine fit plot 42. The boxes in fig. 21 are partly so large because the values of the two fibrils are not close to each other. Fibril 2 exhibits the same phase shift at 0.5 Hz and 1 Hz, which is the reason for the decrease in storage and in loss modulus in this section. Fibril 3 delivered at 1 Hz and 10 Hz results comparable to some data of H170 SDFT with similar very small phase shifts, which are assumed to indicate good data quality. However, why the storage modulus decreases with increasing frequency is not clear. The points located on fibrils 1 to 5 are described in detail in appendix C.

H170 CDET (old)				
frequency	0.1 Hz	0.5 Hz	1 Hz	10 Hz
phase shift ϕ (°)	1.98 ± 0	3 ± 0.8	2.3 ± 1.9	3.2 ± 2.05
loss tangent	0.035 ± 0	0.053 ± 0.015	0.04 ± 0.03	0.06 ± 0.04
storage modulus E' (MPa)	5.41 ± 0	4.5 ± 0.4	4.1 ± 0.8	4.1 ± 0.7
loss modulus E'' (MPa)	0.19 ± 0	0.23 ± 0.05	0.15 ± 0.11	0.2 ± 0.1
dynamic modulus E_{dyn} (MPa)	5.41 ± 0	4.48 ± 0.28	4.13 ± 0.53	4.12 ± 0.48

Table 3: In this table the mean value of the chosen points with the corresponding standard deviation of the tested H170 CDET fibrils are visible.

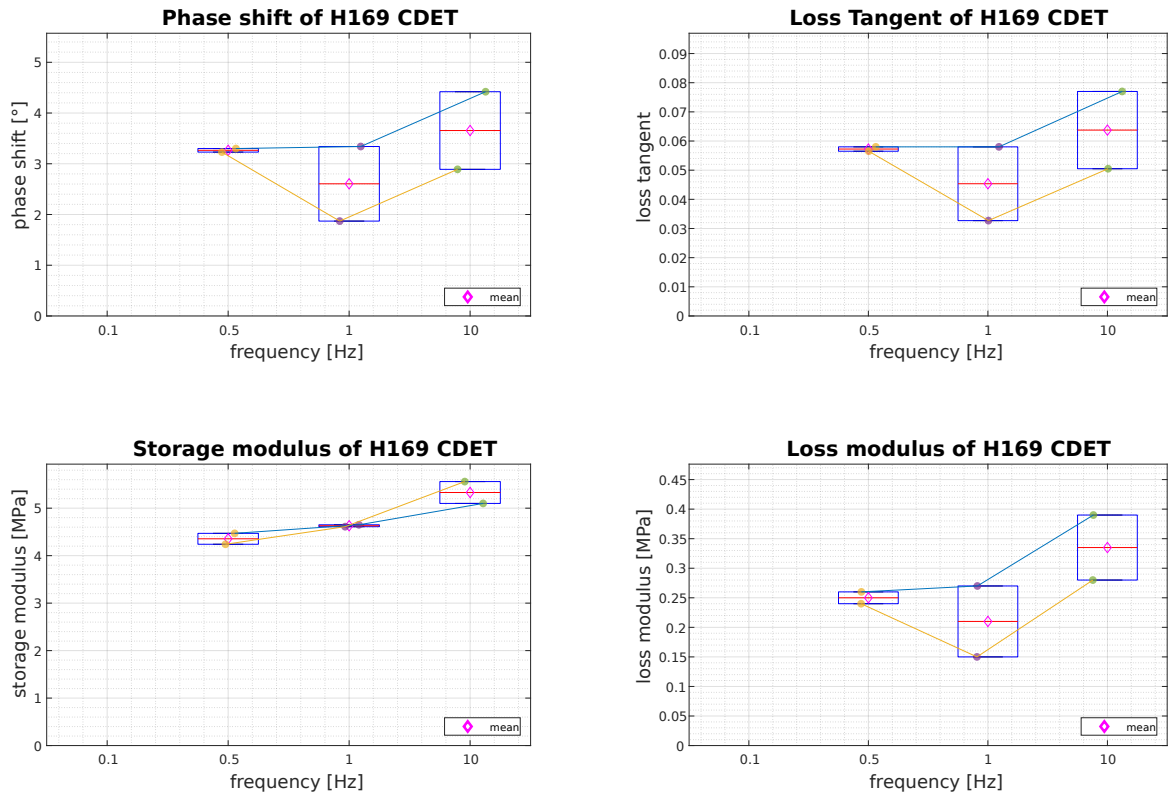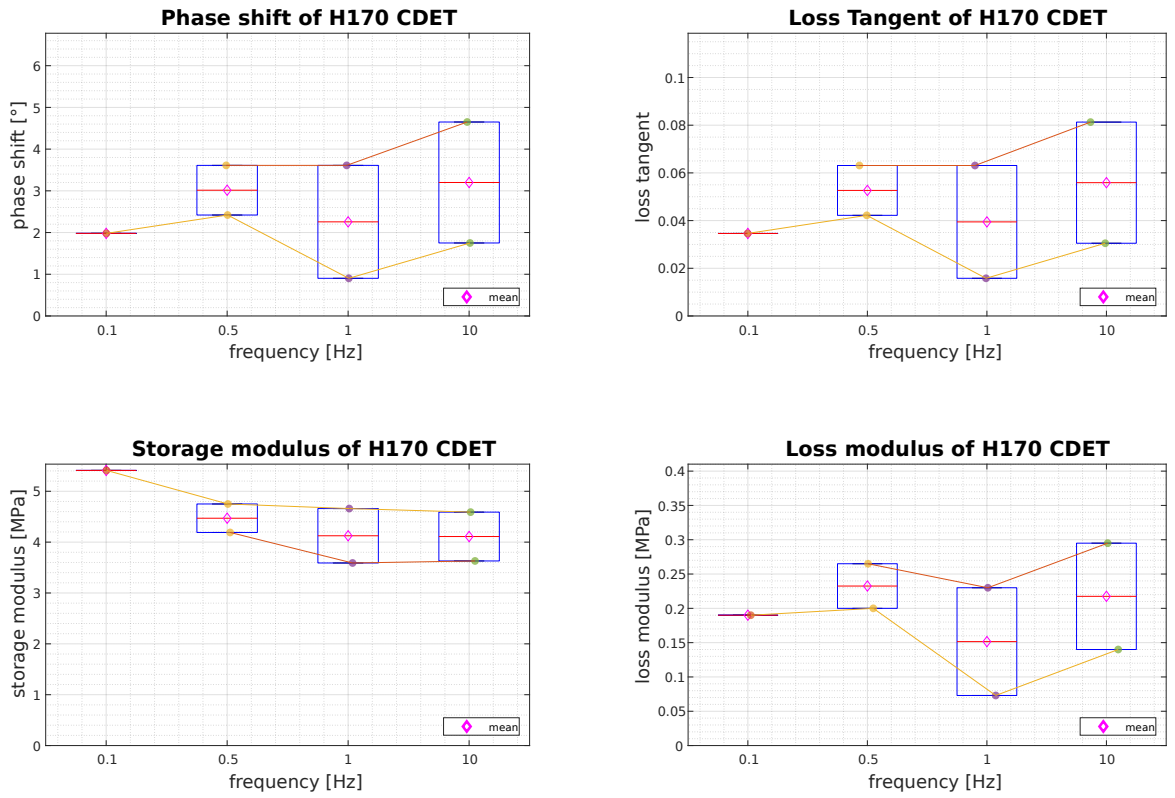Figure 21: The four plots show the results of the tested H170 CDET fibrils in the form of box plots. Additionally the mean of the chosen points is displayed.

H169 SDFT (young horse)

The first thing to notice when looking at the young SDFT fibril data, are seemingly similar storage modulus values compared to the indentation modulus values of Kain in fig. 18. However, the standard deviation for the results is high at 0.5 Hz and 1 Hz, indicating problematic data quality. Furthermore, the slightly higher phase shifts compared to the other samples point to problems with data quality (experience with other samples show phase shifts between 0° and 3° or 4° for good data quality). In addition, the value for the storage modulus appears to be smaller for 10 Hz than for 1 Hz or 0.5 Hz. The storage modulus values of fibril 1 (blue line) and fibril 5 (green line) at 10 Hz are close to each other, which is also visible in the box plot 22. This leads to the assumption that the data quality at 10 Hz is better and more representative of the sample than the values at the lower frequencies. The problems become apparent in the following representations of the force and indentation data with their respective fit at the selected points of a fibril (see fig. 46 - 52). The indentation data at 0.1 Hz from none of the fibrils can be approximated by a sinusoidal fit. Overall fibril 1 provides the best fitted data (10 Hz, 1 Hz, 0.5 Hz).

H169 SDFT (young)				
frequency	0.1 Hz	0.5 Hz	1 Hz	10 Hz
phase shift ϕ (°)	NaN $\pm$ NaN	7.3 $\pm$ 2.6	7.1 $\pm$ 2.4	8 $\pm$ 1
loss tangent	NaN $\pm$ NaN	0.13 $\pm$ 0.05	0.12 $\pm$ 0.04	0.139 $\pm$ 0.018
storage modulus E' (MPa)	NaN $\pm$ NaN	6 $\pm$ 2.2	6.3 $\pm$ 1.6	4.83 $\pm$ 0.08
loss modulus E'' (MPa)	NaN $\pm$ NaN	0.8 $\pm$ 0.4	0.8 $\pm$ 0.3	0.7 $\pm$ 0.1
dynamic modulus E_{dyn} (MPa)	NaN $\pm$ NaN	6.78 $\pm$ 1.88	6.41 $\pm$ 1.59	4.88 $\pm$ 0.07

Table 4: In this table the mean value of the chosen points with the corresponding standard deviation of the tested H169 SDFT fibrils are visible.

Figure 22: The four plots show the results of the tested H169 SDFT fibrils in form of box plots. Additionally the mean of the chosen points is displayed. The blue line connects the points of fibril 1, the green one of fibril 5 and the yellow one fibril 3. Fibril 1 shows the expected trend: Increasing results with increasing frequency, and a stronger increase between 1 Hz and 10 Hz. Overall, the H169 SDFT results are severely affected by data quality.

73

H170 SDFT (old horse)

Compared to the younger sample, the data quality from the older sample is better overall, even if there are dropouts, especially in the 0.1 Hz range, which is why the results from 0.1 Hz are not displayed in fig. 23, but are shown in appendix C. It is noticeable that 1 Hz gives the most useful results (4 of 5 fibrils), followed by 10 Hz (3 of 5 fibrils), 0.5 Hz (2 of 5 fibrils) and finally 0.1 Hz. This becomes comprehensible through the data points drawn in the box plots 23, from which the mean values are calculated. Compared to high phase shift values of H169 SDFT the force curve of H170 SDFT is only a fraction of a degree ahead of the indentation curve - this could be explained with better data quality. This can also be seen from the similar mean values for the storage modulus and the much smaller standard deviation.

As a consequence of different data quality it is difficult to read a trend from comparing the storage modulus values of young and old sample. From Kain's findings H169 SDFT fibrils posses higher indentation modulus than H170 SDFT fibrils, which cannot be confirmed with certainty. Furthermore, 5 MPa is double Kain's indentation modulus value for H170 SDFT fibrils (2.24 ± 0.13 MPa, [9]). The calculated mean values follow a clear upward trend with increasing frequency, which is noticeable in the individual fibrils above all in the phase shift, loss tangent and loss modulus, but not always in the storage modulus (see appendix C).

H170 SDFT (old)				
frequency	0.1 Hz	0.5 Hz	1 Hz	10 Hz
phase shift ϕ (°)	NaN $\pm$ NaN	0.58 $\pm$ 0.08	0.83 $\pm$ 0.06	1.78 $\pm$ 0.27
loss tangent	NaN $\pm$ NaN	0.0101 $\pm$ 0.0014	0.0146 $\pm$ 0.0011	0.031 $\pm$ 0.005
storage modulus E$'$ (MPa)	NaN $\pm$ NaN	5.1 $\pm$ 0.4	5.6 $\pm$ 0.9	5.8 $\pm$ 0.8
loss modulus E$''$ (MPa)	NaN $\pm$ NaN	0.049 $\pm$ 0.005	0.082 $\pm$ 0.016	0.18 $\pm$ 0.04
dynamic modulus E$_{dyn}$ (MPa)	NaN $\pm$ NaN	5.13 $\pm$ 0.28	5.67 $\pm$ 0.87	5.76 $\pm$ 0.65

Table 5: In this table the mean value of the chosen points with the corresponding standard deviation of the tested H170 SDFT fibrils are visible. Although the mean values for the storage modulus show a slight upward trend, they are very close together. This speaks for good data quality. The viscous part (loss modulus) is greatest at the highest storage modulus value.
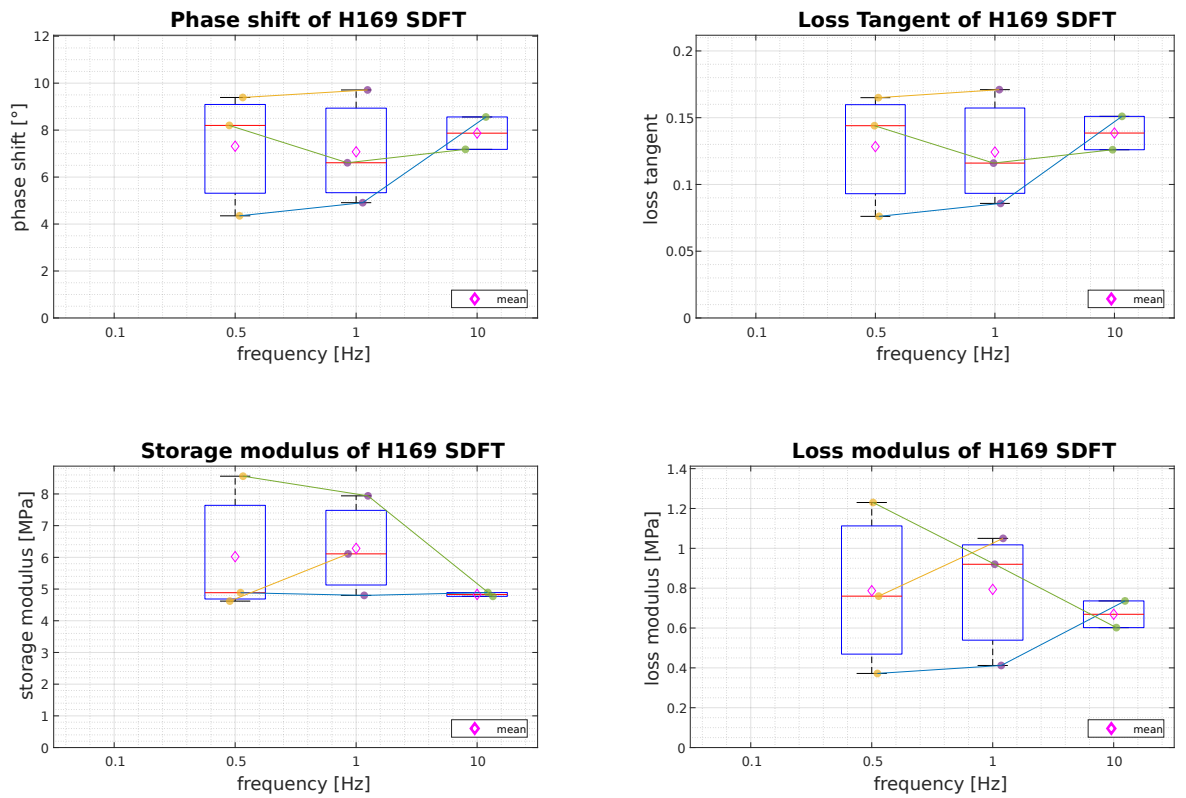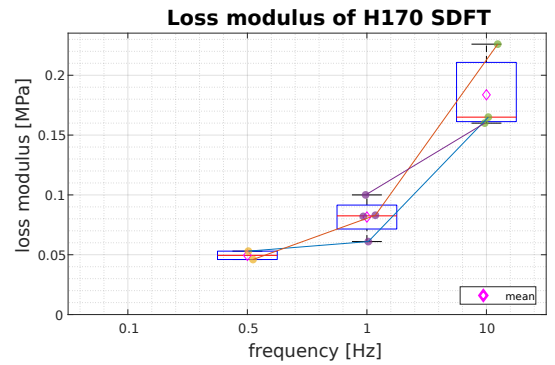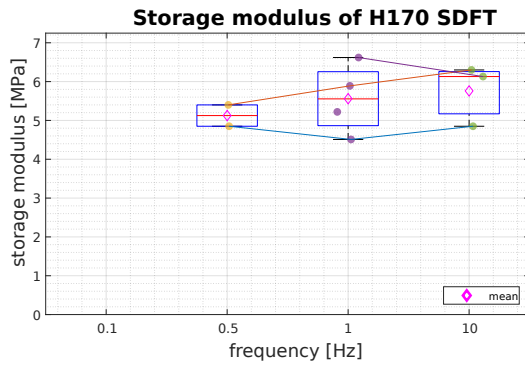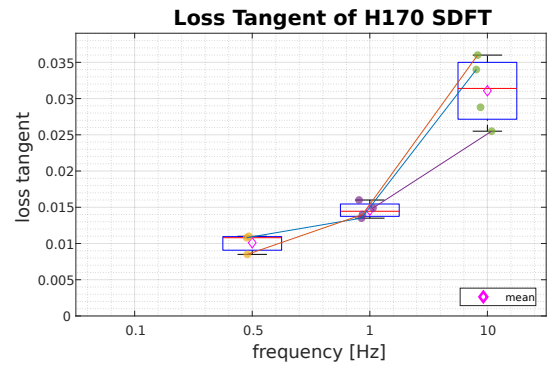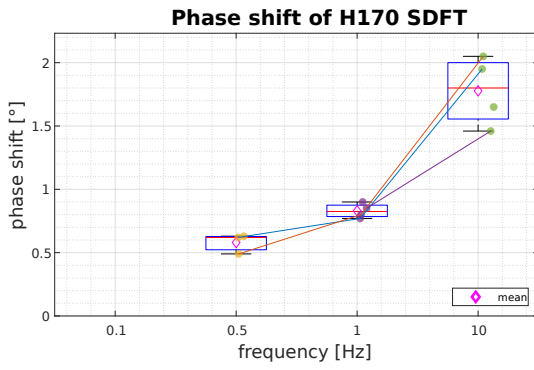
Figure 23: The four plots show the results of the tested H170 SDFT fibrils in form of box plots. Additionally the mean of the chosen points is displayed. While the results for phase shift, loss tangent und loss modulus increase with frequency, this is not always the case for the storage modulus, as clearly visible. The storage modulus of fibril 3 (orange line) is increasing nearly linearly - this results mainly from a good overlapping of raw indentation data and sine fit at 0.5 Hz, see in fig. 55. Conversely, the storage modulus of fibril 1 (blue line) decreases between 0.5 Hz and 1 Hz. These plots also show nicely that the values for 0.5 Hz and 1 Hz are closer together than 1 Hz and 10 Hz.

Conclusion

To summarize the first experiment, the results of the frequency-dependent measurements for all samples should be compared. The sample-dependent differences in phase shift, loss tangent, storage modulus and loss modulus for each frequency (0.1 Hz, 0.5 Hz, 1 Hz and 10 Hz) are visualized in box plots (fig. 24 - 27).

All parameters measured (phase shift, loss tangent, storage and loss modulus and the dynamic modulus) are indicators of the elasticity or viscoelasticity of a material. A phase shift close to zero indicates an almost elastic behaviour. Just like the loss tangent, which is the quotient of storage modulus and loss modulus (see section 3.6). If the loss modulus becomes zero, the material behaves elastically. However, if the storage modulus does not exist, the material behaves viscous.

For each fibril tested, a point, that had a high probability of lying on the fibril, was selected manually. For various reasons and for some fibrils, no point could be chosen, so that often only 2 out of 5 fibrils contributed to the mean value calculation. Exclusion criteria were too high phase shifts (nearly 180°), very similar values for force and indentation amplitude (close to 1) - either an indicator that the glass slide was indented or that the data quality was too bad due to difficulties with the AFM. High storage modulus values (above 20 MPa) were also excluded, which were associated with low indentation depths (below 10 nm). The discussion of plausible points can be found in appendix C.

The data at 0.1 Hz are excluded in most cases from consideration, since a closer look revealed that these unfortunately could not usually be approximated by a sine wave. In a next experiment, this lowest frequency should no longer be repeated. The excitation with the frequencies 0.5 Hz, 1 Hz and 10 Hz led to very low phase shifts and loss tangent values. Overall all samples indicate a highly elastic nature of the collagen fibrils, with storage modulus values a couple MPa higher than loss modulus values. It cannot be said so easily that the trend in Kain's data (fig. 18) is reflected in the results from frequency-dependent experiments presented here. The reason for this may be the small number of samples, which is not sufficient for a statistical evaluation. The following findings are therefore vague attempts at interpreting the available data: Overall differences between the four samples were not particularly evident. The storage modulus usually

is in a range of 4-5 MPa and seems to increase with increasing frequency with an exception of H170 CDET. However, since the experiment starts at 10 Hz, this also means that the storage modulus decreases as the test progresses. So the behaviour of the collagen fibrils seems to become less stiff over time. Often one could also see that the values of 0.5 Hz and 1 Hz are closer together than 1 Hz and 10 Hz. Larger differences in data quality may be noticeable, for example H170 SDFT and one fibril of H170 CDET show phase shifts of almost zero, while in the other plausible cases the phase shift ranges between 3-4° or around 8° for most H169 SDFT fibrils due to really bad data quality (see fig. 24). In the previous analyses, an upward trend in phase shift with increasing frequency was often observed, which agrees with the results of Grant et al., who also did frequency-dependent AFM indentation measurements with frequencies from 0.1 Hz to 2 Hz [10].

The problem that can already be seen here, compared to simple indentation experiments, is that more uncertainties are introduced by more complicated data and additional fitting steps as a result of more complex experiments. Perhaps the disadvantages of a simple indentation measurement, namely the neglect of viscoelasticity due to linear elastic assumptions for the Oliver Pharr calculation of the indentation modulus, are compensated in dynamic measurements by a more difficult acquisition of the data, the longer experiment duration which leads to less (usable) data. In addition, the mathematical effort is higher, which again only represents an approximation. Nonetheless, the results of this experiment provide interesting prospects that will be further enhanced by more data acquisition.
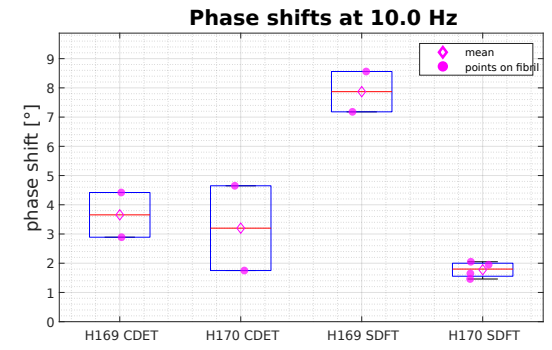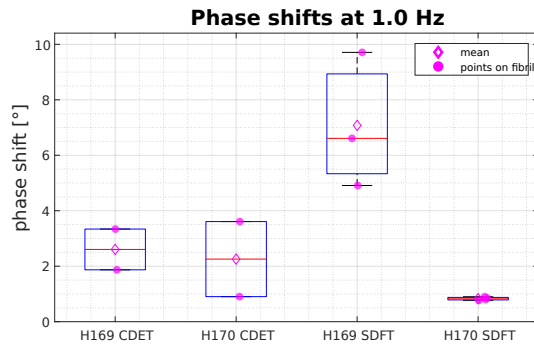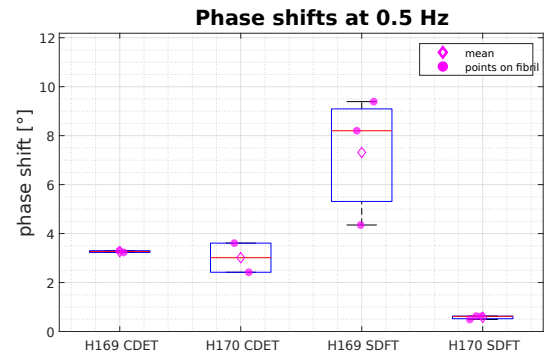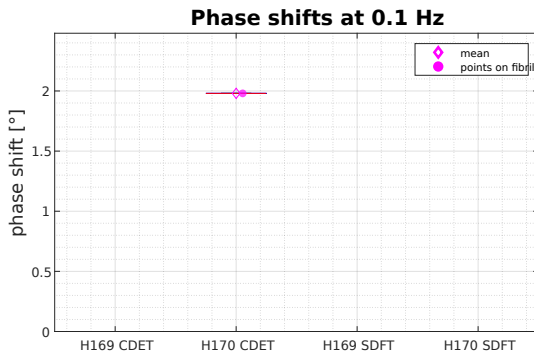
Figure 24: The four plots show the phase shifts at all frequencies for every sample. Additionally the data points and the mean calculated out of them are displayed. H170 SDFT is immediately noticeable with consistently very low phase shifts, which are approximately between 0° and 2° for each frequency - this was justified with good data quality. It also indicates an almost purely elastic material behaviour. Its young counterpart H169 SDFT is the opposite, with comparatively very high phase shifts that can be traced back to difficult measurements. It lacks certainty to say that H169 SDFT behaves more viscoelastic. Both young and old CDET samples show a similar phase shift at all frequencies (2-4 MPa). The increasing phase shift with increasing frequency is not clearly visible here, which also indicates increasingly elastic material behaviour with the duration of the measurement.
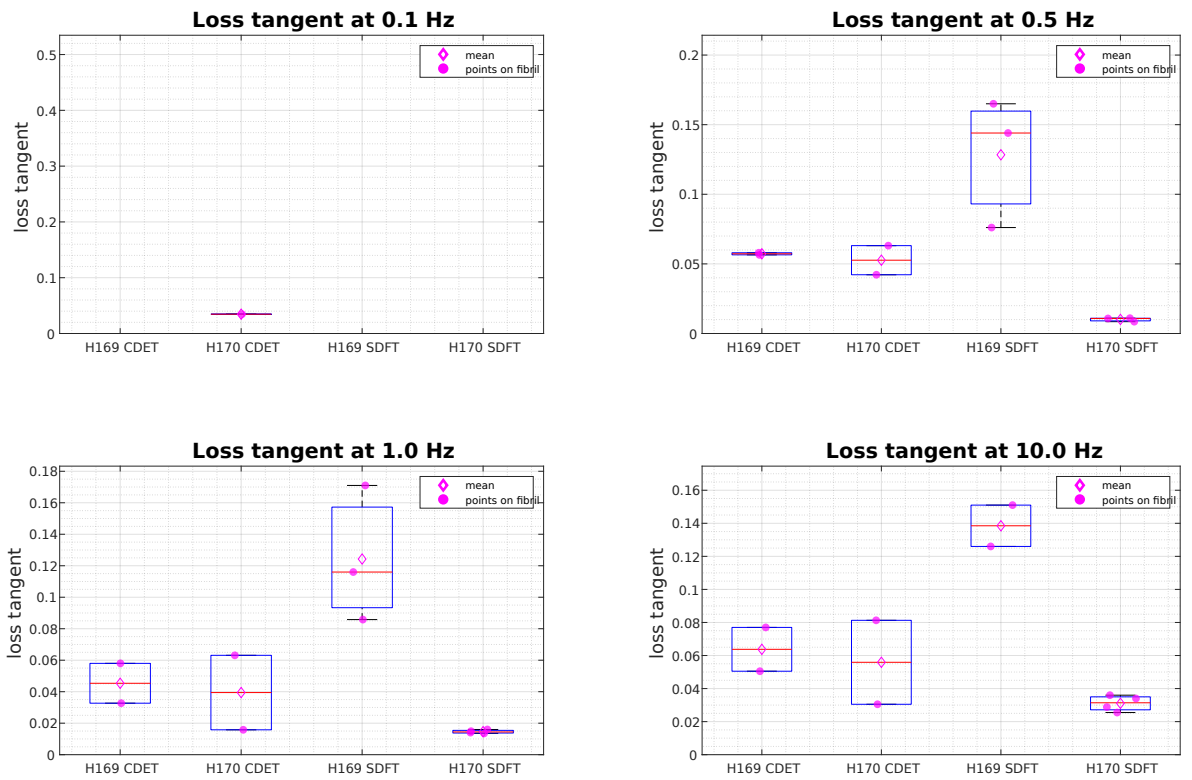
Figure 25: The four plots show the loss tangent at all frequencies for every sample. Additionally the data points and the mean calculated out of them are displayed. Since the loss tangent is calculated using the phase shift, the picture is the same here as in fig. 24. In almost all data points the loss tangent is below 0.1, which indicates a very elastic behaviour of the collagen fibrils.
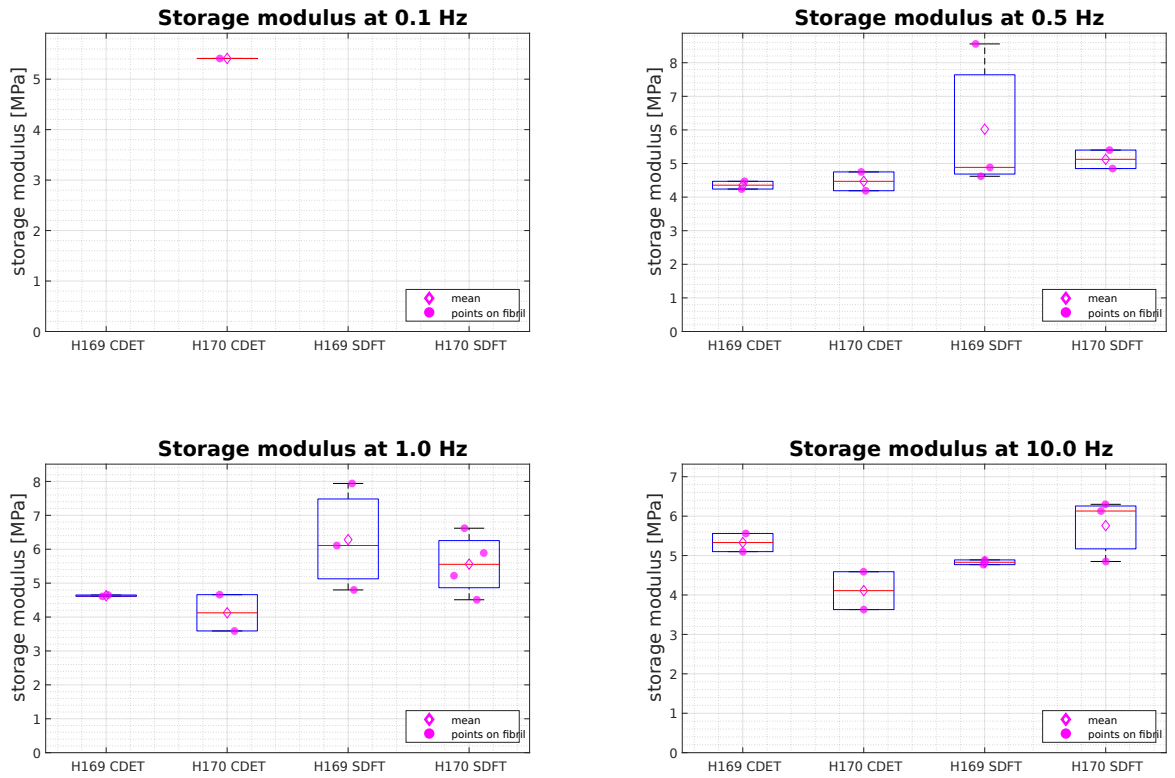
Figure 26: The four plots show the storage modulus at all frequencies for every sample. Additionally the data points and the mean calculated out of them are displayed. The storage modulus of H169 SDFT is widely distributed and appears to decrease with increasing frequency, but this is probably just an artifact. It is more likely that a new experiment with better data will result in values between 4 and 5 MPa. As predicted, the storage modulus of the H170 SDFT sample increases with increasing frequency. If the data are to be trusted, H170 SDFT has the highest storage modulus values of any sample. This could mean that the collagen fibrils of old energy-storing equine tendons are stiffer than young ones and also stiffer than the collagen fibrils of young and old positional tendon. This would correspond to the behavior of the tendon at the macro level, but does not coincide with Kain's results [9]. Storage modulus values of H169 CDET and H170 CDET range very similar between 4 and 5 MPa - no statement can be made as to whether the collagen fibrils lose elasticity with increasing age. The values also agree quite well with the results from the previous quasi-static measurement (see table 1), where there is also no major difference in the indentation modulus between the different samples in terms of age and functionality.
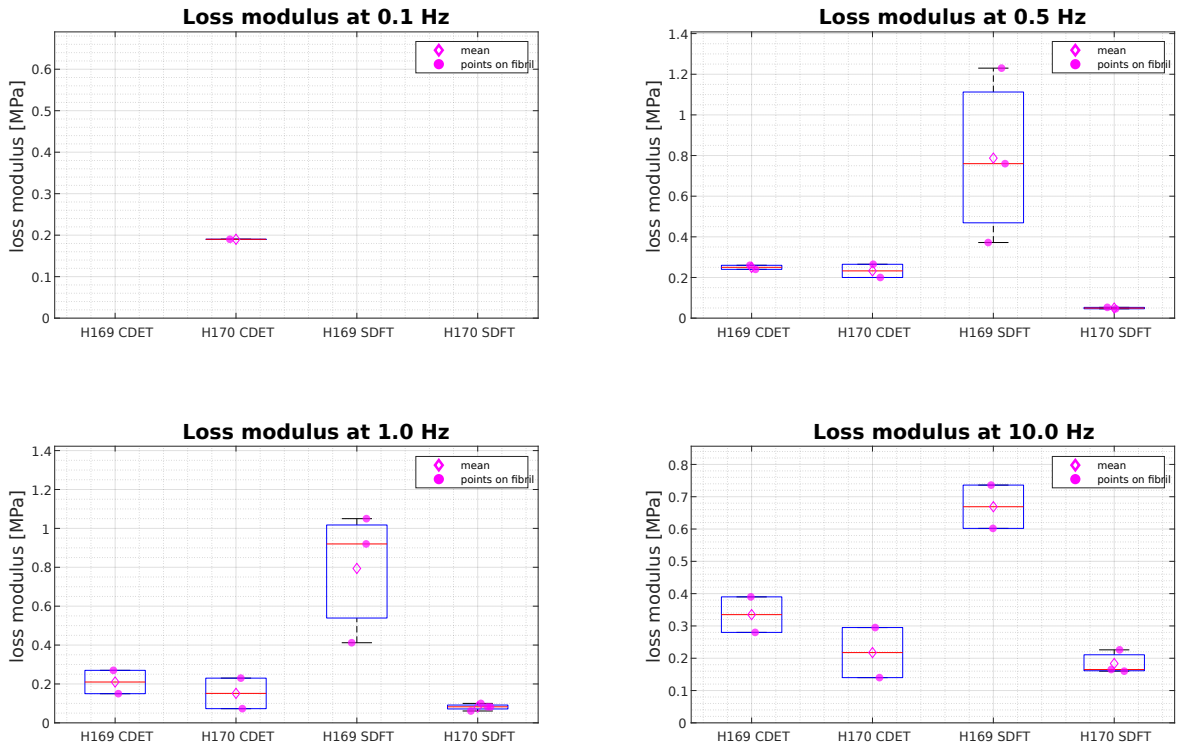
Figure 27: The four plots show the loss modulus at all frequencies for every sample. Additionally the data points and the mean calculated out of them are displayed. What was already evident from the low phase shift continues logically when considering the loss modulus: The values for H170 SDFT are close to zero, which in turn indicates a very elastic behaviour, which decreases slightly with increasing frequency. The loss modulus values for H169 CDET and H170 CDET are around 0.2 MPa and are noticeably a bit higher at 10 Hz than at the lower frequencies. While the other samples do not exceed loss modulus values of 0.4 MPa, collagen fibrils of H169 SDFT exhibt much higher values (nearly or around 1 MPa) - these outliers can be attributed to the poor data quality.

6. Experiment 2

In the second experiment, the test methods of the first experiment are readjusted based on its success. To produce a marked change in behaviour, the aim is now to analyze the effects of AGE cross-links on the mechanics of collagen fibrils in horse tendons. For this, the young samples of SDFT and CDET are exposed to a chemical glycation process. The results of the following dynamic indentation tests are then compared with the results of the old samples from experiment 1. Before going into the details of materials and methods, a few considerations should be made with the attention that there are no known data on chemical glycation in horse tendons in the present literature.

6.1. Practical thoughts on chemically- induced glycation

As shortly depicted in section 2.2, AGEs are non-enzymatic cross-links between collagen fibrils that increase with age and disease. They are formed by reactions of free amino groups with sugars - a process called glycation. In order to better understand how AGEs influence the mechanical qualities of a biological tissue, tissue samples are chemically treated in experiments, such that AGEs are formed rapidly:

To examine what impact AGEs have on hydration and mechanical properties of collagen fibrils, a study treated collagen samples from a mouse tail tendon with ribose which will result in the formation of pentosidone, a naturally ocurring AGE in collagen fibrils [15]. They employed both Brillouin light scattering and atomic force microscopy experiments to find that AGEs can lead to increased hydration, swelling and reduced transverse stiffness. Another study measured tensile mechanics of individual fibrils from rat tendon taking into account the animal's maturity and functionally different tendons (tail vs. Achilles tendons). While age and tissue type seemingly had no significant effect on fibril mechanics, methylglyoxal (MGO) treated fibrils showed increased strength and stiffness but without inducing brittleness as often suggested to be related with AGEs [16]. In his master's thesis, Manuel Rufin treats individual collagen fibrils of mouse tail tendons also with MGO and finds a significantly higher indentation modulus compared to his control groups [53]. Methylglyoxal is a highly reactive by-product of metabolism that binds

to proteins, lipids and DNA to form AGEs [54]. If the samples are treated *in vitro* with MGO, AGEs can be rapidly generated in type-I collagen fibrils [55]. D-ribose, on the other hand, takes days/weeks before glycation is detectable. For this reason, samples of this master thesis are subjected to the chemically induced glycation process with MGO.

6.2. Materials and Methods

6.2.1. Tissue Samples

In the second indentation experiment individual collagen fibrils of the common digital extensor tendon (CDET) and the superficial digital flexor tendon (SDFT) from the younger (3 year old) horse are tested. Both samples are the same as used in experiment 1 (see section 5.2.1). After conducting experiments with a slightly modified testing protocol, both samples undergo MGO treatment. The solution used for glycation consisted of 5 mM/L EDTA (Ethylenediaminetetraacetic Acid) and 20 mM/L MGO (Methylglyoxal) dissolved in 10 mM/L PBS (Phosphate Buffered Saline). The glass slide with the respective sample is immersed in the solution and left in a temperature-controlled incubation chamber at 34°C for 4 hours. The incubation temperature of 34°C is an estimate for typical physiological tendon temperature [53], as the typical horse body temperature is between 36°C and 38°C.

6.2.2. AFM Nanomechanics

Dynamic indentation experiments are first conducted in PBS on 4 selected fibrils (day 1), before undergoing the 4-hour-long MGO treatment (day 2). The exact same fibrils are found and tested again in PBS (day 3). The testing protocol is slightly modified from experiment 1 due to non-sinusoidal output signals at the lowest frequency, 0.1 Hz. While the lowest frequency is left out this time, testing is also done at 5 Hz. This change results in a shorter experiment duration.

1. approach, 1.5 s, force controlled

2. pause, 10 s, height controlled

3. modulation with 10 Hz, 20 periods, height controlled

4. pause, 5 s, height controlled

5. modulation with 5 Hz, 20 periods, height controlled

6. pause, 5 s, height controlled

7. modulation with 1 Hz, 20 periods, height controlled

8. pause, 5 s, height controlled

9. modulation with 0.5 Hz, 10 periods, height controlled

10. pause, 5 s, height controlled

11. retract, 1.5 s, height controlled

Like in the first experiment, a scanning area of 10x1 pixels was chosen, so that the cantilever will indent on glass, fibril and then glass again. The applied indentation load was again 1.5 nN in all experiments.

6.3. Results

Exactly the same four fibrils were measured before and after glycation. As in Experiment 1, a quasi-static measurement was carried out at the same point before each dynamic measurement. An expected result of this second experiment would be higher values for the indentation modulus after treating the young SDFT and CDET samples with MGO.

Unfortunately, the frequency-dependent data generated in this second experiment is unusable. An exception is the third fibril of the MGO treated sample H169 CDET, which is discussed in table 7. Looking at the slopes of the retraction curves, the very high values (mostly around 1) are noticeable, which is an indicator that only glass and not fibril was measured. In some cases it is also evident in the sine fit plots when the indentation curve is obviously 180° out of phase with the force curve. This can be looked up in detail in appendix C. The fact that in the other cases the slopes are still close to 1 and the indentation data are very noisy must be due to problems when recording the data. At this point, the existing problem with the AFM used is pointed out once again. During the experiment, however, it appeared that there were points lying on the fibril. The position of the fibril in the scan window was always checked with a simple indentation measurement before and after the frequency-dependent measurement. On the monitor of the JPK software deflection signals appeared sinusoidal. The problem lays in the calculated indentation data, which is surprisingly noisy. It is striking that no meaningful results were obtained on four different measurement days. Therefore the new measurements (before the MGO treatment) with slightly modified dynamic measurement protocol cannot be directly compared with the results from experiment 1, despite the same samples were tested.

Despite this poor starting position, experiment 2 provides valuable insights. The quasi-static measurements allow cautious statements to be made about the change in collagen fibrils after a glycation process with MGO. Caution is therefore required because, as with the other experiments, only 10 points were indented over a fibril and 1 plausible one was selected from them, which does not lead to a large data yield. The indentation modulus values for the samples treated with MGO are significantly higher than in the untreated state - see table 6. This corresponds to the expectation that an increase in AGEs by MGO stiffens the material. Highly interesting is the comparison with values from experiment 1 in fig. 29. First to notice is the

difference in indentation modulus between the same sample of H169 CDET and H169 SDFT being measured in both experiments. This can be explained by the few selected data points. Even if the differences between young and old samples are not so distinct (like mentioned in section 2.4, [32], [12]) it seems that the young collagen fibrils after glycation are even stiffer than the collagen fibrils of the old horse tendons - this would coincide with findings shared in section 6.1 by Svensson et al. [16] and Rufin [53].

Quasi-static results				
sample	H169 CDET (young)	H169 CDET with MGO (young)	H169 SDFT (young)	H169 SDFT with MGO (young)
indentation modulus (MPa)	6 ± 0.9	7.6 ± 1.9	4.7 ± 0.7	7.3 ± 1.4

Table 6: Visible in this table is the mean value with corresponding standard deviation of the indentation modulus of the 4 different samples tested in a quasi-static experiment 2.
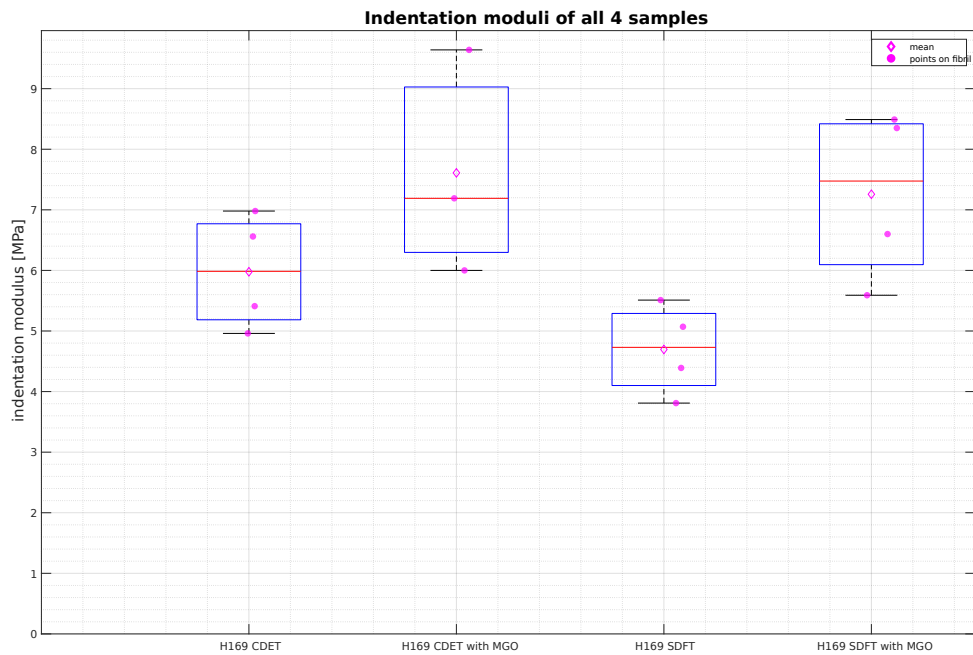
Figure 28: The box plot shows the distribution of the indentation modulus including the calculated mean per 4 samples: H169 CDET, H169 CDET with MGO, H169 SDFT, H169 SDFT with MGO. According to Kain, young SDFT collagen fibrils are stiffer than young CDET collagen fibrils - the opposite is visible in this figure.
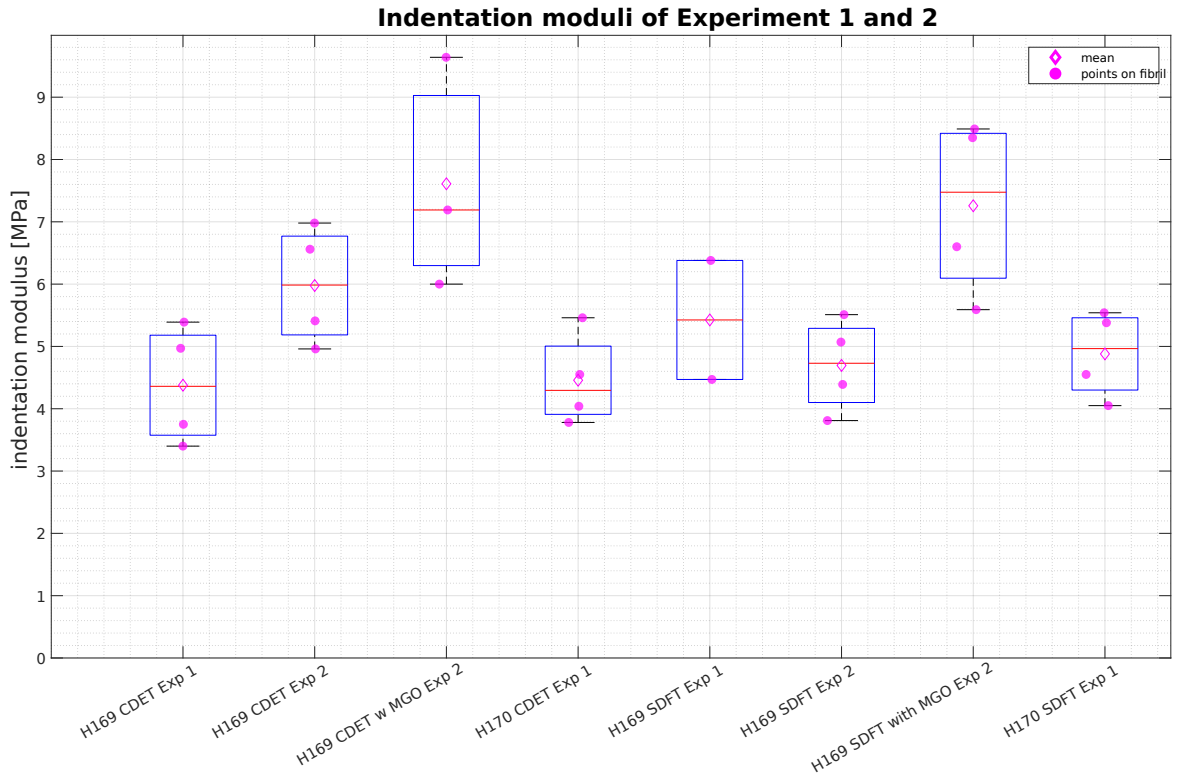
Figure 29: The box plot compares the indentation moduli of all samples that underwent quasi-static indentation with AFM in experiment 1 and experiment 2. The young samples treated with MGO exhibit significantly larger values compared to the untreated young samples, but also compared to the old samples.

H169 CDET with MGO (young)				
frequency	0.5 Hz	1 Hz	5 Hz	10 Hz
phase shift ϕ (°)	2	3.1	3.3	4.7
loss tangent	0.036	0.054	0.058	0.083
storage modulus E′ (MPa)	6.3	8.3	7.5	7.2
loss modulus E″ (MPa)	0.22	0.45	0.44	0.6
dynamic modulus E_{dyn} (MPa)	6.3	8.31	7.51	7.22

Table 7: In this table the material response of fibril 3 of H169 CDET with MGO at the most plausible selected point is visible (see also data and fit in fig. 63). In the absence of alternatives, this result must be representative of the H169 CDET sample treated with MGO. The values of storage and loss modulus seem higher compared with the mean values of H169 CDET in experiment 1 (see table 2). Additionally they are higher than the values of H70 CDET in experiment 1 (see table 3). Since this data set alone shows a similarity to the results of the quasi-static experiment 2, it suggests that the same pattern can be seen in the frequency-dependent results. Of course, in order to be able to evaluate the subtleties, i.e. how the results change over the frequency, as in experiment 1, a problem-free experiment with AFM must be guaranteed.

H169 CDET with MGO (young)				
frequency	0.5 Hz	1 Hz	5 Hz	10 Hz
dynamic modulus E_{dyn} (MPa)	6.3	8.31	7.51	7.22
H169 CDET from Experiment 1 (young)				
frequency	0.5 Hz	1 Hz		10 Hz
dynamic modulus E_{dyn} (MPa)	4.37 ± 0.12	4.64 ± 0.02		5.34 ± 0.23
H170 CDET from Experiment 1 (old)				
frequency	0.5 Hz	1 Hz		10 Hz
dynamic modulus E_{dyn} (MPa)	4.48 ± 0.28	4.13 ± 0.53		4.12 ± 0.48

Table 8: In this table the dynamic moduli of H169 CDET with MGO (experiment 2) are set against the dynamic moduli of H169 CDET (see full table 2) and H170 CDET (see table 2) (both from experiment 1). It should be emphasized that these are not the same fibrils tested. The results for 0.1 Hz were omitted from the data from experiment 1 - the frequency 5 Hz was only measured in the second experiment. The perceived stiffness of the fibrils is higher after treatment with MGO than before.

7. Findings & Conclusion

The aim of this work was to establish and carry out frequency-dependent indentation experiments with AFM in order to test the mechanical properties of collagen fibrils, in particular of two types of tendons of a young and an old horse. Subsequently, the young samples were subjected to a non-enzymatic glycation process in order to induce marked change in chemistry and to increase the number of covalent cross-links (AGEs).

It is emphasized that new ground was broken in many respects: First, developing the framework of frequency-dependent indentation experiments with AFM. Second, using the aforementioned testing method to characterize the viscoelastic properties of collagen fibrils from horse tendons depending on tendon type and age. Additionally, and thirdly, subjecting young collagen fibrils from horse tendons to a chemically induced glycation process to analyze the effect of structural change on mechanical properties with this new testing manner.

Deciding on an adequate AFM measurement protocol required a few attempts. It started with frequencies around 100 Hz and an amplitude of 10 nm. A PhD-candidate at the institute, Mathis Nalbach, did dynamic tensile tests on collagen fibrils with a low frequency range (paper in preparation), which inspired to use a similar frequency range: 1 Hz to 0.1 Hz with an amplitude of 4 nm. The low frequencies on the other hand proved difficult as they required many periods, which led to a long experiment duration, during which uncontrollable factors (e.g. thermal drift of the cantilever) are more plausible to occur impacting the force-displacement data negatively. Higher frequencies such as 5 and 10 Hz were then included in the experiments again, but experiments with even higher frequencies would be advisable in order to reduce experiment duration and therefore increase accuracy.

After analyzing data from the first experiment, it turned out that indentation curves at low frequencies (0.5 Hz and 0.1 Hz) often cannot be described as sinusoidal, which is a prerequisite for the sine fit of the data and the Oliver-Pharr method used. Force-time and indentation-time signals are always to a certain degree disturbed by noise, resulting in the necessity to first detrend and filter the signals before being able to fit them with a simple sine function where the period was a fixed parameter (the input frequency) and just amplitude and phase shift were iterated in a nonlinear minimum search and compared to the original data by a least-squares

cost function.

Force and indentation data, which showed no or a strongly meandering sine profile, could not be approximated by the programmed sine fit. As a result, values for storage and loss modulus turned out disproportionately large and where therefore excluded from further calculations and visualizations, which is disappointing since only a handful fibrils per sample were tested (n1=5, n2=4). This low number is due to the long duration of the experiment, which results from the need for many periods at low frequencies. To counteract this, the 0.1 Hz was removed from the program in the second experiment and measurements at 5 Hz were added instead. As a preview of further dynamic indentation experiments with AFM, it can be said that perhaps the focus should be exclusively on the higher frequencies larger than 10 Hz, and that above all even more care should be taken to ensure that the AFM records the measurement protocol properly, without too many disturbances (it may help to turn off the light of the microscope completely and keep the doors closed). Problems with the data quality in this work are mainly caused by an existing technical problem with the AFM used. Additionally, to complete the bigger picture, it would be necessary to test more fibrils overall, or maybe multiple points or forcemaps on a fibril to counteract the failures and to be able to do a statistical analysis. Still, after those two experiments, frequency-dependent indentation measurements with AFM seem to keep the promise to characterize the viscoelastic behaviour of collagen fibrils better than achieved with simple indentation experiments and data analysis with a linear-elastic Hertz model. Once data acquisition and analysis become more stable, the benefit of the frequency-dependent method can be re-evaluated.

Until now, the mechanical properties of horse tendons have mainly been determined at the macro level. Old energy-storing tendons seem to tear faster, while the young ones are a lot more elastic than the positional tendons. Kain investigated in 2017 the collagen fibrils of such tendons with simple indentation tests with AFM. He observed a trend in the measured indentation modulus that contradicted the behaviour of the tendon on the macroscale, e.g. the collagen fibril of the young SDFT sample seemed to be stiffer than the old one. There were clear differences in the indentation modulus between the four samples, which cannot be confirmed in this work, neither by quasi-static experiments nor by frequency-dependent ones. In fact, the values for storage and loss modulus in this thesis are very similar and range between 4 and 5 MPa. Further tests

could verify the thesis that collagen fibrils of different ages and with different functionality do not show gross differences in terms of their (visco-)elasticity. Even in literature, no changes in mechanical properties with age could be demonstrated in some cases [32], [12] (see the discussion in section 2.4). However, the viscoelastic behaviour of the individual fibrils seems to change over the course of a measurement, namely as a function of the frequency. A measurement starts with the highest frequency (10 Hz), the height-controlled oscillation then decreases further and further until 0.1 Hz. At the highest frequency, the results also show the highest values. Increasing phase shift with increasing frequency has already been reported in literature [10]. Conversely, this also means that in the course of a measurement, phase shift, loss tangent and loss modulus decrease, which can be interpreted as a decrease of the material's viscous character. Since the force signal usually leads the indentation signal by a few degrees, this indicates the viscoelastic character of the material. At first the material seems to react dilatory to the indentation. It might be interesting to see if this is just a subjective observation or can be confirmed by more (and modified) tests and statistical analysis.

Unfortunately, after the second experiment, no statements can be made about the frequency-dependent behaviour of MGO-treated collagen fibrils due to a lack of data. However, the results of the quasi-static measurement complete the picture. As in the literature, a clear increase in the indentation modulus can be determined after glycation [53]. The data evaluated in this work agree with the findings of Svensson et al., who find that there are no major differences between mechanics of collagen fibrils of different ages and types from rat, but chemically treated fibrils show significantly higher stiffness [16].

All these findings are a promising prospect for further development of frequency-dependent indentation measurement with AFM, for which the experience with the measurement protocol and the programmed MATLAB code for data analysis lay a good foundation.

Appendix A   Manual for conducting dynamic mechanical experiments with AFM (JPK)

Quick overview:

- Mount Chip

- Image tgt1

- Place sample

- Calibrate for cantilever stiffness (need to be in air)

- Add liquid

- Do sensitivity calibration again

- Measure

1.) Mount Chip:

- Put in the cable for the camera into the microscope, then turn the microscope on.

- Open the JPK Software.

- Turn on the Motor Control (after turning on the software, otherwise you need to click on "engage" in the motor control panel later on).

- Choose a cantilever and place it in the holder, then place the holder in the AFM head.

- Place a marked glass slide or the glass slide with the sample under the microscope. To center it automatically with the lense, press F4 + Enter on the Motor Control.

- Make sure that the light of the microscope is not too strong.

- Focus on the mark on the glass slide while looking through the microscope. This is important so that you do not make the error to look on the wrong side of the glass slide.

- Place the AFM head: The foot in the back first, then right and then look, if the head has enough space to be put down fully.

- Go into JPK Software: Turn on Camera. (Turn the wheel on the microscope to switch to computer camera. Choose e.g. orestisimaging to get good contrast.)

- Use Z Stepper Motors to slowly go 100μm, 50μm,.. down until Cantilever and Chip appear on the screen (dark shadow first).

- Focus on the Cantilever with wheels on the microscope.

- Move AFM head in position with the silver screws if necessary (back one moves arched, front one moves vertically).

2.) Laser Alignment:

- Push in the filter to see the bright light = Laser (if you do not see the light, then go to a microscope magnitude of 5).

- First two screws from right will move the Laser horizontally and vertically, with the goal to point him on the tip of the tip.

- Middle screw is to tilt the mirror: You turn it until "Sum" in the Software reaches a max between two corners. Most times the red point will be somewhere at -11,96V on the scale of the Vertical Deflection, that's ok!

- Now move the last two screws until the red point finds itself right in the middle of the cross.

3.) Calibration:

- Focus on glass slide, so turn the focus wheel in your direction until the marking (or fibrils) on the glass slide has sharp contours.

- Z Stepper Motors in small steps down until cantilever appears again.

- Choose "Contact mode" and "Force mapping".

- Take a look at the setpoint in the Software. A large setpoint means a large deflection of the cantilever which means a large force. If you use a stiffer cantilever then use a setpoint like 0.1 V. If you use a softer cantilever then use a setpoint like 1 V.

- Click the blue arrow or "Start approach" (if it might not do anything now, you must possibly click on "engage" in the panel of the motorized stage).

- How to doublecheck if your approach was successful: The red line of the Z Range should not move!

- Now choose your Pixels, ideally the smallest amount: 4x4.

- Make sure you checked "Autosave" when you click the tab "Setup".

- Click on the white "Go"-Button.

- In the panel of the force scan map oscilloscope you will see your approach and retraction curves – if those seems strange, then you might not be in contact with the sample: Try to increase the setpoint!

- Push the red arrow to retract the piezo (Attention: If you want to retract a bigger space through the Z Stepper Motors, make sure to click twice "up" then. With the first click it will just retract the piezo as if you clicked the red arrow).

- Open the JPK Data Processing Software.

- Drag your force map from your folder into the window.

- Then choose from the icon range the one "Use this map for batch processing".

- Choose the sensitivity process, deselect the option to save the force curves.

- Click the icons in the range as presented: The first one will select you the region where the baseline fit should be made.

- The next icon addresses the linear fit height, where you click through the curves, zoom in and mark the first 20% of the linear graph. Zoom in to check if the graphs are smooth, if so choose "keep" once you marked the 20%, if not choose "discard".

- At the end click on the statistics icon above "save final results".

- Take the "Mean Value" and put it in the Excel sheet, where the sensitivity is calculated in the next row automatically. Copy the sensitivity value.

- Go back into the JPK Software: Click on the icon "Calibration Manager".

- Choose the "contact-based" method, where you put in the copied sensitivity value.

- Now the unknown value is the spring constant.

- Check the box next to the unlimited sign and click on "Run thermal noise". (For this it is important to be retracted! Red arrow.)

- After a time, click on "Stop".

- Click on "Choose a fit range with mouse", and select the highest peak. A red curve will overlay the turquoise signal. Center the curve and zoom in.

- Insert the received value for the spring constant into the third column of the excel data sheet.

- If you did not reach the wished setpoint, set it to your goal force and deselect Sensitivity and Spring Constant. Now repeat all steps beginning with a new approach. For dry experiments you might choose a max force in a range from 150 to 200 nN. For experiments in liquid the max force will find itself between 1nN and 1.5 nN.

4.) TGT1 Measurement:

- Place the TGT1 glass slide (from the tube with the pink lid) under the microscope.

- The glass slide is higher than usual ones, so take care to be far away through the Z Stepper Motors.

- On the TGT1 glass slide there is a smaller square. Place the head as such that it could measure the area of this square. Adjust with the silver screws if necessary.

- Go down with the Z Stepper Motors and then approach. If you have not done the calibration yet, do first a quick "contact free" calibration in the Calibration Manager, to have the right setpoint.

- Choose "Contact mode" and "Imaging".

- Choose for fast and slow axis 3x3.

- From this image choose a 1.5x1.5μm area and image again one single beam.

- Also look at the Error Signal of the Data Viewer!

5.) Fibril Measurement:

Zoom on the glass slide and search for a fibril with Motion Control. For measurements in dry circumstances use "QI Mode" and "Advanced Imaging".

- Set the fast and the slow axis to 20x20. The X and Y Offset to 0.0 and choose 256x256 pixels.

- You can press one icon to see in the camera which area will be imaged.

- After approaching and taking the image, select an area where the fibril is displayed well in a square for example 2.5x2.5.

- Retract.

- Switch to "Contact Mode" and "Force Mapping".

- Round the Fast Axis.

- Choose more Pixels in Length than in Height, e.g. 64x16, 64x8. Deselect "square image".

- Approach.

For **measurements in liquid** choose first, still in dry condition, "Contact mode" and "Imaging" instead of "QI Mode". You use "Contact Mode/Imaging" when you use soft cantilevers otherwise the fibrils will be scratched off.

- Drive the cantilever to a promising position to image several image at once. Chose a region of 20 μm by 20 μm with a resolution of 256 x 256 pixels.

- Choose higher values for "IGain", so that the light and the dark blue curve overlap.

- Optionally you can increase the setpoint to obtain a better result.

- Now you have an image of a region with fibrils, ideally with a few ones and the fibrils must be on the glass surface and not on top of other fibrils.

- Select the channel "Error Signal" in the Data Viewer to see if there is D-Banding and to measure if fibril is in diameter larger than 100nm: Right mouseclick on image and select "Measure Distance".

Then add the PBS

Option 1: remove the AFM head, once the AFM head is down add some PBS using a pipette (eppendorf Research R plus), perhaps up to half the depth of the fluid cell. When you add the AFM head back in you need to check the optical image because there could be a bubble forming right close to the cantilever. If it happens remove the head again, take a tissue and carefully place it from the rear side of the AFM chip holder just a bit above the screw that you mount the AFM chip. This should suck up the water and destroy the bubble of air. Place AFM head back in PBS and check again. Bubble should not form after this. If it is, to the same thing. After a while it is gone.

Option 2: place the pipette carefully in the narrow space between AFM head and sample and slowly let the PBS fill the fluid cell half full.

- After adding the PBS the laser will be off. You need to readjust the mirror with the middle and the two screws on the left. After having the red point in the middle of the

100

cross again, you will notice that all three values are changing constantly. Wait for 15 minutes approximately that the system can calm down.

- Then the calibration steps must be repeated because the sensitivity changed.

- After that take an image in "QI mode" and "Advanced Imaging". The QI Image will give you the height and you can locate the fibrils you imaged in air.

- When we hydrate the sample we want to image the same location of fibrils because we know also how much they swell from the contact mode imaging, which is an indication of how much water they adsorb. You can of course move to another location. If you wish to do so then you can choose a couple of areas in air, image them along with taking an optical microscope image of the area so that you can go back again when in PBS. Try to find features like crossings of fibrils etc that you can easily find again. Ideally, do not move too far away but rather go in the vicinity.

- Collect the single force maps for every fibril with "Contact Mode" and "Force Mapping" as described for dry condition.

- Once you are done from this area, you can use the motorized stage to go to a near region to find other fibrils. Approach, select a region of interest of 20 um x 20 um and do the QI image. Then from the QI do your individual force maps.

6.) After Measurements:

Clean sample and chip holder with distilled water.

Appendix B   MATLAB Code for Visualization of microrheology data

The code parts for generating the plots with MATLAB that help to visualize the data of dynamic mechanical experiments with AFM are shown below and comprise:

1. Display of force and indentation data

2. Force and indentation data over time including the sine fit

3. Phase shift between force and indentation fit

4. Results (phase shift, losstangent, elastic and storage modulus) over frequency

1.) Display force and indentation data

```matlab
function show_modulation(obj)


close all


DirectoryPath = uigetdir();


for i=1:obj.NCurves


    %Identify position of first modulation for Multiplier later
    frequencies = zeros(obj.NumSegments,1);
    for j=1:obj.NumSegments
        frequencies(j,:) = obj.SegFrequency{j};
    end
    FirstFreq = find(frequencies,1,'first');


```

```matlab
17                     % Multiplier
18                     [MultiplierF,UnitF,~] = AFMImage.parse_unit_scale(range(obj
                           .BasedForce{i,FirstFreq}),'N',10);
19                     [MultiplierI,UnitI,~] = AFMImage.parse_unit_scale(range(obj
                           .Indentation{i,FirstFreq}),'m',10);
20
21
22                     % find min/max of indentation and force modulation
23                     Hmin = zeros(obj.NumSegments,1);
24                     Hmax = zeros(obj.NumSegments,1);
25                     Fmin = zeros(obj.NumSegments,1);
26                     Fmax = zeros(obj.NumSegments,1);
27                     for j=1:obj.NumSegments
28                         if obj.SegFrequency{j} > 0
29
30                             Hmin(j,:) = min(obj.Indentation{i,j});
31                             Hmax(j,:) = max(obj.Indentation{i,j});
32                             Fmin(j,:) = min(obj.BasedForce{i,j});
33                             Fmax(j,:) = max(obj.BasedForce{i,j});
34                         else
35                             Hmin(j,:) = NaN;
36                             Hmax(j,:) = NaN;
37                             Fmin(j,:) = NaN;
38                             Fmax(j,:) = NaN;
39
40                         end
41                     end
42
43                     yHmin = min(Hmin)*MultiplierI;
44                     yHmax = max(Hmax)*MultiplierI;
45                     yFmin = min(Fmin)*MultiplierF;
46                     yFmax = max(Fmax)*MultiplierF;
47
```

```matlab
48        if yHmin > 0
49            yHmin = yHmin * 0.7;
50
51        else
52            yHmin = yHmin * 1.2;
53        end
54
55        if yHmax > 0
56            yHmax = yHmax * 1.2;
57
58        else
59            yHmax = yHmax * 0.7;
60        end
61
62        if yFmin > 0
63            yFmin = yFmin * 0.7;
64
65        else
66            yFmin = yFmin * 1.2;
67        end
68
69        if yFmax > 0
70            yFmax = yFmax * 1.2;
71
72        else
73            yFmax = yFmax * 0.7;
74        end
75
76
77        %Colours
78        lila = [0.368, 0.058, 0.721];
79        lightblue = [0.101, 0.701, 0.976];
80        darkblue = [0.109, 0.078, 0.941];
```

```matlab
81
82                 for  j=1:obj.NumSegments
83
84                     lengthApp = length(obj.App{i});
85                     obj.SecPerPoint{1} = obj.SegDuration{1}/lengthApp;
86                     obj.TStart{1} = obj.SecPerPoint{1}/2;
87                     obj.TEnd{1} = obj.SeriesTime{1};
88                     obj.SegTime{1} = obj.TStart{1}:obj.SecPerPoint{1}:
                         obj.TEnd{1};
89                     obj.SegTime{1} = obj.SegTime{1}.';
90
91                     lastseg = obj.NumSegments - 1;
92                     lengthRet = length(obj.Ret{i});
93                     obj.SecPerPoint{obj.NumSegments} = obj.SegDuration{
                         obj.NumSegments}/lengthRet;
94                     obj.TStart{obj.NumSegments} = obj.SeriesTime{lastseg
                         }+(obj.SecPerPoint{obj.NumSegments}/2);
95                     obj.TEnd{obj.NumSegments} = obj.SeriesTime{obj.
                         NumSegments};
96                     obj.SegTime{obj.NumSegments} = obj.TStart{obj.
                         NumSegments}:obj.SecPerPoint{obj.NumSegments}:obj
                         .TEnd{obj.NumSegments};
97                     obj.SegTime{obj.NumSegments} = obj.SegTime{obj.
                         NumSegments}.';
98
99
100                end
101
102            % Plot
103            figure('Name',sprintf('Microrheology Curves %i',i))
104            hold on
105            for  j=1:obj.NumSegments
106
```

```matlab
107                 %subplot 1: force time
108                 subplot(3,2,1)
109                 hold on
110                 plot(obj.SegTime{j},obj.BasedForce{i,j}*MultiplierF,'m'
                        )
111                 title(sprintf('Force Time Curve %i',i),'FontSize', 18)
112                 xlabel('time in s','FontSize', 12)
113                 ylabel(sprintf('vDeflection-Force [%s]',UnitF),'
                        FontSize', 12)
114                 grid on
115                 grid minor
116
117                 %subplot 2: indentation time
118                 subplot(3,2,2)
119                 hold on
120                 plot(obj.SegTime{j},obj.Indentation{i,j}*MultiplierI,'-
                        ','color',lightblue)
121             ylim([yHmin yHmax])
122                 title(sprintf('Indentation Time Curve %i',i),'FontSize'
                        , 18)
123                 xlabel('time in s','FontSize', 12)
124                 ylabel(sprintf('Indentation [%s]',UnitI),'FontSize',
                        12);
125                 grid on
126                 grid minor
127
128                 %subplot 3: force and indentation over time
129                 subplot(3,2,5)
130                 hold on
131
132             yyaxis left
133             ylim([yFmin yFmax])
```

```matlab
134                plot(obj.SegTime{j},obj.BasedForce{i,j}*MultiplierF,'--m'
                       )
135                set(gca, 'YColor', 'm')
136                xlabel('time in s','FontSize', 12)
137                ylabel(sprintf('vDeflection-Force [%s]',UnitF),'FontSize
                       ', 12)
138
139
140                yyaxis right
141                ylim([yHmin yHmax])
142                plot(obj.SegTime{j},obj.Indentation{i,j}*MultiplierI,'-'
                       ,'color',lightblue)
143                set(gca, 'YColor', lightblue)
144                title(sprintf('Force and Indentation over Time Curve %i'
                       ,i),'FontSize', 18)
145                ylabel(sprintf('Indentation [%s]',UnitI),'FontSize', 12)
                       ;
146                grid on
147                grid minor
148
149
150            % subplot 4: force vs indentation
151            subplot(3,2,6)
152            plot(obj.Indentation{i,1}*MultiplierI,obj.BasedForce{i
                   ,1}*MultiplierF,'--r',obj.Indentation{i,obj.
                   NumSegments}*MultiplierI,obj.BasedForce{i,obj.
                   NumSegments}*MultiplierF,'--b')
153            hold on
154            plot(obj.Indentation{i,j}*MultiplierI,obj.BasedForce{i,j
                   }*MultiplierF,':m')
155            xlim([-200 200])
156            title(sprintf('Force Indentation Curve %i',i),'FontSize'
                   , 18)
```

107

```matlab
157                    xlabel(sprintf('Indentation [%s]',UnitI),'FontSize', 12)
                           ;
158                    ylabel(sprintf('vDeflection−Force [%s]',UnitF),'FontSize
                           ', 12);
159                    grid on
160                    grid minor
161
162                    l1 = plot(nan, nan, '−r');
163                    hold on
164                    l2 = plot(nan, nan, '−b');
165                    l3 = plot(nan, nan, ':m');
166                    l1.LineWidth = 2;
167                    l2.LineWidth = 2;
168                    l3.LineWidth = 2;
169                    legend([l1, l2, l3], {'approach', 'retract','modulation'
                           }, 'FontSize', 8)
170
171
172                end
173
174
175            if DirectoryPath~=0
176                whereToStore=fullfile(DirectoryPath,['
                       microrheology_curve_' num2str(i) '.svg']);
177                saveas(gcf, whereToStore);
178            end
179
180
181
182
183            %force indentation only segments
184 %              s=2*obj.NCurves + 10*i;
185 %              for j=1:obj.NumSegments
```

108

```matlab
%
%
%                              if obj.SegFrequency{j} > 0
%
%                                  Freq = obj.SegFrequency{j};
%
%                                  figure(s)
%                                  plot(obj.Indentation{i,j}*MultiplierI,obj.
    BasedForce{i,j}*MultiplierF,'b')
%                                  title(sprintf('Force Indentation Curve %i, %.1f [
    Hz]',i,Freq),'FontSize', 18)
%                                  xlabel(sprintf('Indentation [%s]',UnitI),'
    FontSize', 16);
%                                  ylabel(sprintf('vDeflection-Force [%s]',UnitF),'
    FontSize', 16);
%                                  grid on
%                                  grid minor
%
%                                  if DirectoryPath~=0
%                                      whereToStore=fullfile(DirectoryPath,['
    force_indentation_curve_' num2str(i) '_segment_' num2str(j) '.svg']);
%                                      saveas(gcf, whereToStore);
%                                  end
%
%
%
%                          end
%                          s=s+1;
%
%                  end
```

109

```
214              end
215
216          end
```

Listing 7: MATLAB Code for displaying force and indentation data.

2.) Force and indentation data over time including sine fit

```matlab
1              function show_sine_special(obj)
2          % this function is to display the filtered force and
3          % indentation data and the respective fits to see the quality
4          % of the fit
5          close all
6          DirectoryPath = uigetdir();
7          k=1;
8
9
10         for i=1:obj.NCurves
11
12             %Identify position of first modulation for Multiplier later
13              frequencies = zeros(obj.NumSegments,1);
14              time = obj.SegTime;
15              for j=1:obj.NumSegments
16                  frequencies(j,:) = obj.SegFrequency{j};
17
18              end
19             %frequencies = cell2mat(obj.SegFrequency);
20             FF = obj.FilterF;
21             FH = obj.FilterH;
22             SVF = obj.SineVarsF;
23             SVH = obj.SineVarsH;
24             BF = obj.BasedForce;
25             BH = obj.Indentation;
```

```matlab
26              empty_fields = cellfun(@isempty,FF);
27              FF(:,empty_fields(1,:))=[];
28              FH(:,empty_fields(1,:))=[];
29              SVF(:,empty_fields(1,:))=[];
30              SVH(:,empty_fields(1,:))=[];
31
32              time = time(frequencies ~= 0);
33              BF = BF(:,frequencies ~= 0);
34              BH = BH(:,frequencies ~= 0);
35              frequencies = frequencies(frequencies ~= 0);
36              lf = length(frequencies);
37
38              maxfreq = max(frequencies);
39              minfreq = min(frequencies);
40              faktor = maxfreq/minfreq;
41
42 %               if faktor > 10
43 %
44 %               end
45
46              %Colours
47              lila = [0.368, 0.058, 0.721];
48              lightblue = [0.101, 0.701, 0.976];
49              darkblue = [0.109, 0.078, 0.941];
50
51
52
53
54              %Plot
55              figure('Name',sprintf('Normalized curves with Fit %i',i))
56              set(gcf,'units','normalized','outerposition',[0 0 1 1])
57              %set(gcf,'Resize','off')
58
```

```matlab
59              t = tiledlayout(2,2);
60              t.TileSpacing = 'none';
61
62              %n = 1*lf;
63              %h = gobjects(2,n);
64
65              hold on
66
67              for j = 1:lf
68
69                  x = time(j);
70                  x =cell2mat(x);
71                  a = 0.99*time{j}(1);
72                  e = 1.01*time{j}(end);
73
74                  % range of data
75                  rangeF = range(BF{i,j});
76                  rangeH = range(BH{i,j});
77
78                  %Y-values fitted sine of indentation and force:
79                  ypF = SVF{i,j}(1)*(sin(2*pi*x.*SVF{i,j}(2) + SVF{i,j}(3)));
80                  ypH = SVH{i,j}(1)*(sin(2*pi*x.*SVH{i,j}(2) + SVH{i,j}(3)));
81
82
83
84                  nexttile
85
86                  yyaxis left
87                  [MultiplierF,UnitF,~] = AFMImage.parse_unit_scale(range(BF{i,j}),'N',10);
88                  semilogx(time{j},FF{i,j}*rangeF*MultiplierF,'—m')
```

```matlab
89                    hold on
90                    semilogx(x,ypF*MultiplierF,'--m')
91                    set(gca, 'YColor', 'm')
92                    xlabel('time [s]','FontSize', 14)
93                    ylabel(sprintf('vDeflection-Force [%s]',UnitF),'...
                          FontSize', 14)
94
95
96                    yyaxis right
97                    [MultiplierI,UnitI,~] = AFMImage.parse_unit_scale(range
                          (BF{i,j}),'m',10);
98                    semilogx(x,FH{i,j}*rangeH*MultiplierI,'--','color',...
                          lightblue);
99                    hold on
100                   semilogx(x,ypH*MultiplierI,'-','color',lightblue)
101                   set(gca, 'YColor', lightblue)
102                   title(sprintf('Curve %i, %.1f [Hz]',i,frequencies(j)),'...
                          FontSize', 16)
103                   ylabel(sprintf('Indentation [%s]',UnitI),'FontSize',...
                          14);
104                   grid on
105                   grid minor
106
107
108               end
109
110
111           % Title
112           %title(sprintf('Force and Indentation over Time incl. Fit...
                      Curve %i',i),'FontSize', 18)
113
114
115           % Legend
```

113

```matlab
116         l1 = plot(nan, nan, 'm—');
117         hold on
118         l2 = plot(nan, nan, '-m');
119         l3 = plot(nan, nan, '—', 'color', lightblue);
120         l4 = plot(nan, nan, '-','color',lightblue);
121         l1.LineWidth = 3;
122         l2.LineWidth = 3;
123         l3.LineWidth = 3;
124         l4.LineWidth = 3;
125         legend([l1, l2, l3, l4], {'normalized force data', 'force
                fit','normalized indentation data', 'indentation fit'},
                'Location', 'southoutside','FontSize', 12)
126
127         % Save
128         k = obj.RectApexIndex;
129         if DirectoryPath~=0
130             whereToStore=fullfile(DirectoryPath,['
                    filtered_force_indentation_fit_curve_' num2str(i) '.
                    svg']);
131             saveas(gcf, whereToStore);
132         end
133     end
134 end
```

Listing 8: MATLAB Code for displaying the sine fit of force and indentation data over time.

3.) Phase shift between force and indentation fit

```matlab
1         function show_phaseshift(obj)
2         close all
3         DirectoryPath = uigetdir();
4         k=1;
5         for i=1:obj.NCurves
```

114

```matlab
                        %Identify position of first modulation for Multiplier later
                        frequencies = zeros(obj.NumSegments,1);
                        for j=1:obj.NumSegments
                                frequencies(j,:) = obj.SegFrequency{j};
                        end
                        FirstFreq = find(frequencies,1,'first');



                    % Plot
                        figure('Name',sprintf('Phaseshift Curve %i',i))
                        %lastseg = obj.NumSegments - 2;
                        hold on
                        for j=1:obj.NumSegments


                            if obj.SegFrequency{j} > 0


                                Freq = obj.SegFrequency{j};


                                Period = 2*pi/obj.SegFrequency{j};
                                End = obj.TStart{j} + 2/obj.SegFrequency{j};
                                x = linspace(obj.TStart{j},End);




                                %Y-values fitted sine of indentation and force:
                                try
                                    ypF = obj.SineVarsF{i,j}(1)*(sin(2*pi*x.*obj.
                                        SineVarsF{i,j}(2) + obj.SineVarsF{i,j}(3)));
                                    ypH = obj.SineVarsH{i,j}(1)*(sin(2*pi*x.*obj.
                                        SineVarsH{i,j}(2) + obj.SineVarsH{i,j}(3)));
                                catch
                                    ypF = zeros(length(x),1);
```

115

```matlab
37          ypH = zeros(length(x),1);
38      end
39
40
41
42  hold on
43
44  [MultiplierI,UnitI,~] = AFMImage.parse_unit_scale(
        range(obj.Indentation{i,FirstFreq}),'m',10);
45  [MultiplierF,UnitF,~] = AFMImage.parse_unit_scale(
        range(obj.BasedForce{i,FirstFreq}),'N',10);
46  subplot(1,obj.NumSegments,j)
47  findpeaks(ypF*MultiplierF,x)
48  hold on
49  findpeaks(ypH*MultiplierI,x)
50  title(sprintf('Curve %i, %.1f [Hz]',i,Freq),'
        FontSize', 16)
51  xlabel('time [s]','FontSize', 14)
52  ylabel(sprintf('fit of vDeflection-Force [%s] and
        Indentation [%s]',UnitF, UnitI),'FontSize', 14)
53  legend({'force fit','force fit peak','indentation
        fit','indentation fit peak'},'Location','
        southoutside','FontSize', 12)
54  drawnow
55  grid on
56  grid minor
57
58
59
60  if DirectoryPath~=0
61      whereToStore=fullfile(DirectoryPath,['
            force_indentation_fit_curve_' num2str(i) '.
            svg']);
```

116

```matlab
62                          saveas(gcf, whereToStore);
63                      end
64
65                  end
66
67              end
68          end
69      end
```

Listing 9: MATLAB Code for showing the phase shift between force and indentation fit.

4.) Results over frequency

```matlab
1       function show_emodmicro(obj)
2       close all
3       DirectoryPath = uigetdir();
4       k=1;
5
6       figure('Name',sprintf('Results'))
7       hold on
8       for i=1:obj.NCurves
9
10          for j=1:obj.NumSegments
11              EModMicro1 = num2cell(obj.EModMicro1);
12              EModMicro2 = num2cell(obj.EModMicro2);
13          end
14
15          Dphi = zeros(obj.NumSegments,1);
16          frequencies = zeros(obj.NumSegments,1);
17          losstangent = zeros(obj.NumSegments,1);
18          emodmicro1 = zeros(obj.NumSegments,1);
19          emodmicro2 = zeros(obj.NumSegments,1);
20          for j=1:obj.NumSegments
```

117

```matlab
21              if obj.SegFrequency{j} > 0
22                  Dphi(j,:) = obj.DeltaPhi{i,j};
23                  frequencies(j,:) = obj.SegFrequency{j};
24                  losstangent(j,:) = obj.LossTangent{i,j};
25
26                  emodmicro1(j,:) = EModMicro1{i,j};
27                  emodmicro2(j,:) = EModMicro2{i,j};
28              end
29          end
30          Dphi = Dphi(Dphi ~= 0);
31          frequencies = frequencies(frequencies ~= 0);
32          losstangent = losstangent(losstangent ~= 0);
33          emodmicro1 = emodmicro1(emodmicro1 ~= 0);
34          emodmicro2 = emodmicro2(emodmicro2 ~= 0);
35
36          minfreq = min(frequencies);
37          maxfreq = max(frequencies);
38
39          xq = 0:0.1:maxfreq;
40          vqDphi = interp1(frequencies,Dphi,xq,'spline');
41          vqLosstangent = interp1(frequencies,losstangent,xq,'spline'
                );
42          vqEmodmicro1 = interp1(frequencies,emodmicro1,xq,'spline');
43          vqEmodmicro2 = interp1(frequencies,emodmicro2,xq,'spline');
44
45          %figure('Name',sprintf('Results'))
46          hold on
47
48          subplot(2,2,1)
49          plot(xq,vqDphi,'-','DisplayName',sprintf('Curve %i',i))
50          hold on
51          plot(frequencies, Dphi,'o','HandleVisibility','off')
52          title('Phaseshift of all curves','FontSize', 18)
```

118

```matlab
53      xlabel('frequency [Hz]','FontSize', 16)
54      ylabel('phaseshift[U+FFFD]','FontSize', 16)
55      legend show
56      %drawnow
57      grid on
58      grid minor
59
60      subplot(2,2,2)
61      plot(xq,vqLosstangent,'-','DisplayName',sprintf('Curve %i',
            i))
62      hold on
63      plot(frequencies, losstangent,'o','HandleVisibility','off')
64      title('Loss Tangent of all curves','FontSize', 18)
65      xlabel('frequency [Hz]','FontSize', 16)
66      ylabel('losstangent','FontSize', 16)
67      legend show
68      %drawnow
69      grid on
70      grid minor
71
72      subplot(2,2,3)
73      plot(xq,vqEmodmicro1,'-','DisplayName',sprintf('Curve %i',i
            ))
74      hold on
75      plot(frequencies, emodmicro1,'o','HandleVisibility','off')
76      title('Elastic modulus of all curves','FontSize', 18)
77      xlabel('frequency [Hz]','FontSize', 16)
78      ylabel('elastic modulus [N/mm2]','FontSize', 16)
79      legend show
80      %drawnow
81      grid on
82      grid minor
83
```

```matlab
84                subplot(2,2,4)
85                plot(xq,vqEmodmicro2,'-','DisplayName',sprintf('Curve %i',i
                    ))
86                hold on
87                plot(frequencies,emodmicro2,'o','HandleVisibility','off')
88                title('Viscous modulus of all curves','FontSize', 18)
89                xlabel('frequency [Hz]','FontSize', 16)
90                ylabel('viscous modulus [N/mm2]','FontSize', 16)
91                legend show
92                %drawnow
93                grid on
94                grid minor
95
96                if DirectoryPath~=0
97                    whereToStore=fullfile(DirectoryPath,['results_' num2str(
                        i) '.svg']);
98                    saveas(gcf, whereToStore);
99                end
100
101
102
103          end
```

Listing 10: MATLAB Code for showing the results, namely phase shift, loss tangent, elastic and storage modulus, over the frequency range.

120

Appendix C   Additional results

Results from Experiment 1

In this chapter of the appendix, the results of Experiment 1 are analyzed in detail. It starts with a consideration of all quasi-static measurements followed by the dynamic ones (H169 CDET, H170 CDET, H169 SDFT, H170 SDFT). Based on the slopes of the approach and retraction curves, the indentation depth and the ratio of force to indentation amplitude, it is determined whether a point on the fibril has been hit. The used, adapted and supplemented MATLAB program calculates an apex from the 10 points, but other points often give more plausible results for phase shift, loss tangent, storage and loss modulus - these are presented in detail below. The presentation of the raw data with the associated sine fits provides additional insight.

Quasi-static

H169 CDET				
quasistatic test				
fibril	indentation modulus (MPa)	Q. approach slope	Q. retraction slope	Q. indentation depth (nm)
1	3.75	0.475	0.516	7.6
2	NaN	0.48	0.695	-2.87
3	4.97	0.497	0.604	8.94
4	3.4	0.372	0.577	14
5	5.39	0.44	0.608	7.75

Table 9: In this table the results of quasistatic (stephold) experiments on 5 fibrils of H169 CDET are visible.

H170 CDET			
quasistatic test			
fibril	indentation modulus (MPa)	Q. approach slope	Q. retraction slope	Q. indentation depth (nm)
1	4.55	0.416	0.64	16.5
2	4.04	0.349	0.582	13.85
3	3.78	0.371	0.539	10.98
4	7.57	0.491	0.637	6.99
5	5.46	0.484	0.579	7.84

Table 10: In this table the results of quasistatic (stephold) experiments on 5 fibrils of H170 CDET are visible. Fibril 4 was excluded from the mean value calculation for showing a larger indentation modulus value.

H169 SDFT			
quasistatic test			
fibril	indentation modulus (MPa)	Q. approach slope	Q. retraction slope	Q. indentation depth (nm)
1	4.47	0.56	0.6	12.74
2	6.38	0.52	0.72	16.84
3	13.4	0.64	0.84	18.55
4	10	0.61	0.73	8.96
5	11.4	0.58	0.79	14.32

Table 11: In this table the results of quasistatic (stephold) experiments on 5 fibrils of H169 SDFT are visible. The values for the indentation modulus can be questioned as to their reasonableness in cases in which they exceed 10 MPa (for fibrils 3,4,5). This leads to a false upward shift in the mean, which is why they should be excluded from the calculation.

H170 SDFT			
quasistatic test			
fibril	indentation modulus (MPa)	Q. approach slope	Q. retraction slope	Q. indentation depth (nm)
1	4.05	0.378	0.476	5.93
2	5.38	0.452	0.595	8.32
3	4.55	0.257	0.709	27.44
4	5.54	0.559	0.675	14.53
5	7.11	0.345	0.72	13.84

Table 12: In this table the results of quasistatic (stephold) experiments on 5 fibrils of H170 SDFT are visible.

H169 CDET

H169 CDET				
fibril 1 (apex 4)				
dynamic			D. approach slope	D. retraction slope	D. indentation depth (nm)
apex 4			0,661	0,734	30,04
frequency	0.1 Hz	0.5 Hz	1 Hz	10 Hz
amplitude force (nm)	0,545	0,5	0,51	0,52
amplitude indentation (nm)	0,8	1,08	1,05	0,977
phase shift ϕ (°)	-11,77	3,3	3,34	4,42
loss tangent	-0,21	0,058	0,058	0,077
storage modulus E$'$ (MPa)	6,41	4,47	4,65	5,1
loss modulus E$''$ (MPa)	NaN	0,26	0,27	0,39

Table 13: In this table the material response of fibril 1 of H169 CDET at point 4 is visible. Indentation amplitude is double force amplitude except for 0.1 Hz. Phase shifts are a couple degree, increasing with frequency - so do storage and loss modulus.
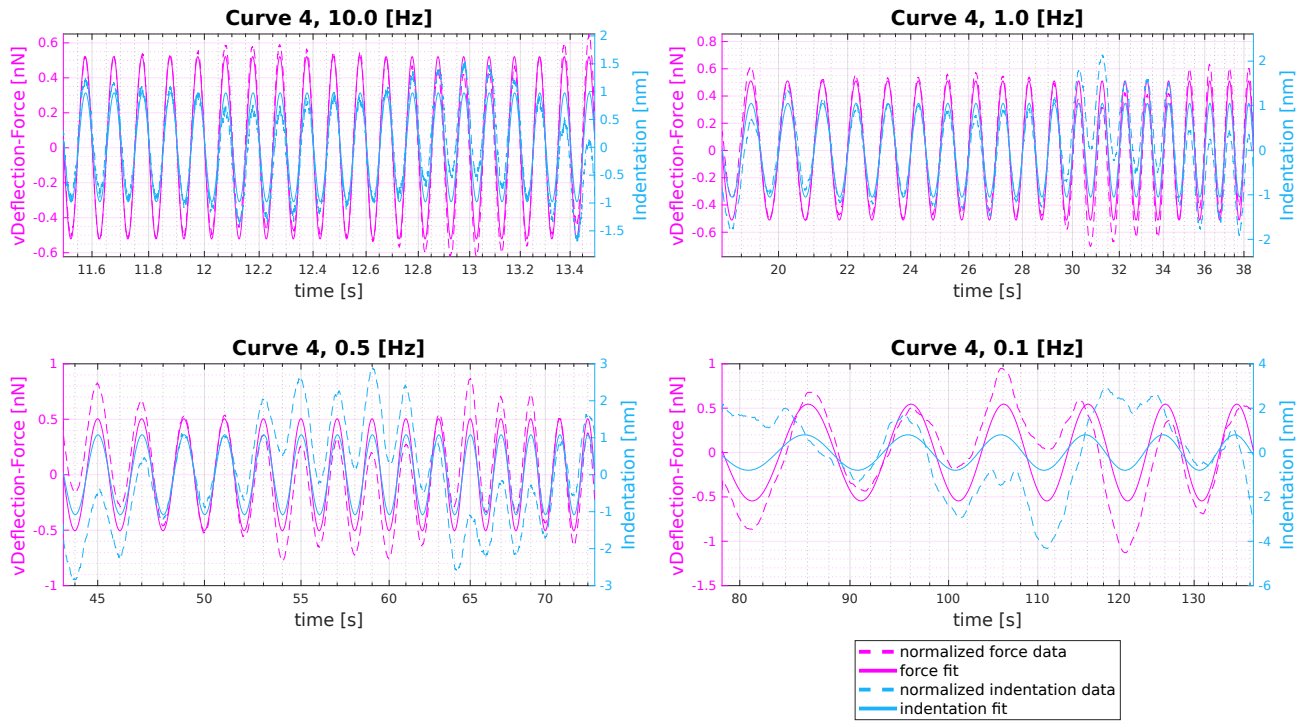
Figure 30: These four plots show the force and indentation signals over all measured frequencies with the respective sine fit of H169 CDET fibril 1 curve 4, which was identified as point on fibril.

H169 CDET				
fibril 2 (apex 5)				
dynamic		D. approach slope	D. retraction slope	D. indentation depth (nm)
apex 5		0,641	0,875	4,03
frequency	0.1 Hz	0.5 Hz	1 Hz	10 Hz
amplitude force (nm)	0,62	0,54	0,55	0,52
amplitude indentation (nm)	0,34	0,86	0,85	0,98
phase shift ϕ (°)	5,82	-0,5	4,8	5,5
loss tangent	0,102	-0,0087	0,084	0,096
storage modulus E' (MPa)	63,64	22,01	22,31	18,38
loss modulus E'' (MPa)	6,5	NaN	1,88	1,77

Table 14: In this table the material response of fibril 2 of H169 CDET at point 5 is visible. Storage modulus values seem strangely high, for this reason this point will not be considered in the mean value calculation. Perhaps the higher storage modulus values can be explained by the quite low indentation depth of 4 nm. However, it is the only point that has values for the storage modulus when measuring fibril 2.
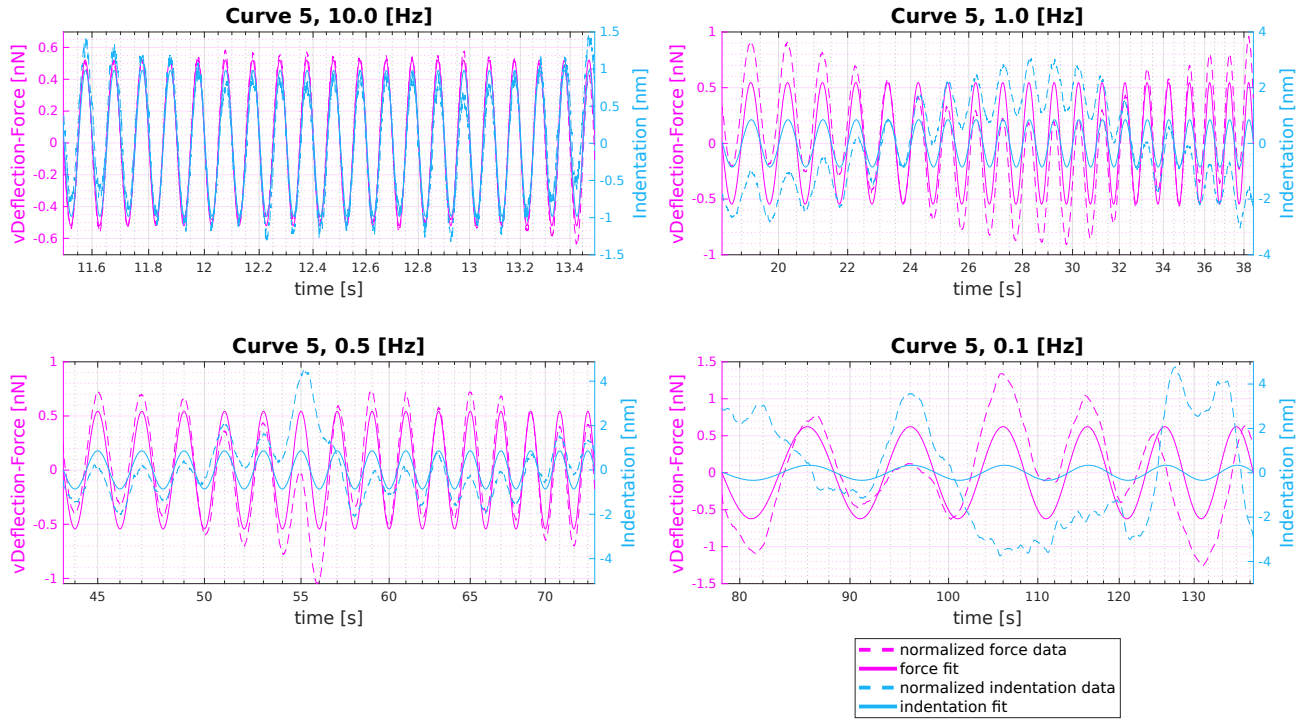
Figure 31: These four plots show the force and indentation signals over all measured frequencies with the respective sine fit of H169 CDET fibril 2 curve 5.

H169 CDET				
fibril 3 (apex 4)				
dynamic		D. approach slope	D. retraction slope	D. indentation depth (nm)
apex 4		0,656	0,723	7,13
frequency	0.1 Hz	0.5 Hz	1 Hz	10 Hz
amplitude force (nm)	0,498	0,51	0,51	0,49
amplitude indentation (nm)	1,07	1,07	1,06	1,13
phase shift ϕ (°)	10	-1,66	-0,783	-0,003
loss tangent	0,176	-0,0289	-0,0137	-5,3*10-5
storage modulus E′ (MPa)	9,98	10,3	10,42	9,52
loss modulus E″ (MPa)	1,76	NaN	NaN	NaN

Table 15: In this table the material response of fibril 3 of H169 CDET at point 4 is visible. Although the amplitude ratios for the point are consistent, negative phase shifts occur for all frequencies greater than 0.1 Hz, which is why point 5 is preferred.
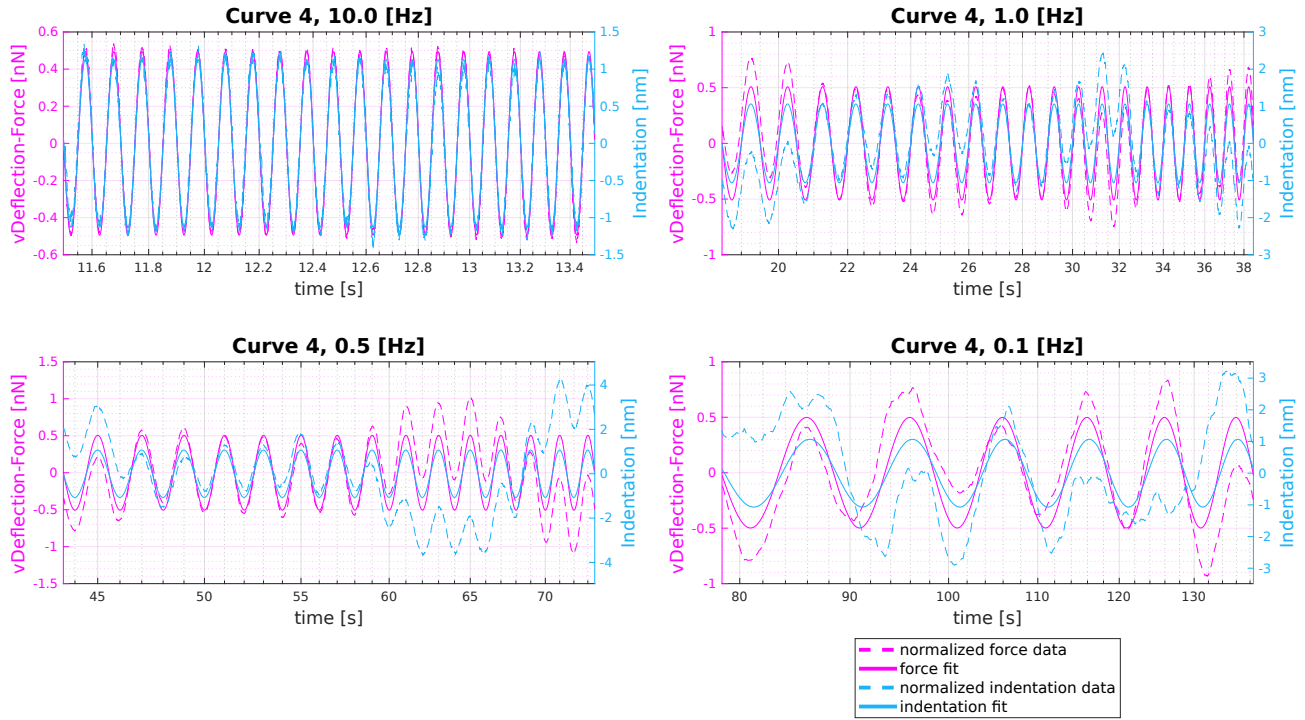
Figure 32: These four plots show the force and indentation signals over all measured frequencies with the respective sine fit of H169 CDET fibril 3 curve 4.

H169 CDET				
fibril 3 (point 5)				
dynamic			D. approach slope	D. retraction slope	D. indentation depth (nm)
point 5			0,604	0,705	16,45
frequency	0.1 Hz	0.5 Hz	1 Hz	10 Hz
amplitude force (nm)	0,41	0,45	0,46	0,49
amplitude indentation (nm)	1,56	1,4	1,33	1,16
phase shift ϕ (°)	0,003	3,23	1,87	2,89
loss tangent	4,74*10-5	0,0565	0,0327	0,0505
storage modulus E' (MPa)	3,49	4,24	4,61	5,56
loss modulus E'' (MPa)	0,000165	0,24	0,15	0,28

Table 16: In this table the material response of fibril 3 of H169 CDET at point 5 is visible. Results are comparable to fibril 1 H169 CDET (table 13). Frequency of 1 Hz delivers the overall smallest results in comparison to 0.5 Hz and 10 Hz.
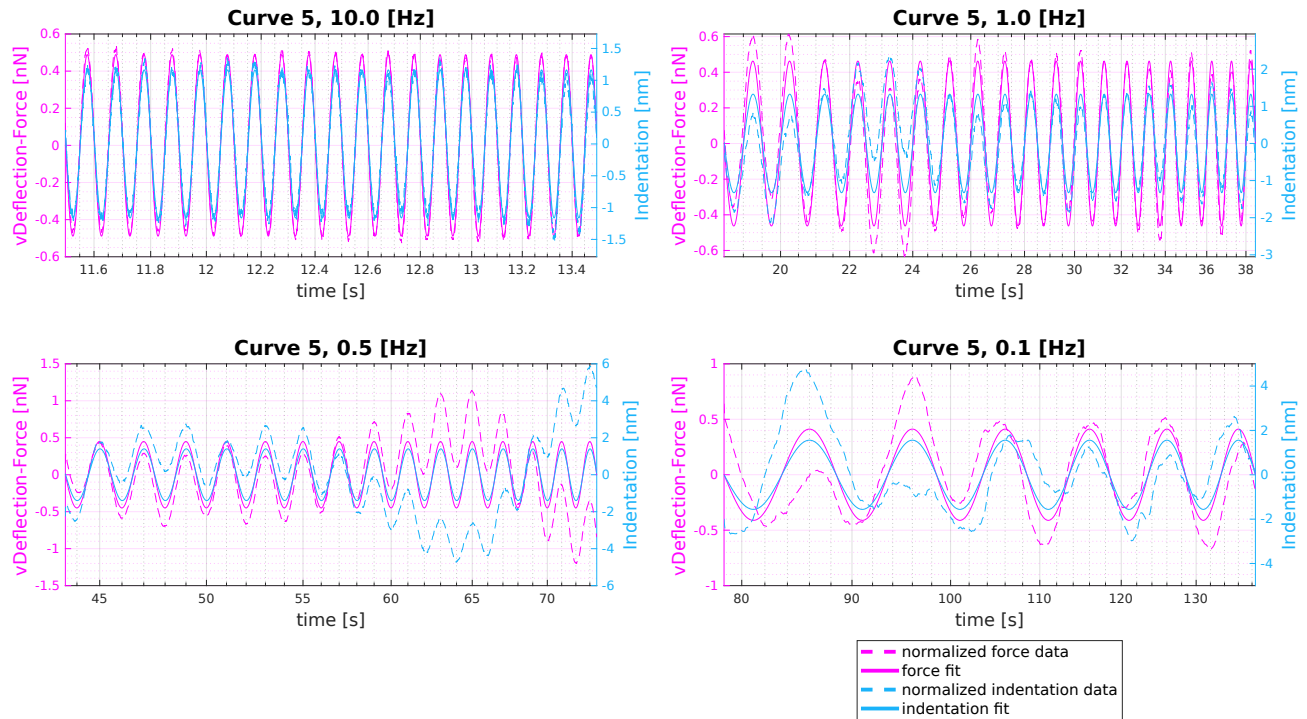
Figure 33: These four plots show the force and indentation signals over all measured frequencies with the respective sine fit of H169 CDET fibril 3 curve 5, which was identified as point on fibril.

H169 CDET				
fibril 4 (apex 4)				
dynamic		D. approach slope	D. retraction slope	D. indentation depth (nm)
apex 4		0,655	0,701	8,35
frequency	0.1 Hz	0.5 Hz	1 Hz	10 Hz
amplitude force (nm)	0,53	0,5	0,48	0,51
amplitude indentation (nm)	0,88	1,1	1,23	1,03
phase shift ϕ (°)	11,04	0,557	2,97	0,387
loss tangent	0,195	0,0097	0,0518	0,0068
storage modulus E' (MPa)	11,73	8,99	7,67	9,8
loss modulus E'' (MPa)	2,3	0,087	0,397	0,066

Table 17: In this table the material response of fibril 4 of H169 CDET at point 4 is visible. Since the results differ more strongly from the previous ones from H169 CDET, it can be considered to exclude them from further calculations in order to avoid falsifying shifts.
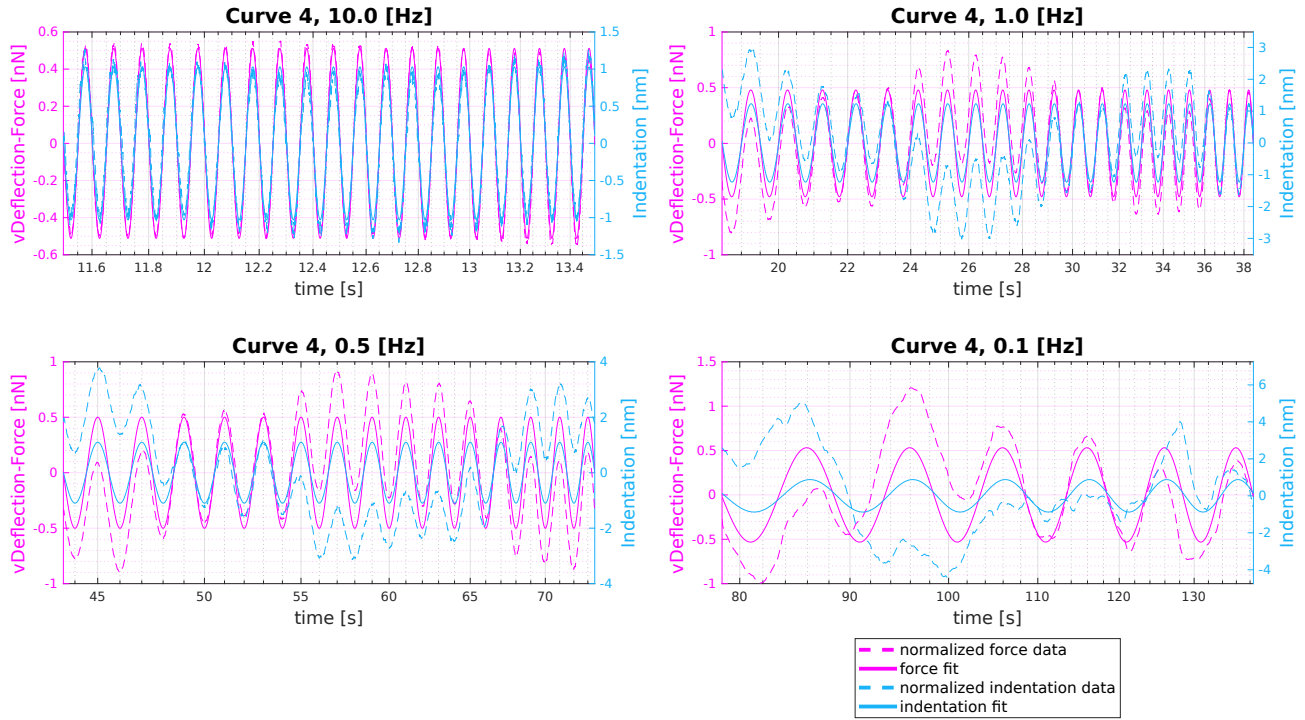
Figure 34: These four plots show the force and indentation signals over all measured frequencies with the respective sine fit of H169 CDET fibril 4 curve 4.

H169 CDET				
fibril 5 (apex 4)				
dynamic		D. approach slope	D. retraction slope	D. indentation depth (nm)
apex 4		0,749	0,819	-0,85
frequency	0.1 Hz	0.5 Hz	1 Hz	10 Hz
amplitude force (nm)	0,59	0,6	0,56	0,57
amplitude indentation (nm)	0,61	0,52	0,78	0,7
phase shift ϕ (°)	-28,35	9,04	5,46	6,77
loss tangent	-0,54	0,159	0,0956	0,119
storage modulus E' (MPa)	NaN	NaN	NaN	NaN
loss modulus E'' (MPa)	NaN	NaN	NaN	NaN

Table 18: In this table the material response of fibril 5 of H169 CDET at point 4 is visible. Force and indentation amplitude coincide, suggesting that no material is being measured, so another point in the data is being sought.
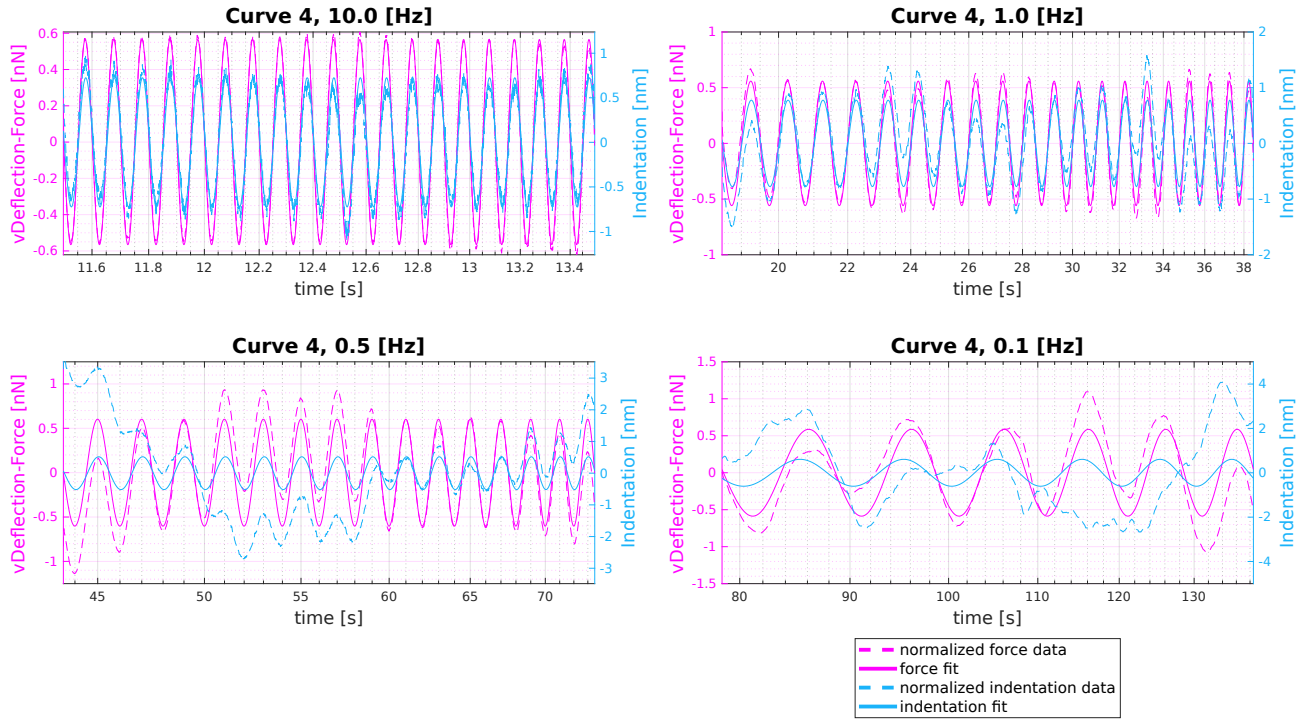
Figure 35: These four plots show the force and indentation signals over all measured frequencies with the respective sine fit of H169 CDET fibril 5 curve 4, which was identified not as point on fibril - see table 18.

H169 CDET				
fibril 5 (point 5)				
dynamic		D. approach slope	D. retraction slope	D. indentation depth (nm)
point 5		0,58	0,739	2,42
frequency	0.1 Hz	0.5 Hz	1 Hz	10 Hz
amplitude force (nm)	0,62	0,525	0,524	0,54
amplitude indentation (nm)	0,54	0,96	0,98	0,88
phase shift ϕ (°)	48,04	5,52	7,76	8,29
loss tangent	1,11	0,0966	0,136	0,146
storage modulus E' (MPa)	45,01	31,85	31,21	35,72
loss modulus E'' (MPa)	50,07	3,08	4,25	5,2

Table 19: In this table the material response of fibril 5 of H169 CDET at point 5 is visible. Instead of point 4, point 5 is considered, which has a lower slope of the approach and retraction curves and whose indentation amplitude is twice as high as the force amplitude for frequencies higher than 0.1 Hz. Is it because of the low indentation depth that storage modulus values are exorbitantly high? Physically, these are completely out of the ordinary and can therefore not be taken into account.
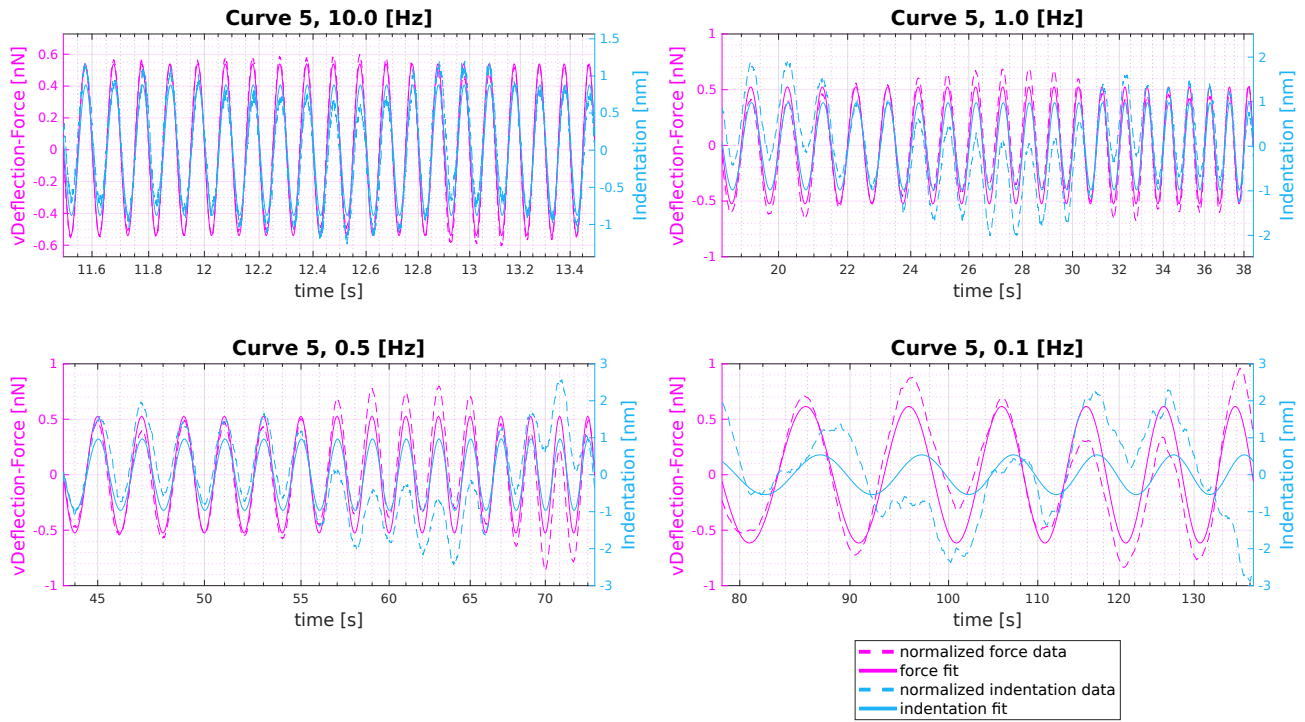
Figure 36: These four plots show the force and indentation signals over all measured frequencies with the respective sine fit of H169 CDET fibril 5 curve 5.

H170 CDET

H170 CDET				
fibril 1 (apex 3)				
dynamic		D. approach slope	D. retraction slope	D. indentation depth (nm)
apex 3		0,786	0,83	44,88
frequency	0.1 Hz	0.5 Hz	1 Hz	10 Hz
amplitude force (nm)	0,62	0,72	0,685	0,73
amplitude indentation (nm)	1	0,38	0,57	0,33
phase shift ϕ (°)	36,57	11,1	5,69	6,96
loss tangent	0,742	0,196	0,0996	0,122
storage modulus E' (MPa)	3,72	14,29	9,03	16,56
loss modulus E'' (MPa)	2,76	2,8	0,9	2,02

Table 20: In this table the material response of fibril 1 of H170 CDET at point 3 is visible. The indentation amplitude is much smaller than the force amplitude, storage and loss modulus are larger than expected, so a better point is sought.

Figure 37: These four plots show the force and indentation signals over all measured frequencies with the respective sine fit of H170 CDET fibril 1 curve 3, which was not chosen for further calculations because of the amplitude ratio (see table 20). The plots for 1 Hz, 0.5 Hz and 0.1 Hz also show that the indentation is not sinusoidal at all.

H170 CDET				
fibril 1 (point 5)				
dynamic		D. approach slope	D. retraction slope	D. indentation depth (nm)
point 5		0,731	0,839	46,75
frequency	0.1 Hz	0.5 Hz	1 Hz	10 Hz
amplitude force (nm)	0,66	0,64	0,63	0,65
amplitude indentation (nm)	0,65	0,8	0,87	0,73
phase shift ϕ (°)	-10,86	3,88	6,05	4,54
loss tangent	-0,192	0,0679	0,106	0,0794
storage modulus E' (MPa)	7,35	5,84	5,28	6,54
loss modulus E'' (MPa)	NaN	0,4	0,56	0,52

Table 21: In this table the material response of fibril 1 of H170 CDET at point 5 is visible. The problem here are the small height differences between amplitudes. It wouldn't be that noticeable with just a look at the storage modulus values. Since it is not certain whether glass was tested instead of fibril, one should refrain from this point.
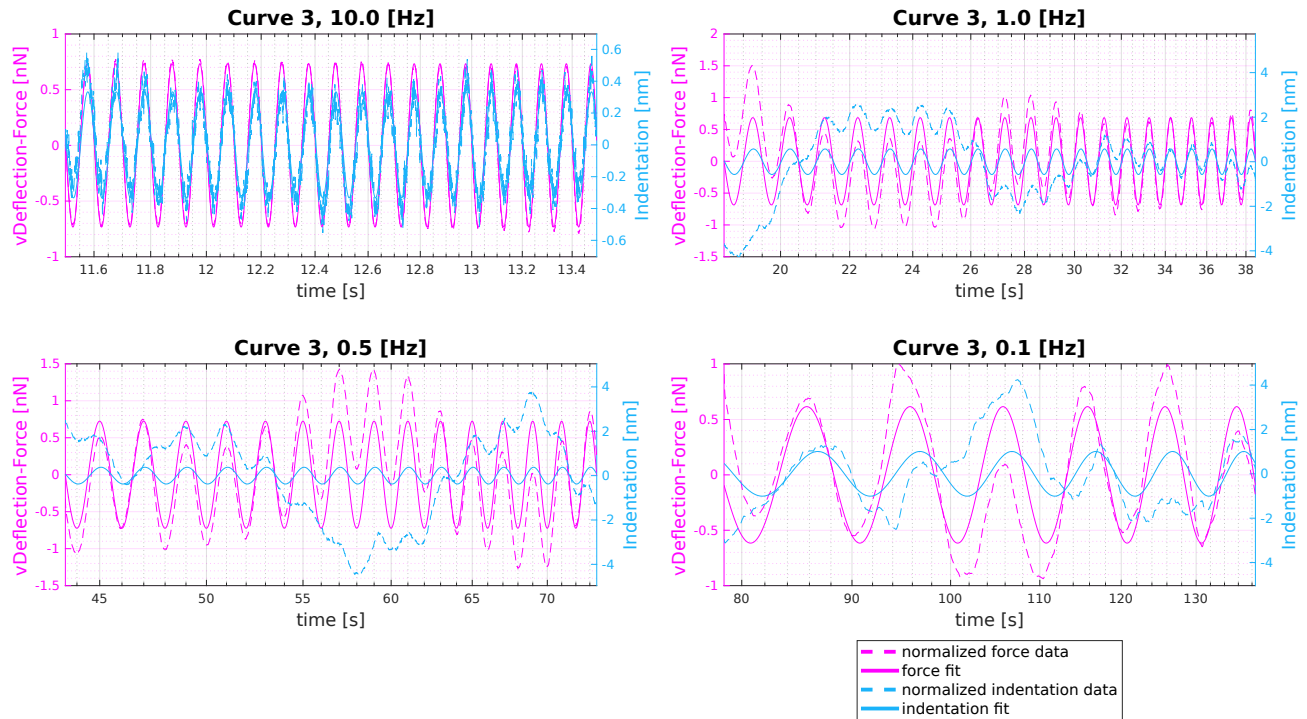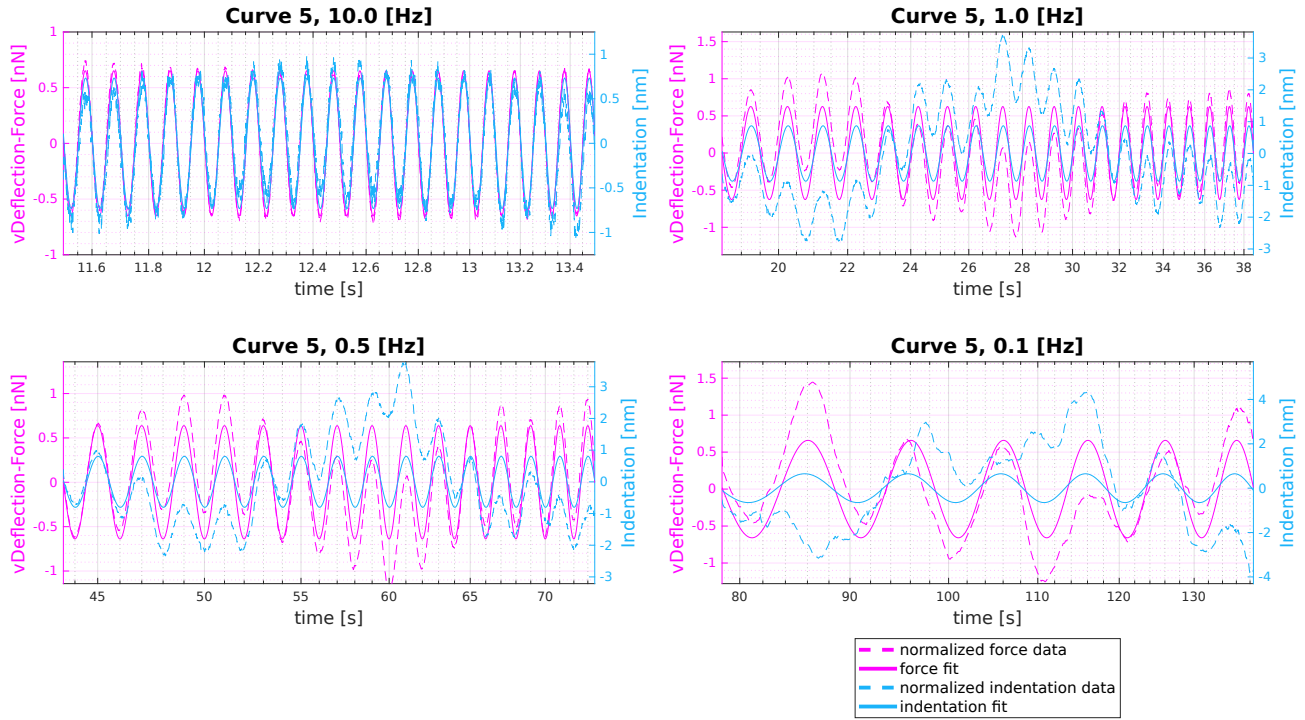
Figure 38: These four plots show the force and indentation signals over all measured frequencies with the respective sine fit of H170 CDET fibril 1 curve 5, which is not clearly identified as a point on fibril.

H170 CDET				
fibril 2 (apex 4)				
dynamic		D. approach slope	D. retraction slope	D. indentation depth (nm)
apex 4		0,666	0,78	8,31
frequency	0.1 Hz	0.5 Hz	1 Hz	10 Hz
amplitude force (nm)	0,64	0,62	0,618	0,62
amplitude indentation (nm)	0,74	0,89	0,91	0,89
phase shift ϕ (°)	10,34	-1,1	0,166	1,38
loss tangent	0,183	-0,019	0,0029	0,024
storage modulus E′ (MPa)	16,85	13,71	13,38	13,82
loss modulus E″ (MPa)	3,08	NaN	0,039	0,33

Table 22: In this table the material response of fibril 2 of H170 CDET at point 4 is visible. Force amplitude and indentation amplitude lay closer at this point and the storage modulus values are higher, that's why another point is searched for.
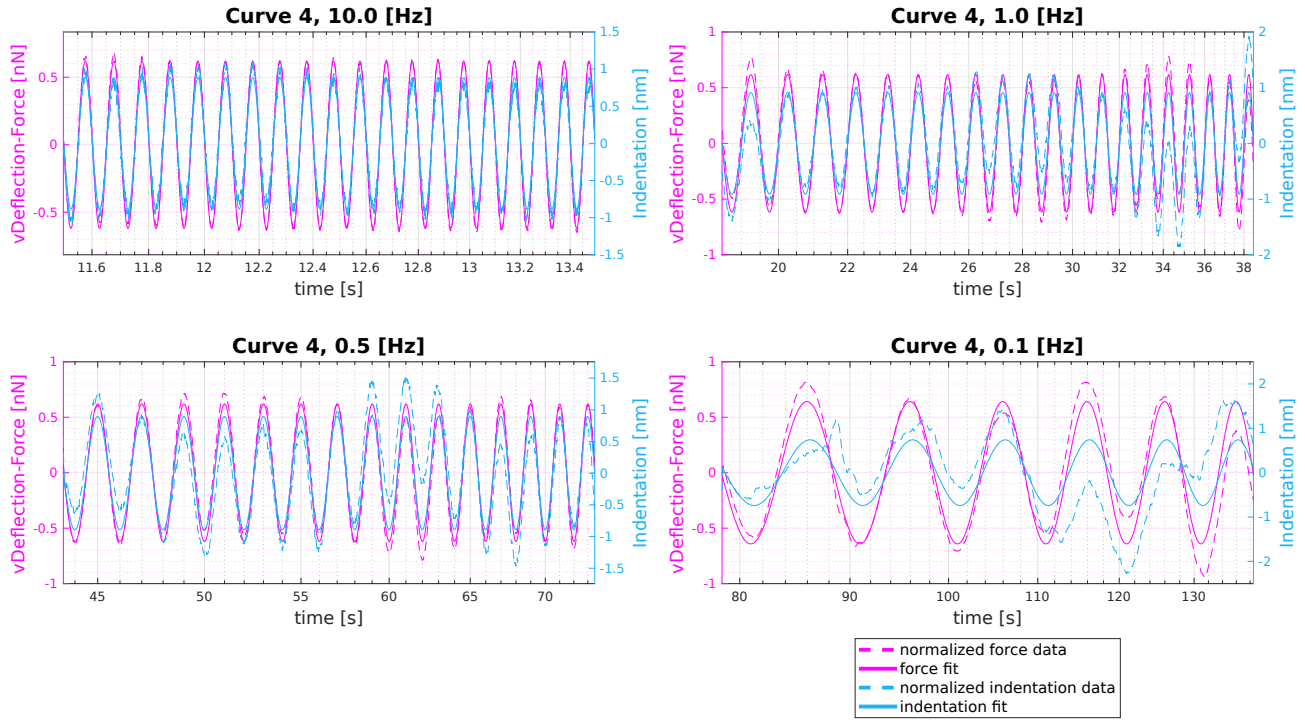
Figure 39: These four plots show the force and indentation signals over all measured frequencies with the respective sine fit of H170 CDET fibril 2 curve 4.

H170 CDET				
fibril 2 (point 6)				
dynamic		D. approach slope	D. retraction slope	D. indentation depth (nm)
point 6		0,509	0,759	45,21
frequency	0.1 Hz	0.5 Hz	1 Hz	10 Hz
amplitude force (nm)	0,6	0,59	0,56	0,56
amplitude indentation (nm)	0,92	1,06	1,18	1,17
phase shift ϕ (°)	-9,25	3,61	3,61	4,65
loss tangent	-0,163	0,0631	0,0631	0,0813
storage modulus E' (MPa)	4,89	4,19	3,59	3,63
loss modulus E'' (MPa)	NaN	0,265	0,23	0,295

Table 23: In this table the material response of fibril 2 of H170 CDET at point 6 is visible. The indentation depth seems high, but indentation amplitude is nearly twice as big as force amplitude and storage modulus range is also plausible.
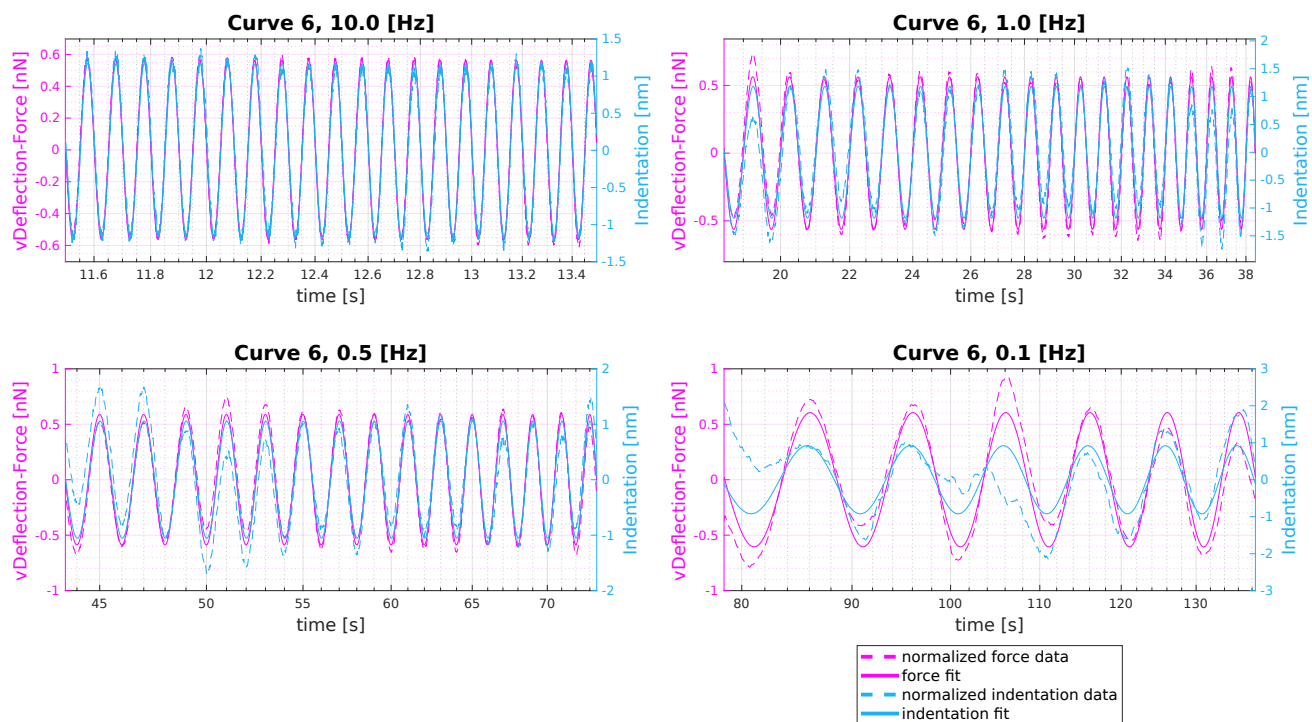
Figure 40: These four plots show the force and indentation signals over all measured frequencies with the respective sine fit of H170 CDET fibril 2 curve 6, which was identified as point on fibril.

H170 CDET				
fibril 3 (apex 5)				
dynamic		D. approach slope	D. retraction slope	D. indentation depth (nm)
apex 5		0,585	0,653	2,56
frequency	0.1 Hz	0.5 Hz	1 Hz	10 Hz
amplitude force (nm)	0,52	0,546	0,54	0,55
amplitude indentation (nm)	1,33	1,26	1,29	1,25
phase shift ϕ (°)	1,63	1,86	2,3	2,95
loss tangent	0,0284	0,0324	0,0401	0,0516
storage modulus E′ (MPa)	20,58	22,66	22,11	22,82
loss modulus E″ (MPa)	0,58	0,73	0,89	1,18

Table 24: In this table the material response of fibril 3 of H170 CDET at point 5 is visible. The values for the storage modulus are disproportionately high, which may have something to do with the very low indentation depth.
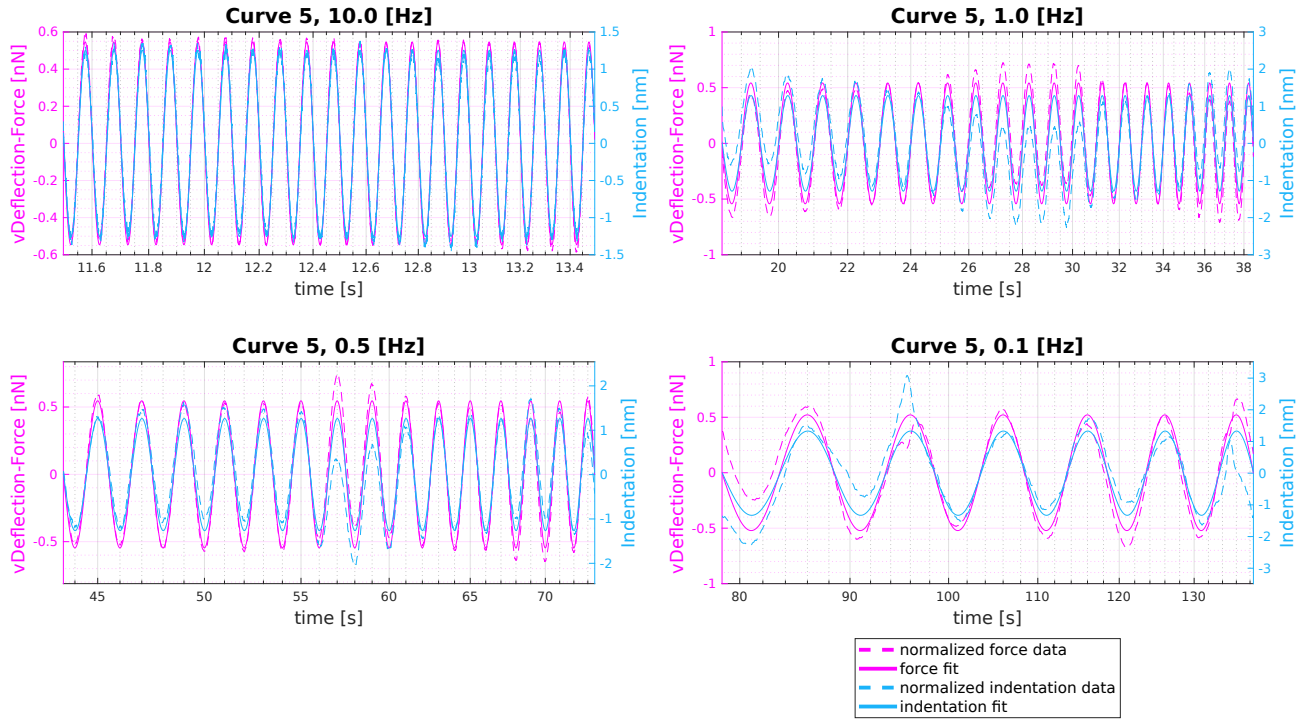
Figure 41: These four plots show the force and indentation signals over all measured frequencies with the respective sine fit of H170 CDET fibril 3 curve 5.

H170 CDET				
fibril 3 (point 6)				
dynamic		D. approach slope	D. retraction slope	D. indentation depth (nm)
point 6		0,531	0,632	16,96
frequency	0.1 Hz	0.5 Hz	1 Hz	10 Hz
amplitude force (nm)	0,53	0,52	0,51	0,51
amplitude indentation (nm)	1,28	1,41	1,43	1,44
phase shift ϕ (°)	1,98	2,42	0,903	1,75
loss tangent	0,0346	0,0422	0,0158	0,0305
storage modulus E$'$ (MPa)	5,41	4,75	4,66	4,59
loss modulus E$''$ (MPa)	0,19	0,2	0,073	0,14

Table 25: In this table the material response of fibril 3 of H170 CDET at point 6 is visible. Here storage modulus are again in a plausible range. The phase shifts at this point are very small compared to the other points on H170 CDET, which could be due to good data quality. Following this assumption, data at 1 Hz is expected to be good. This becomes more apparent when looking at the sine fit plots 42. Storage modulus values decrease with increasing frequency, but this can easily be a coincidence.

Figure 42: These four plots show the force and indentation signals over all measured frequencies with the respective sine fit of H170 CDET fibril 3 curve 6, which was identified as point on fibril. This is a rare example where the indentation data at 0.1 Hz can be fitted quite well with a simple sine wave.

H170 CDET				
fibril 4 (apex 3)				
dynamic		D. approach slope	D. retraction slope	D. indentation depth (nm)
apex 3		0,867	0,894	13,61
frequency	0.1 Hz	0.5 Hz	1 Hz	10 Hz
amplitude force (nm)	0,72	0,71	0,708	0,725
amplitude indentation (nm)	0,34	0,43	0,46	0,37
phase shift ϕ (°)	1,09	0,87	4,28	7,51
loss tangent	0,019	0,0152	0,0748	0,1318
storage modulus E' (MPa)	31,7	24,72	22,86	29,29
loss modulus E'' (MPa)	0,6	0,38	1,71	3,86

Table 26: In this table the material response of fibril 4 of H170 CDET at point 3 is visible. The indentation amplitude is much smaller than the force amplitude, storage and loss modulus are larger than expected - unfortunately no other point shows better results, therefore this fibril does not contribute to the mean value calculation.
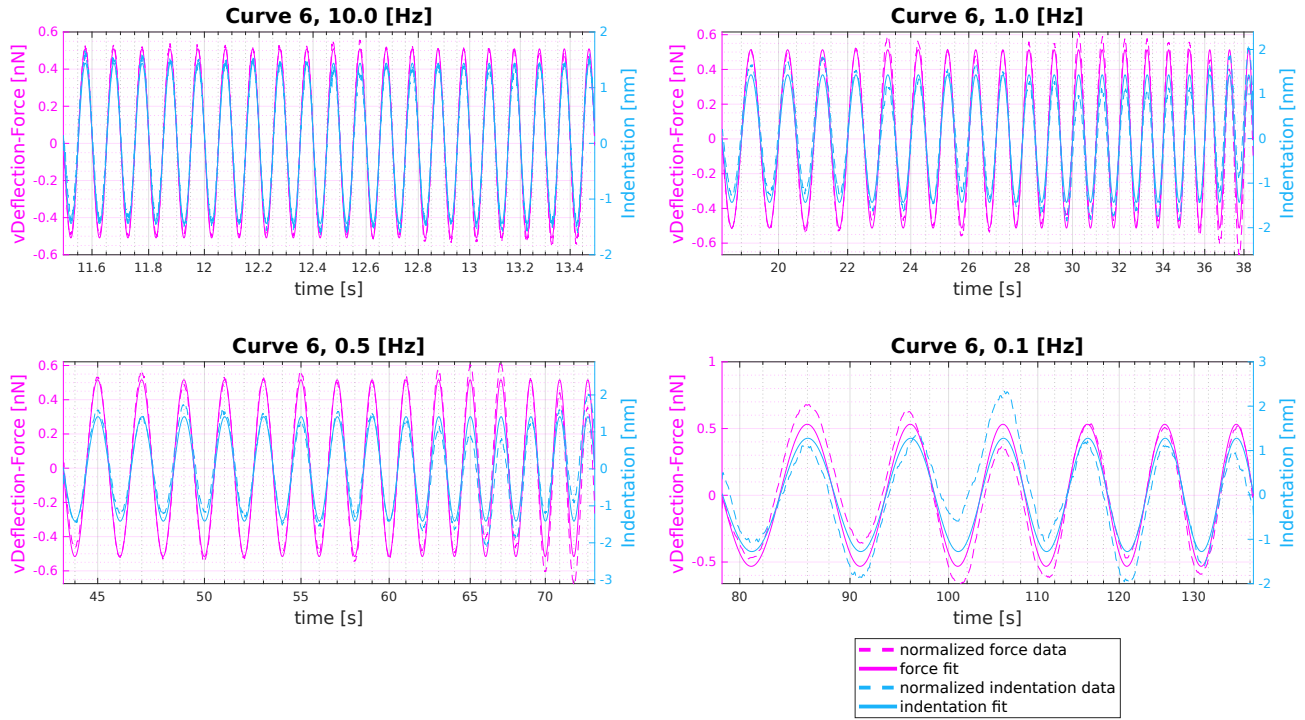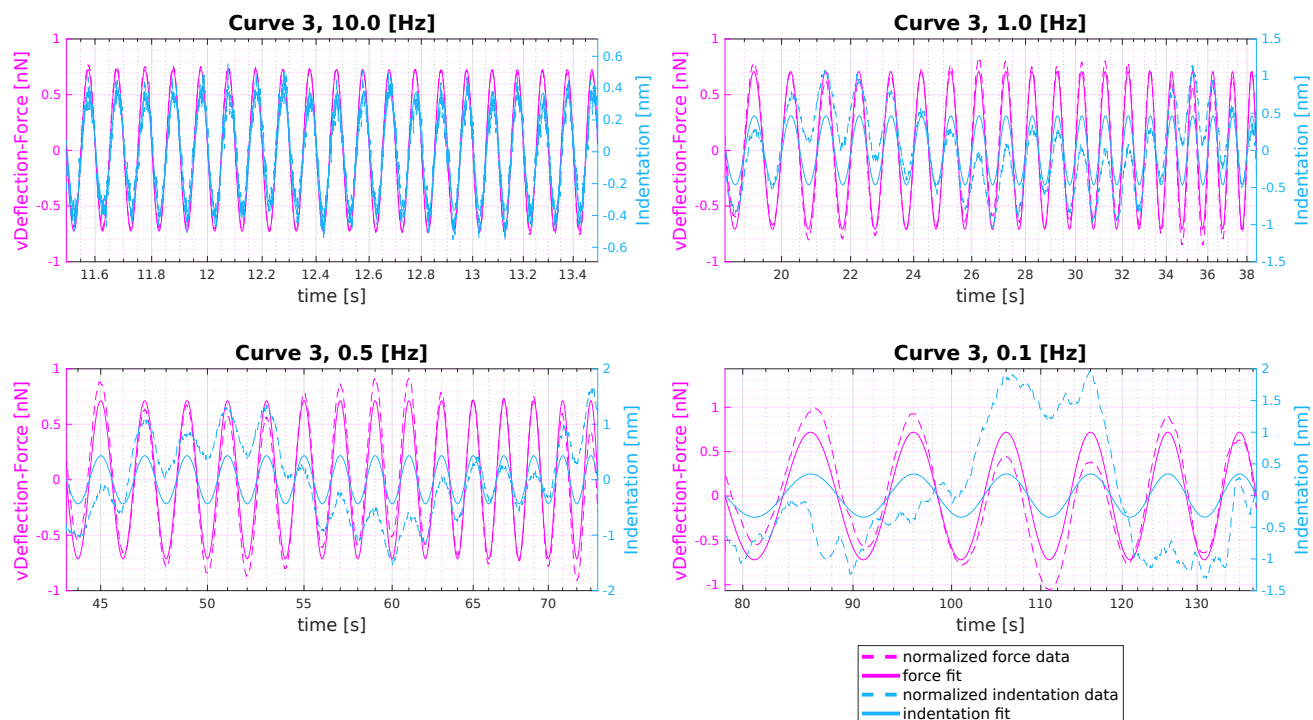
Figure 43: These four plots show the force and indentation signals over all measured frequencies with the respective sine fit of H170 CDET fibril 4 curve 3. The plots show very noisy data across all frequencies.

H170 CDET				
fibril 5 (apex 4)				
dynamic		D. approach slope	D. retraction slope	D. indentation depth (nm)
apex 4		0,693	0,789	9,42
frequency	0.1 Hz	0.5 Hz	1 Hz	10 Hz
amplitude force (nm)	0,56	0,62	0,596	0,61
amplitude indentation (nm)	1,15	0,87	1,02	0,93
phase shift ϕ (°)	4,42	2,03	2,41	4,96
loss tangent	0,0773	0,0355	0,042	0,0868
storage modulus E' (MPa)	8,77	13,02	10,64	11,85
loss modulus E'' (MPa)	0,68	0,46	0,45	1,03

Table 27: In this table the material response of fibril 5 of H170 CDET at point 4 is visible. Storage modulus is higher than expected with values around 10 MPa, which is why another plausible point on fibril 5 should be analyzed.
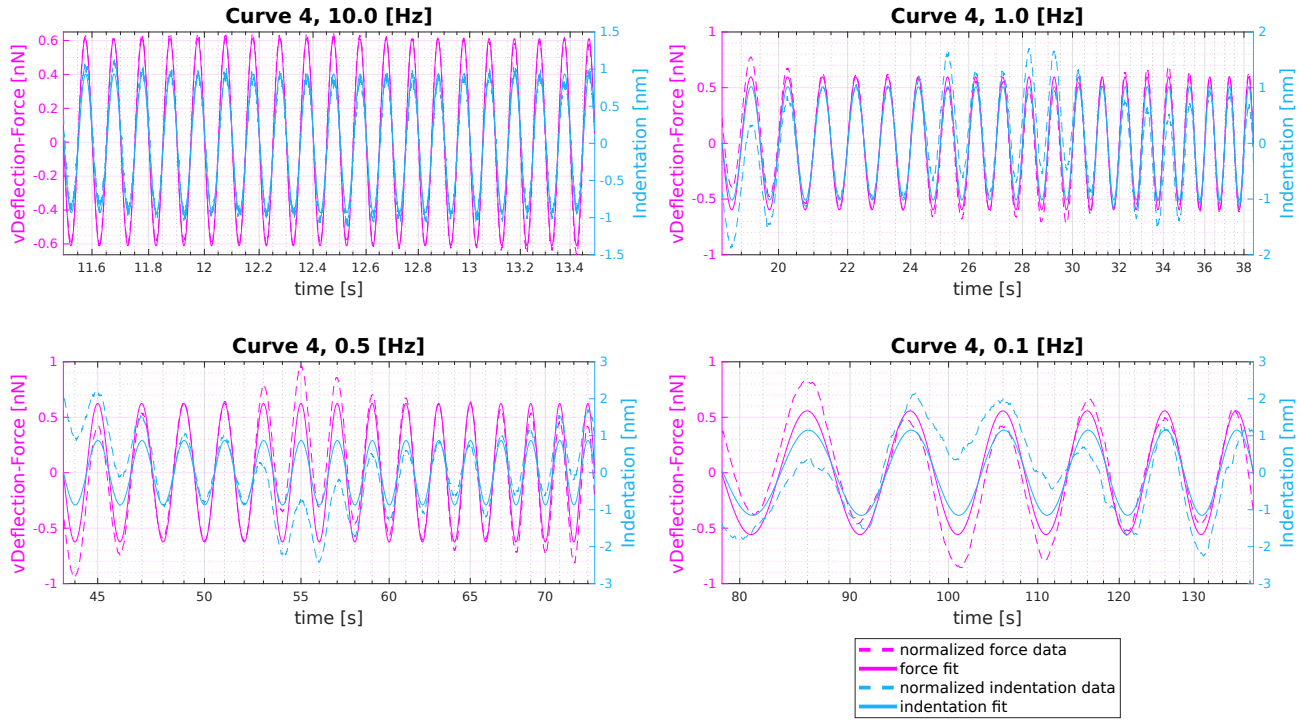
Figure 44: These four plots show the force and indentation signals over all measured frequencies with the respective sine fit of H170 CDET fibril 5 curve 4.

H170 CDET			
fibril 5 (point 5)			
dynamic		D. approach slope	D. retraction slope	D. indentation depth (nm)
point 5		0,579	0,71	98,98
frequency	0.1 Hz	0.5 Hz	1 Hz	10 Hz
amplitude force (nm)	0,59	0,57	0,569	0,567
amplitude indentation (nm)	0,99	1,13	1,155	1,15
phase shift ϕ (°)	-8,8	-1,66	4,56	5,11
loss tangent	-0,155	-0,0291	0,0798	0,0894
storage modulus E$'$ (MPa)	2,64	2,29	2,21	2,21
loss modulus E$''$ (MPa)	NaN	NaN	0,18	0,2

Table 28: In this table the material response of fibril 5 of H170 CDET at point 5 is visible. The indentation depth is very high and the storage modulus values are very low, which is why this point should not be included in the mean value calculation.
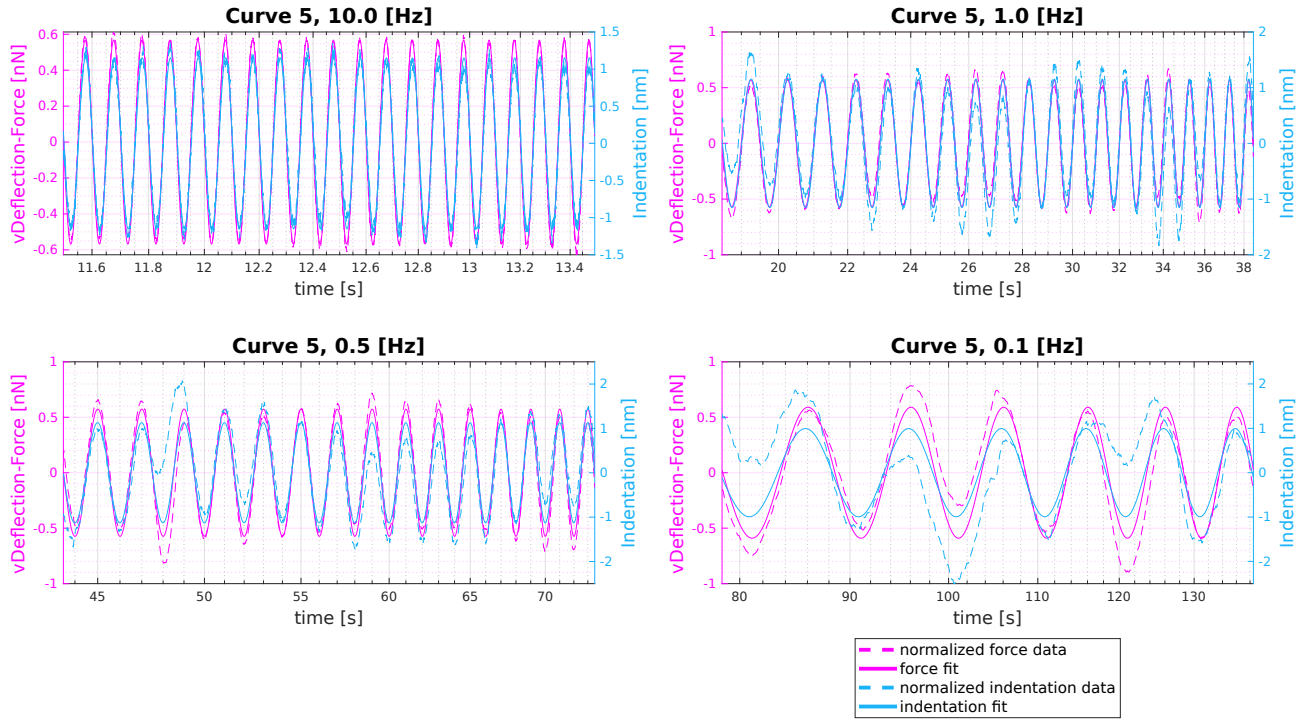
Figure 45: These four plots show the force and indentation signals over all measured frequencies with the respective sine fit of H170 CDET fibril 5 curve 5.

H169 SDFT				
fibril 1 (apex 5)				
		D. approach slope	D. retraction slope	D. indentation depth (nm)
		0,586	0,861	37,8
frequency	0.1 Hz	0.5 Hz	1 Hz	10 Hz
amplitude force (nm)	0,686	0,58	0,578	0,58
amplitude indentation (nm)	0,491	0,996	1	0,988
phase shift ϕ (°)	41,31	4,35	4,91	8,56
loss tangent	0,879	0,0761	0,0858	0,151
storage modulus E' (MPa)	8,83	4,885	4,8	4,89
loss modulus E'' (MPa)	7,76	0,372	0,412	0,736

Table 29: In this table the material response from fibril 1 of H169 SDFT at his automatically calculated 'apex' (point 5) is visible. The indentation modulus from the quasistatic indentation experiment, which took place before the dynamic experiment, is comparable to the resulting storage modulus values of the dynamic experiment (see table 11). Over the different frequencies, with an exception for 0.1 Hz, there is no great change in storage modulus. It is noticeable that the force amplitude is always half the indentation amplitude, except for the measurement at 0.1 Hz. The phase shift is ten times higher than at the higher frequencies, which also leads to a relatively high loss modulus at 0.1 Hz leads. The Sine Fit Plot shows that the signal at 0.1 Hz cannot be fitted so easily.

Figure 46: These four plots show the force and indentation signals over all measured frequencies with the respective sine fit of H169 SDFT fibril 1 curve 5, which was identified as point on fibril. The strange results from table 29 are easy to understand when looking at the indentation curve at 0.1 Hz.

H169 SDFT			
fibril 2 (apex 5)			
dynamic		D. approach slope	D. retraction slope	D. indentation depth (nm)
		0,696	0,82	18
frequency	0.1 Hz	0.5 Hz	1 Hz	10 Hz
amplitude force (nm)	0,61	0,64	0,66	0,71
amplitude indentation (nm)	0,81	0,67	0,56	0,35
phase shift ϕ (°)	14,15	3,94	6.73	15,34
loss tangent	0,252	0,0689	0,118	0,274
storage modulus E' (MPa)	9,34	12,28	15,19	24,73
loss modulus E'' (MPa)	2,36	0,846	1,79	6,78

Table 30: In this table the material response from fibril 2 of H169 SDFT at his automatically calculated 'apex' (point 5) is visible. Larger force amplitudes than indentation amplitudes may indicate that tissue is not being tested at that selected point. Compared to the other selected points, results for storage and loss modulus are also significantly higher, which is why this data set is excluded from the mean value calculation.
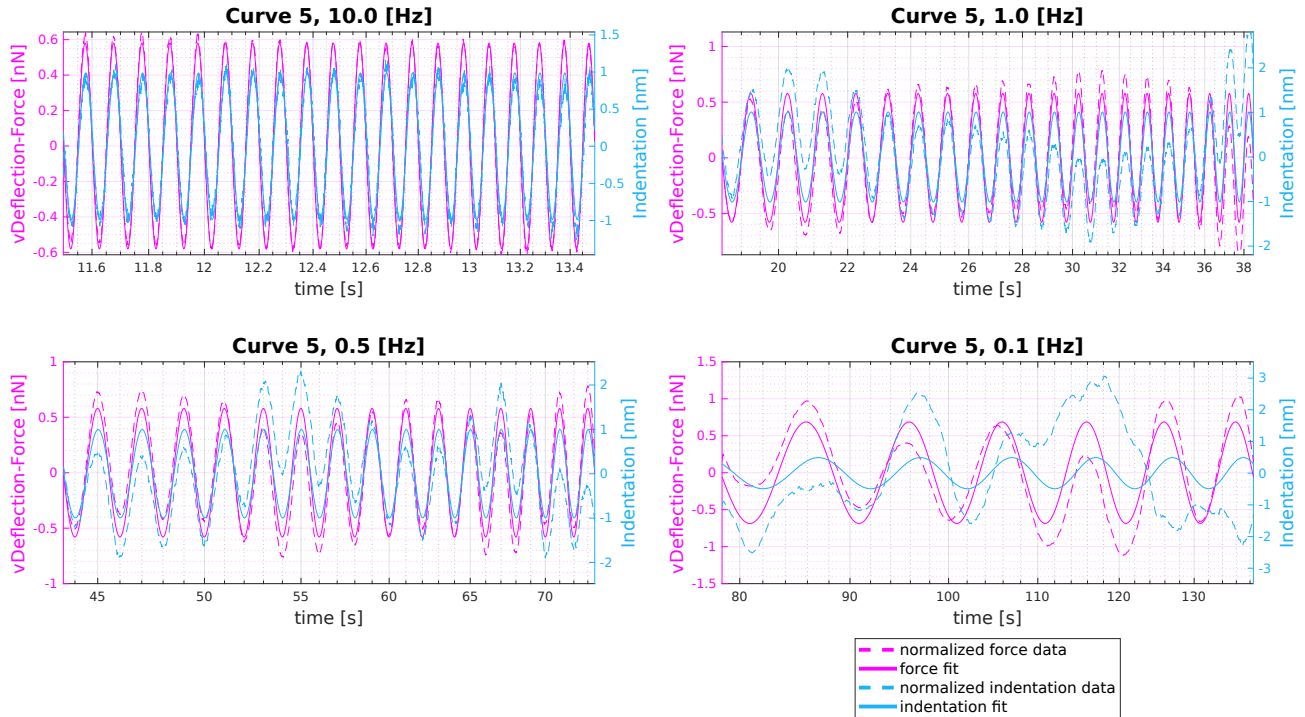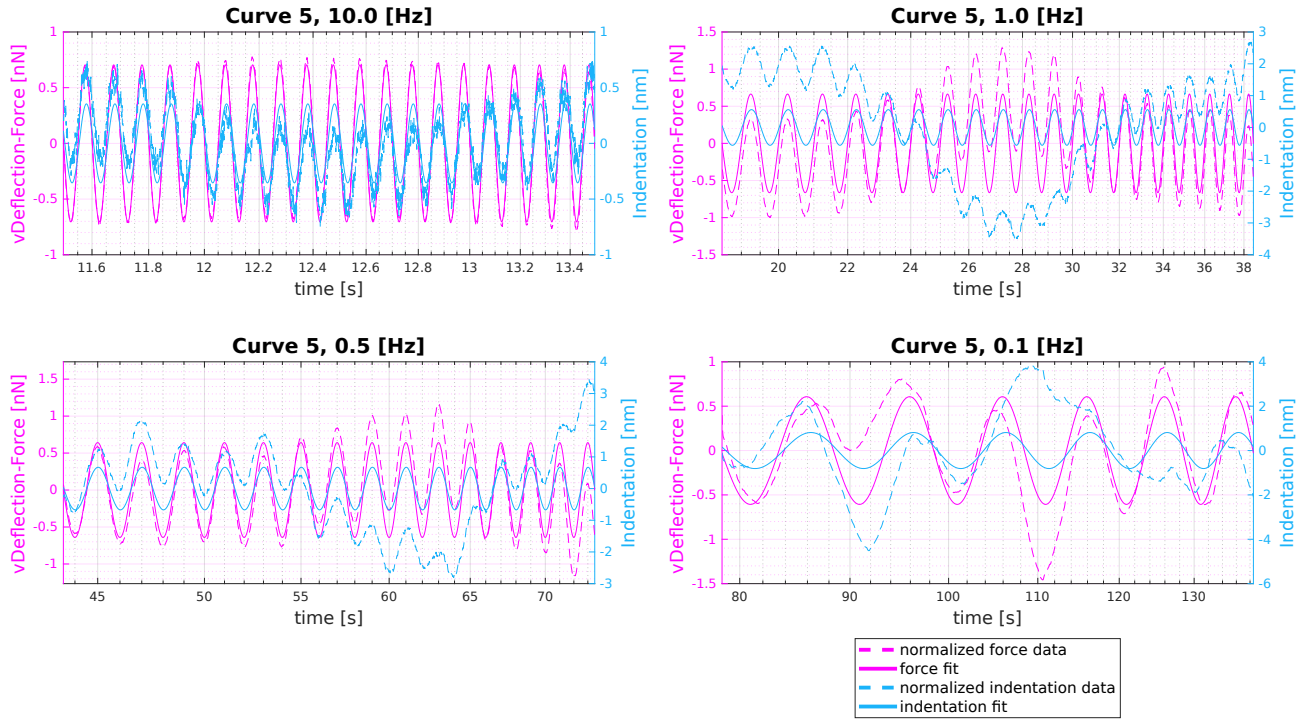
Figure 47: These four plots show the force and indentation signals over all measured frequencies with the respective sine fit of H169 SDFT fibril 2 curve 5.

H169 SDFT				
fibril 3 (apex 5)				
dynamic		D. approach slope	D. retraction slope	D. indentation depth (nm)
		0,926	1,07	3,16
frequency	0.1 Hz	0.5 Hz	1 Hz	10 Hz
amplitude force (nm)	0,74	0,85	0,78	0,77
amplitude indentation (nm)	0,25	0,42	0,11	0,11
phase shift ϕ (°)	-299,15	-187,84	135,89	101,16
loss tangent	1,79	-0,14	-0,97	-5,07
storage modulus E' (MPa)	58,32	NaN	NaN	NaN
loss modulus E'' (MPa)	104,55	10,97	196,2	283,93

Table 31: In this table the material response from fibril 3 of H169 SDFT at his automatically calculated 'apex' (point 5) is visible. Very high phase shifts, larger force amplitudes relative to indentation amplitudes, and a slope of the retraction curve of 1 suggest that not fibril is indented at this point, so a more plausible point is chosen - point 6.
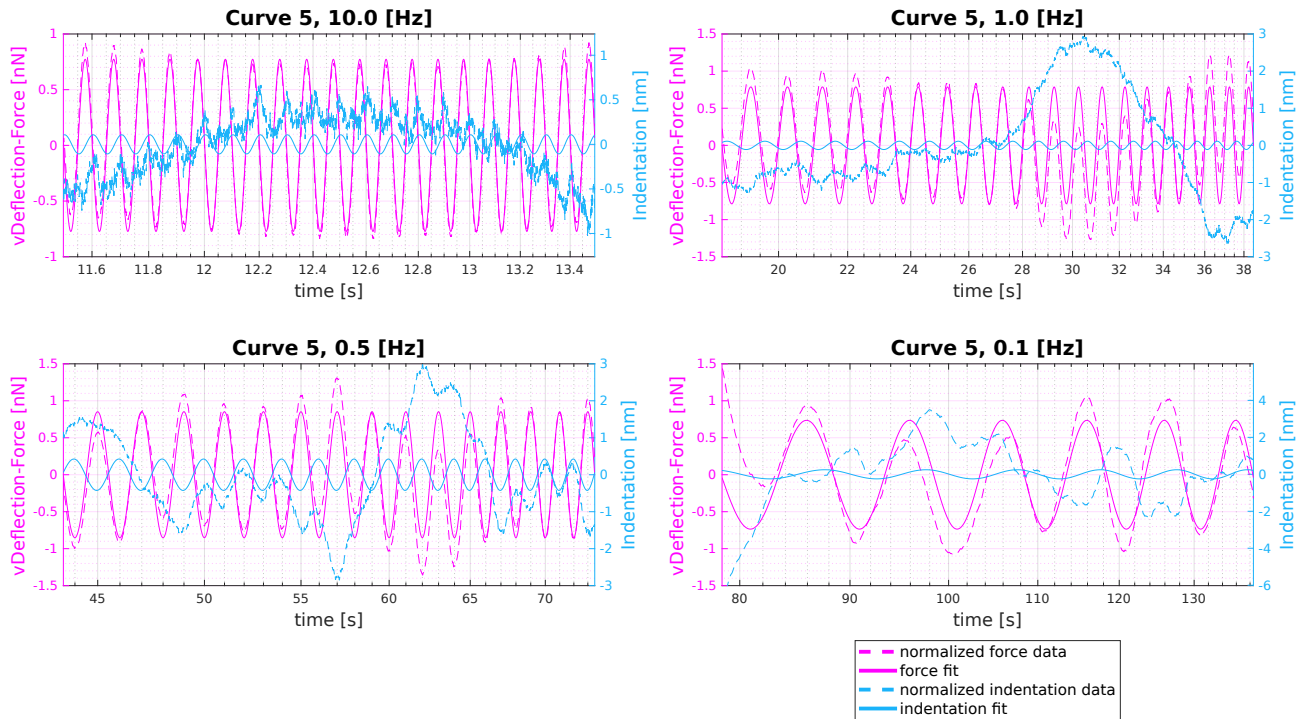
Figure 48: These four plots show the force and indentation signals over all measured frequencies with the respective sine fit of H169 SDFT fibril 3 curve 5, which was identified as point on glass.

H169 SDFT				
fibril 3 (point 6)				
dynamic		D. approach slope	D. retraction slope	D. indentation depth (nm)
		0,679	0,876	15,6
frequency	0.1 Hz	0.5 Hz	1 Hz	10 Hz
amplitude force (nm)	0,62	0,49	0,54	0,62
amplitude indentation (nm)	0,75	1,45	1,2	0,82
phase shift ϕ (°)	14,55	9,39	9,71	14,45
loss tangent	0,26	0,165	0,171	0,258
storage modulus E′ (MPa)	10,96	4,62	6,11	10,02
loss modulus E″ (MPa)	2,84	0,76	1,05	2,58

Table 32: In this table the material response of fibril 3 of H169 SDFT at point 6 is visible. When looking at fibril 1 (see table 29), it is noticeable that the storage modulus differs only slightly at the higher frequencies. However, this point of fibril 3 shows strongly fluctuating storage modulus data. Also, the amplitudes of force and indentation are closer together at 0.1 Hz and 10 Hz. In order to be able to explain this behavior, one has to look at the sine fit plot 49. One can consider excluding the data at 0.1 Hz and at 10 Hz in order to counteract implausible outliers in the mean value calculation.
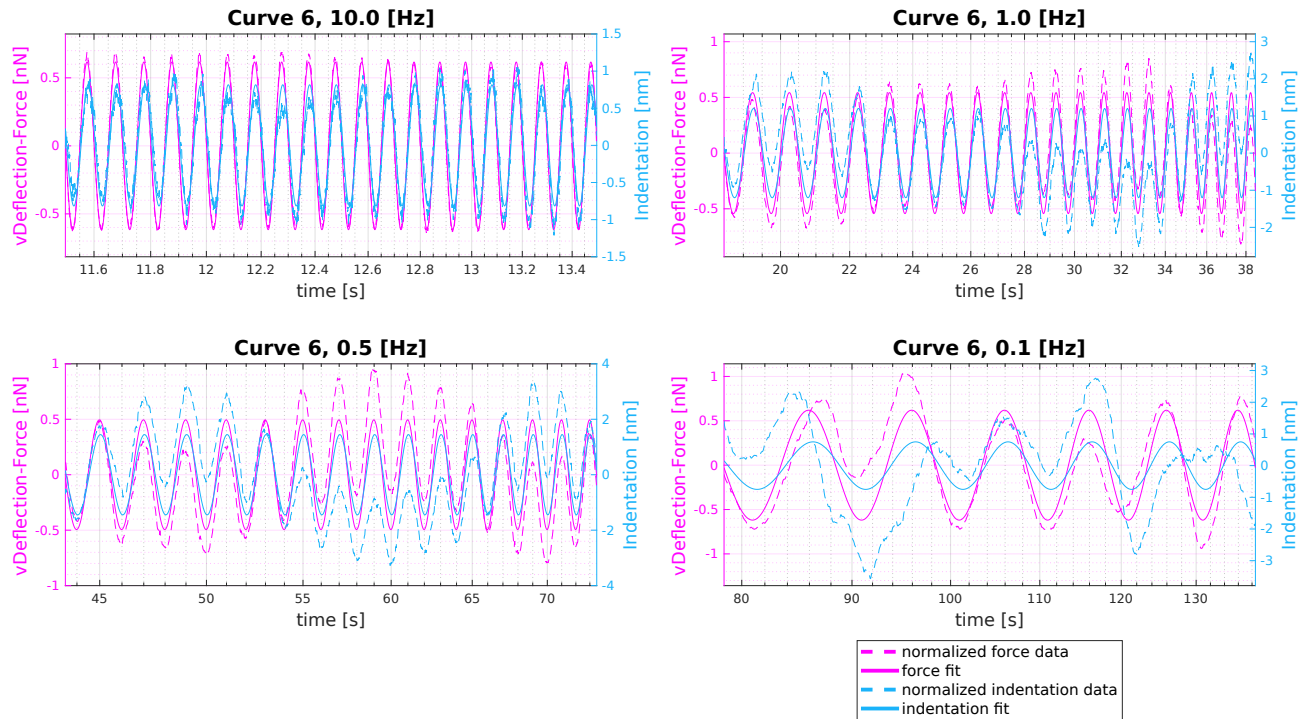
Figure 49: These four plots show the force and indentation signals over all measured frequencies with the respective sine fit of H169 SDFT fibril 3 curve 6.

H169 SDFT				
fibril 4 (apex 6)				
dynamic		D. approach slope	D. retraction slope	D. indentation depth (nm)
		0,807	0,912	14,64
frequency	0.1 Hz	0.5 Hz	1 Hz	10 Hz
amplitude force (nm)	0,66	0,7	0,7	0,7
amplitude indentation (nm)	0,77	0,36	0,38	0,38
phase shift ϕ (°)	52,08	6,97	12,08	21,91
loss tangent	1,28	0,122	0,214	0,402
storage modulus E' (MPa)	7,49	27,37	25,85	24,43
loss modulus E'' (MPa)	9,62	3,35	5,53	9,82

Table 33: In this table the material response of fibril 4 of H169 SDFT at his automatically calculated 'apex' (point 6) is visible. Also here the larger force amplitudes relative to indentation amplitudes suggest that not fibril is indented at this point, so a more plausible point is chosen - point 2.

Figure 50: These four plots show the force and indentation signals over all measured frequencies with the respective sine fit of H169 SDFT fibril 4 curve 6, which was identified as point on glass.

H169 SDFT				
fibril 4 (point 2)				
dynamic		D. approach slope	D. retraction slope	D. indentation depth (nm)
		0,287	0,769	69,42
frequency	0.1 Hz	0.5 Hz	1 Hz	10 Hz
amplitude force (nm)	0,49	0,45	0,45	0,42
amplitude indentation (nm)	1,46	1,66	1,66	1,8
phase shift ϕ (°)	23,77	4,7	5,49	5,75
loss tangent	0,44	0,082	0,096	0,1
storage modulus E$'$ (MPa)	1,78	1,53	1,55	1,34
loss modulus E$''$ (MPa)	0,78	0,126	0,149	0,134

Table 34: In this table the material response of fibril 4 of H169 SDFT at point 6 is visible. Indentation amplitude is much bigger than force amplitude. Storage modulus and loss modulus data is very small and close together for frequencies higher than 0.5 Hz.
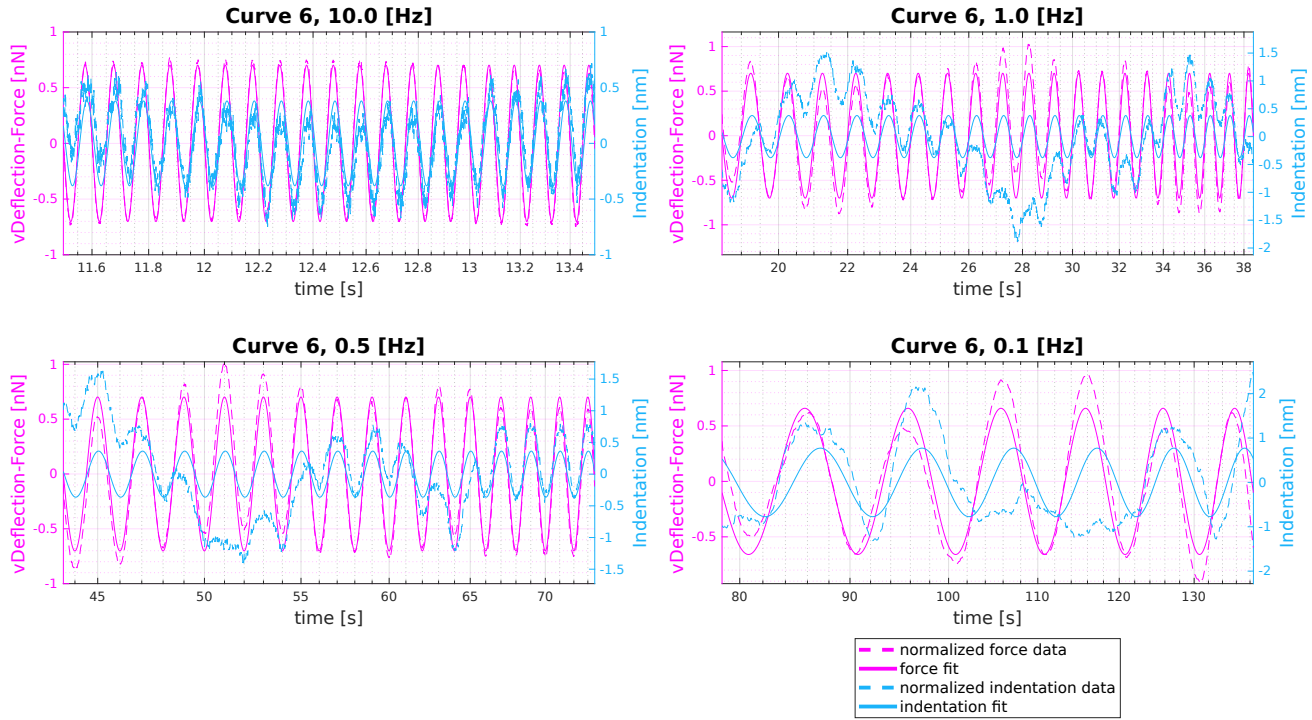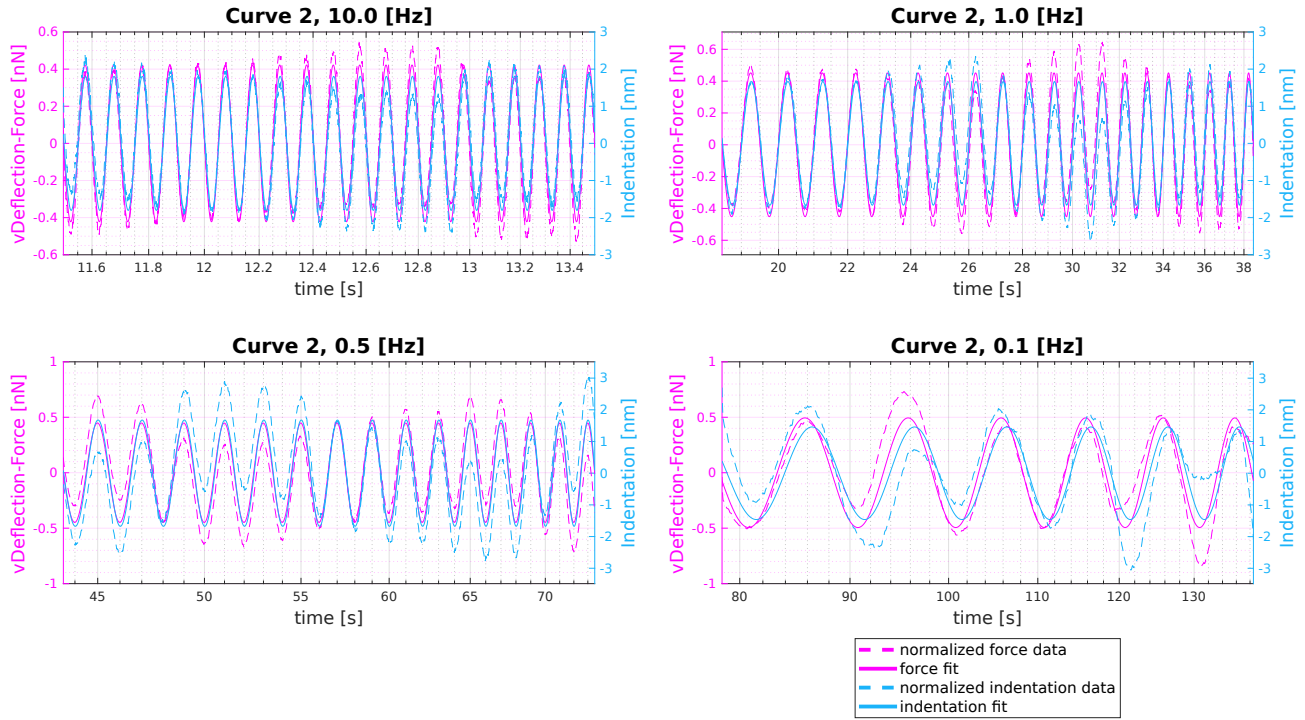
Figure 51: These four plots show the force and indentation signals over all measured frequencies with the respective sine fit of H169 SDFT fibril 4 curve 2.

H169 SDFT				
fibril 5 (point 3)				
dynamic		D. approach slope	D. retraction slope	D. indentation depth (nm)
		0,965	0,921	22,2
frequency	0.1 Hz	0.5 Hz	1 Hz	10 Hz
amplitude force (nm)	0,68	0,67	0,66	0,57
amplitude indentation (nm)	0,97	0,87	0,92	1,33
phase shift ϕ (°)	-294,85	8,2	6,61	7,18
loss tangent	2,16	0,144	0,116	0,126
storage modulus E' (MPa)	3,33	8,56	7,94	4,77
loss modulus E'' (MPa)	7,19	1,23	0,92	0,602

Table 35: In this table the material response of fibril 5 of H169 SDFT at point 3 is visible. After looking at 5 fibrils of H169 SDFT one could say that the bigger the difference between force and indentation amplitude, the smaller the storage modulus. The middle frequencies lead to comparable storage and loss modulus values.
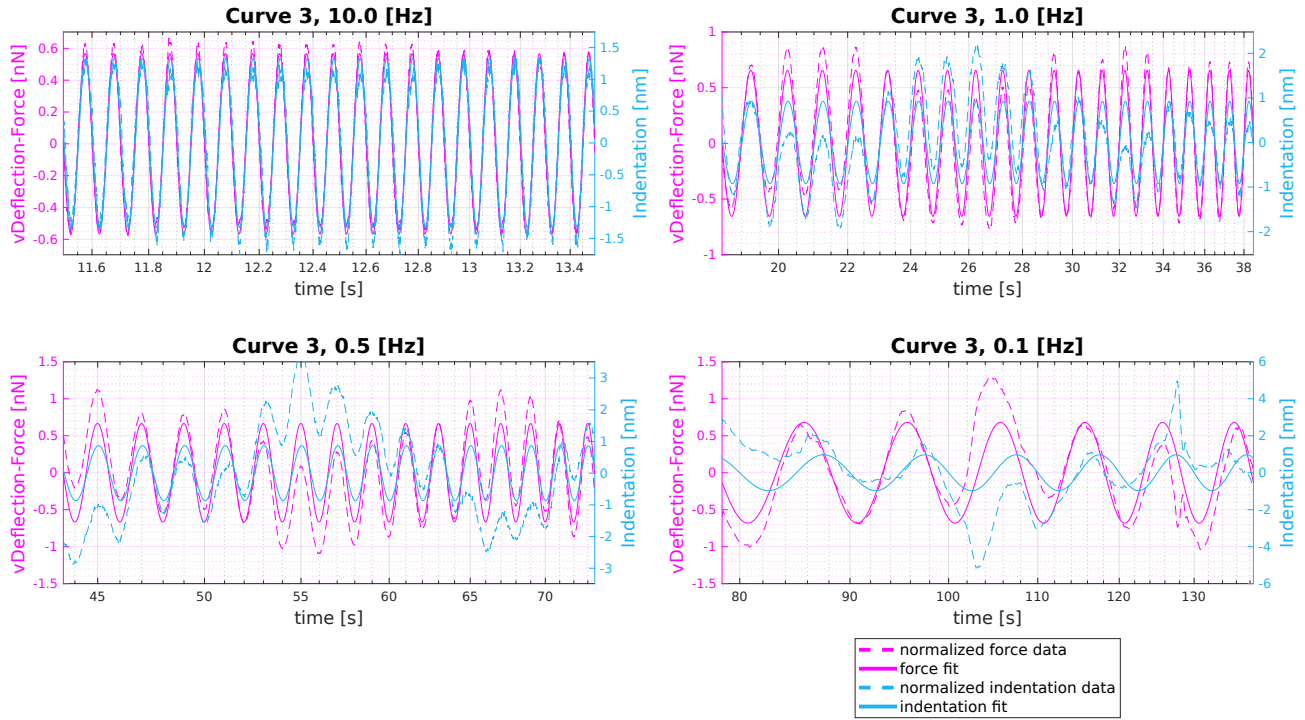
Figure 52: These four plots show the force and indentation signals over all measured frequencies with the respective sine fit of H169 SDFT fibril 5 curve 3.

H170 SDFT

H170 SDFT				
fibril 1 (apex 5)				
dynamic		D. approach slope	D. retraction slope	D. indentation depth (nm)
		0,586	0,683	21,4
frequency	0.1 Hz	0.5 Hz	1 Hz	10 Hz
amplitude force (nm)	0,41	0,52	0,51	0,52
amplitude indentation (nm)	1,83	1,24	1,31	1,24
phase shift ϕ (°)	-16,8	0,62	0,77	1,95
loss tangent	-0,302	0,0108	0,0135	0,034
storage modulus E' (MPa)	2,45	4,85	4,51	4,85
loss modulus E'' (MPa)	NaN	0,053	0,061	0,165

Table 36: In this table the material response of fibril 1 of H170 SDFT at point 5 is visible. Phase shifts are here quite small compared to the phase shifts visible in H169 SDFT fibrils. Again results from 0.5 Hz and 1 Hz are closer together compared to those from 10 Hz, whereas 0.1 Hz is neglectable. The phase shift might be bigger at 10 Hz, storage modulus is not affected by it compared to the loss modulus.
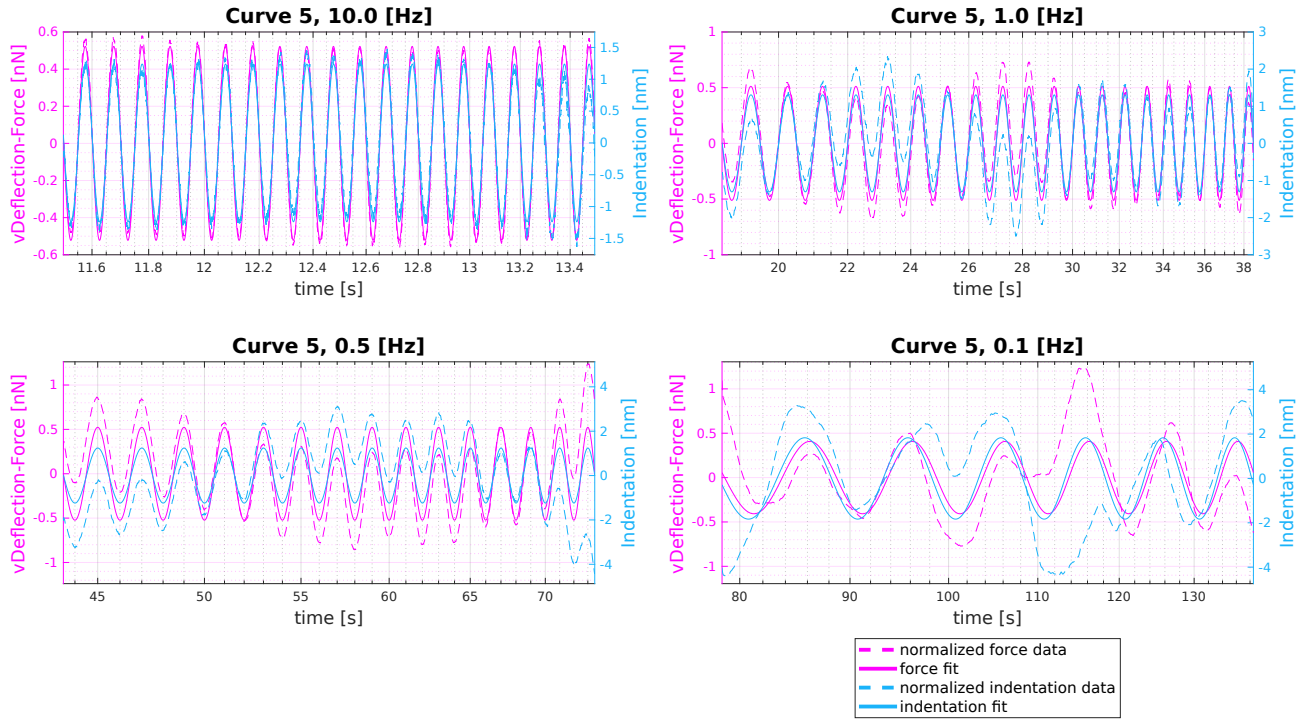
Figure 53: These four plots show the force and indentation signals over all measured frequencies with the respective sine fit of H170 SDFT fibril 1 curve 5, which was identified as point on fibril.

H170 SDFT				
fibril 2 (apex 6)				
dynamic			D. approach slope	D. retraction slope	D. indentation depth (nm)
apex 6			0,67	0,735	13,25
frequency	0.1 Hz	0.5 Hz	1 Hz	10 Hz
amplitude force (nm)	0,48	0,57	0,55	0,55
amplitude indentation (nm)	1,5	1	1,1	1,07
phase shift ϕ (°)	30,02	-1,12	2,34	1,97
loss tangent	0,58	-0,02	0,041	0,034
storage modulus E' (MPa)	4,23	8,54	7,71	7,93
loss modulus E'' (MPa)	2,44	NaN	0,316	0,273

Table 37: In this table the material response of fibril 2 of H170 SDFT at point 6 is visible. Because of the negative phase shift at 0.5 Hz at point 6 of the fibril, point 5 was also considered - the difference between the two points can be seen in the sine fit plots.
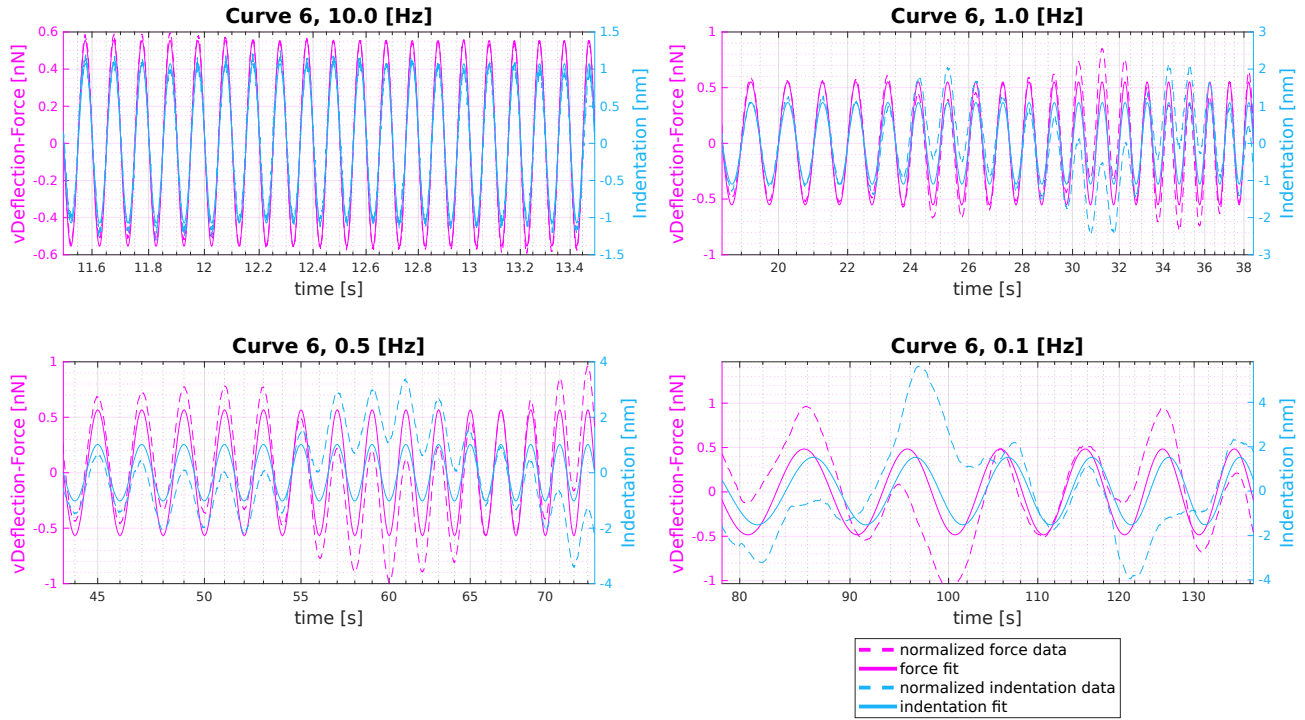
Figure 54: These four plots show the force and indentation signals over all measured frequencies with the respective sine fit of H170 SDFT fibril 2 curve 6.

H170 SDFT				
fibril 2 (point 5)				
dynamic		D. approach slope	D. retraction slope	D. indentation depth (nm)
point 5		0,63	0,753	22,72
frequency	0.1 Hz	0.5 Hz	1 Hz	10 Hz
amplitude force (nm)	0,58	0,55	0,56	0,57
amplitude indentation (nm)	0,98	1,12	1,06	1
phase shift ϕ (°)	27,6	0,49	0,8	2,05
loss tangent	0,52	0,0085	0,014	0,036
storage modulus E' (MPa)	5,83	5,4	5,89	6,3
loss modulus E'' (MPa)	3,05	0,046	0,083	0,226

Table 38: In this table the material response of fibril 2 of H170 SDFT at point 5 is visible. Both slopes of approach and retraction curves are similar to those of point 6, but the indentation depth is higher in this case. Looking at force and indentation amplitudes also assumes a measurement on the material. The phase shifts are comparable to those from fibril 1 of H170 SDFT (see table 36). In storage and loss modulus values a slight increase with frequency is noticeable.
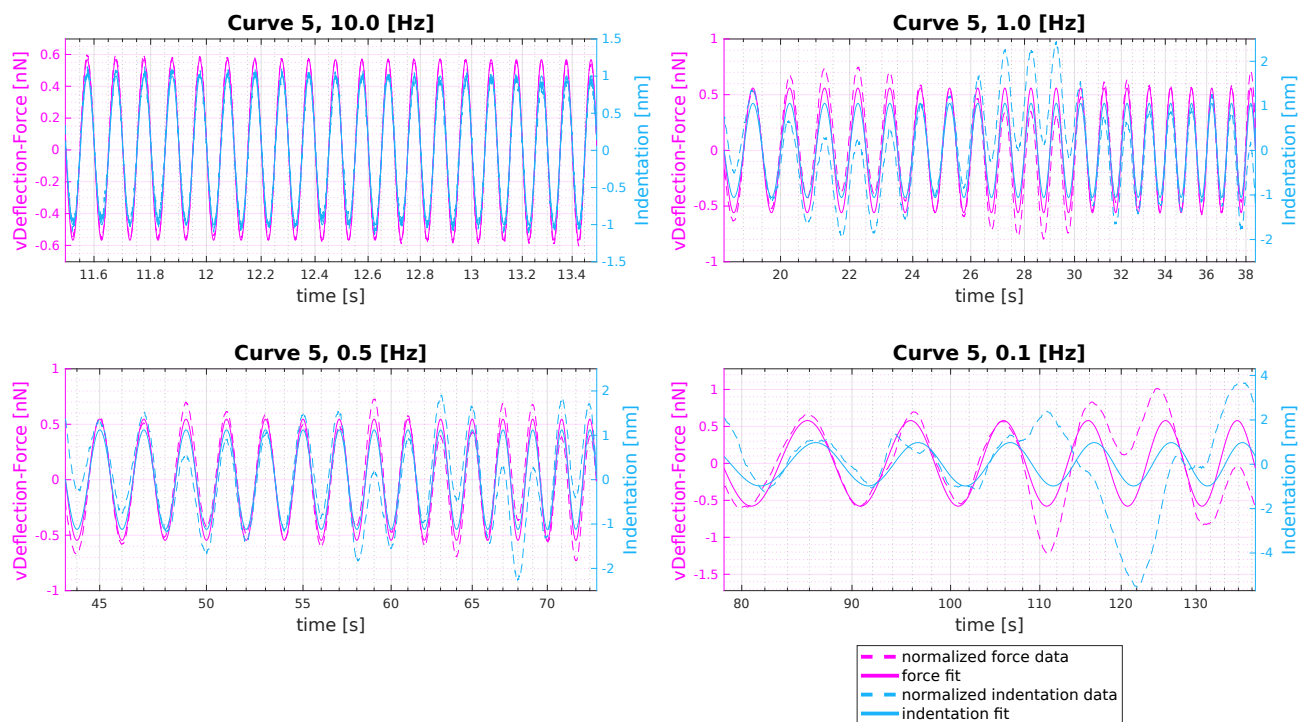
Figure 55: These four plots show the force and indentation signals over all measured frequencies with the respective sine fit of H170 SDFT fibril 2 curve 5, which was identified as point on fibril.

H170 SDFT			
fibril 3 (apex 4)			
dynamic		D. approach slope	D. retraction slope	D. indentation depth (nm)
apex 4		0,63	0,753	22,72
frequency	0.1 Hz	0.5 Hz	1 Hz	10 Hz
amplitude force (nm)	0,55	0,61	0,61	0,64
amplitude indentation (nm)	1,05	0,81	0,79	0,64
phase shift ϕ (°)	-15,23	1,33	2,2	1,65
loss tangent	-0,27	0,023	0,039	0,029
storage modulus E' (MPa)	8,02	11,77	12,17	15,47
loss modulus E'' (MPa)	NaN	0,272	0,468	0,445

Table 39: In this table the material response of fibril 3 of H170 SDFT at point 4 is visible. Except for 0.1 Hz, the force and indentation amplitudes are too close together, so it is better to find a more plausible point - point 7.
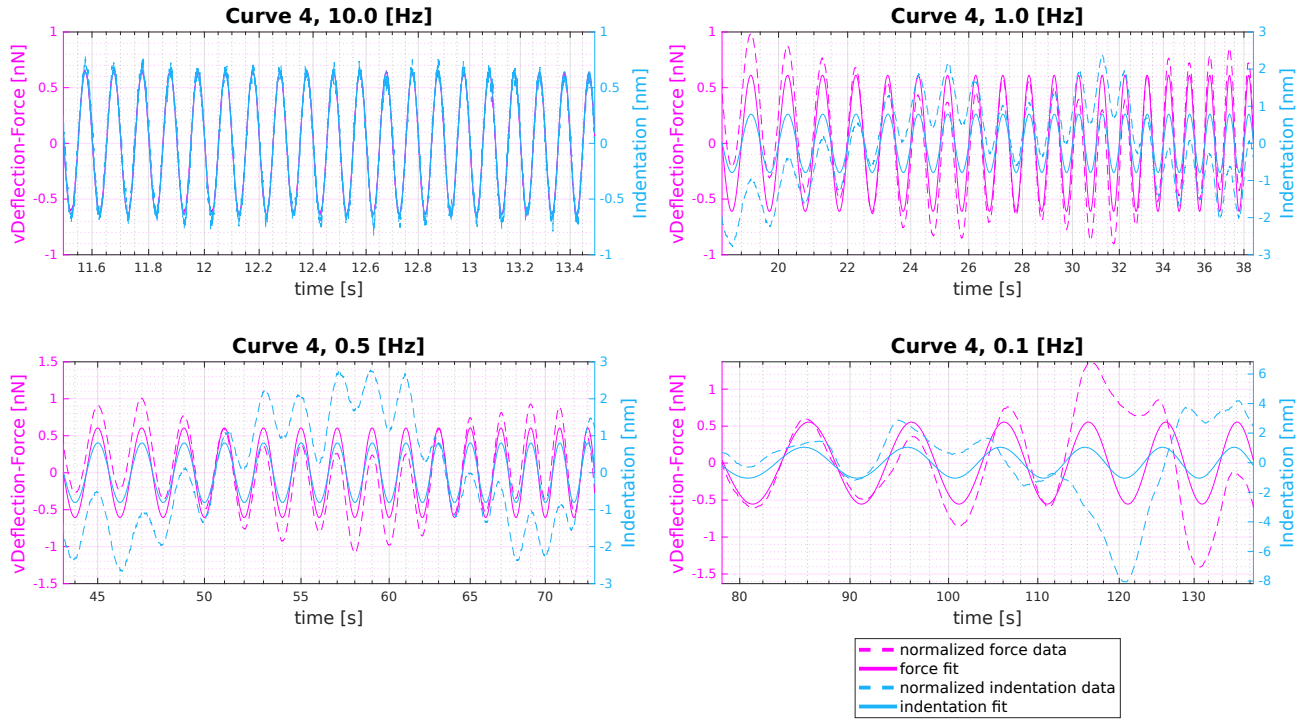
Figure 56: These four plots show the force and indentation signals over all measured frequencies with the respective sine fit of H170 SDFT fibril 3 curve 4.

H170 SDFT				
fibril 3 (point 7)				
dynamic		D. approach slope	D. retraction slope	D. indentation depth (nm)
point 7		0,63	0,753	22,72
frequency	0.1 Hz	0.5 Hz	1 Hz	10 Hz
amplitude force (nm)	0,52	0,57	0,55	0,56
amplitude indentation (nm)	1,2	1	1,12	1,06
phase shift ϕ (°)	-1,99	-1,91	0,9	-1,76
loss tangent	-0,035	-0,033	0,016	-0,031
storage modulus E′ (MPa)	4,65	6,12	5,22	5,66
loss modulus E″ (MPa)	NaN	NaN	0,082	NaN

Table 40: In this table the material response of fibril 3 of H170 SDFT at point 7 is visible. Here the ratio of the amplitudes is again constant over all frequencies. Unfortunately at this point negative phase shifts occur for 0.1Hz, 0.5Hz and 10Hz. This leads to a single loss modulus value for 1 Hz, but which is nearly the same as for fibril 2 (see table 38). As a consequence, only 1 Hz is used from this point for the mean value calculation.
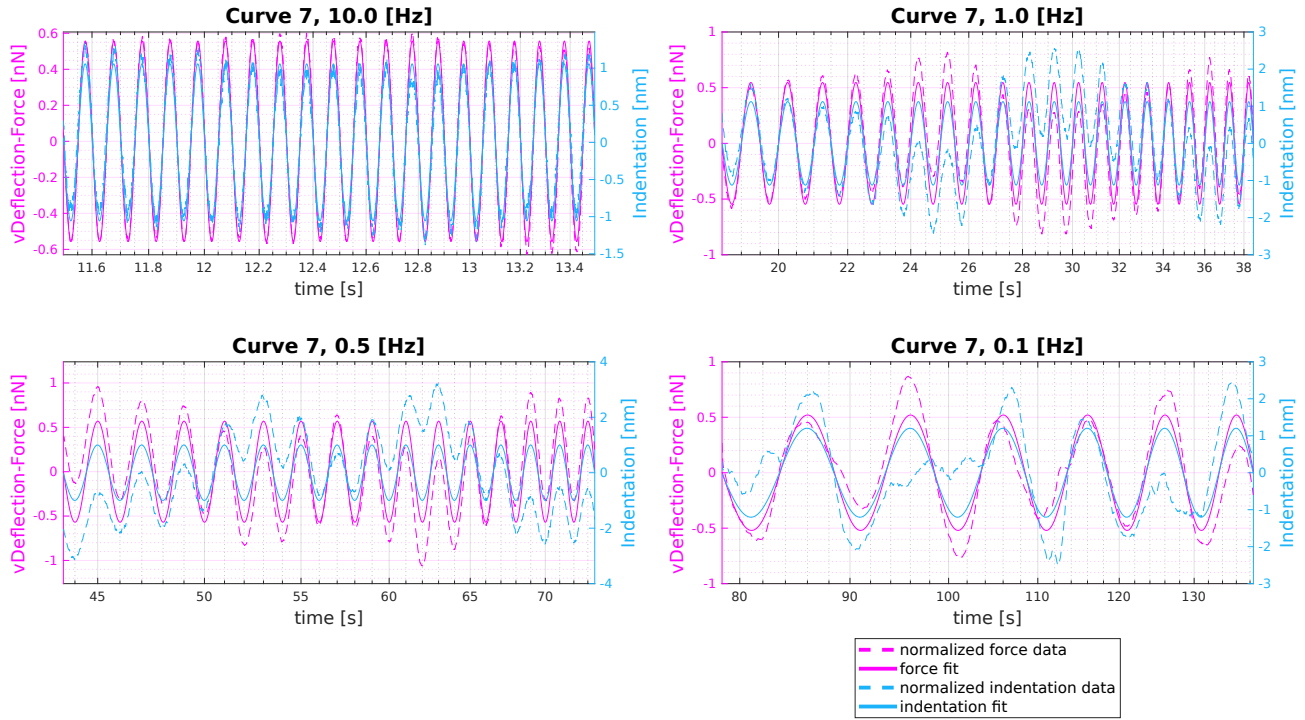
Figure 57: These four plots show the force and indentation signals over all measured frequencies with the respective sine fit of H170 SDFT fibril 3 curve 7.

H170 SDFT				
fibril 4 (apex 5)				
dynamic		D. approach slope	D. retraction slope	D. indentation depth (nm)
apex 5		0,773	0,81	-0,76
frequency	0.1 Hz	0.5 Hz	1 Hz	10 Hz
amplitude force (nm)	0,67	0,62	0,62	0,6
amplitude indentation (nm)	0,52	0,73	0,76	0,81
phase shift ϕ (°)	42,21	-0,55	-1,32	0,48
loss tangent	0,91	-0,01	-0,023	0,0084
storage modulus E$'$ (MPa)	NaN	NaN	NaN	NaN
loss modulus E$''$ (MPa)	NaN	NaN	NaN	NaN

Table 41: In this table the material response of fibril 4 of H170 SDFT at point 5 is visible. In several places the data of this point 5 indicates that it is unusable.
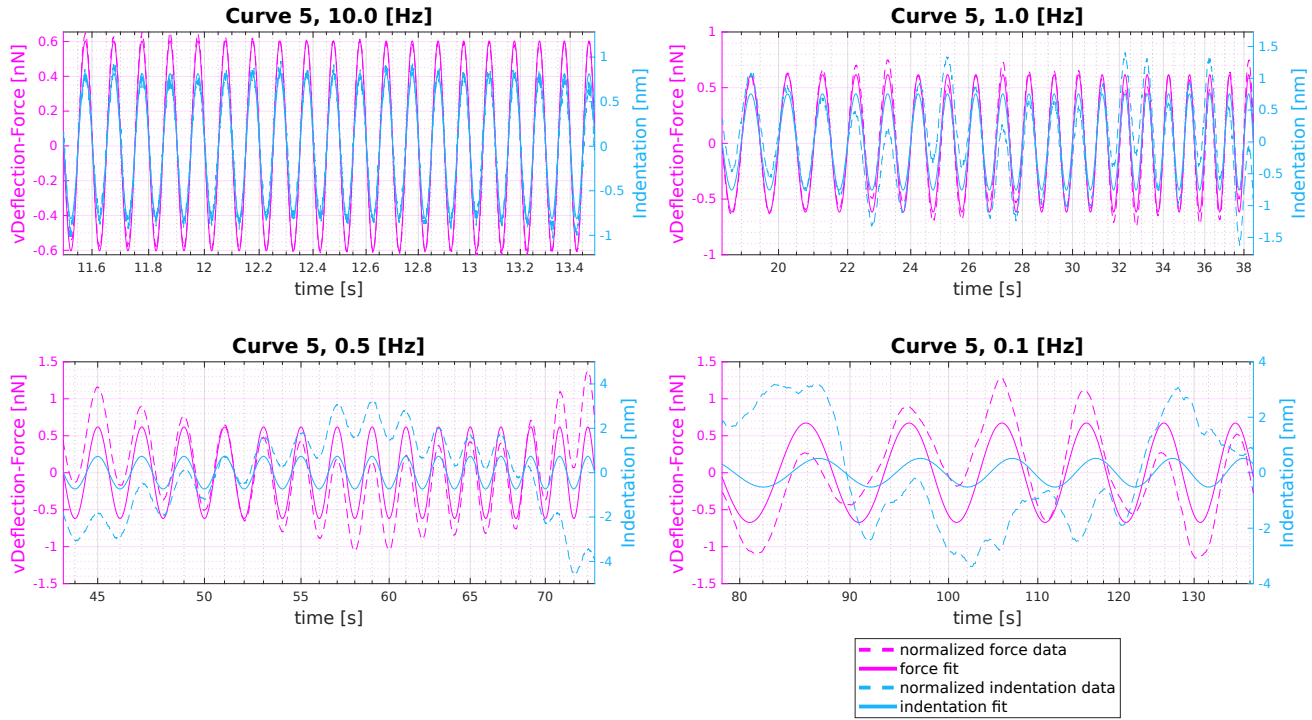
180

Figure 58: These four plots show the force and indentation signals over all measured frequencies with the respective sine fit of H170 SDFT fibril 4 curve 5.

H170 SDFT				
fibril 4 (point 7)				
dynamic			D. approach slope	D. retraction slope	D. indentation depth (nm)
point 7			0,468	0,831	31,63
frequency	0.1 Hz	0.5 Hz	1 Hz	10 Hz
amplitude force (nm)	0,605	0,605	0,6	0,59
amplitude indentation (nm)	0,76	0,81	0,84	0,89
phase shift ϕ (°)	-9,3	-0,86	0,85	1,46
loss tangent	-0,164	-0,0151	0,0149	0,0255
storage modulus E' (MPa)	7,31	6,91	6,62	6,13
loss modulus E'' (MPa)	NaN	NaN	0,1	0,16

Table 42: In this table the material response of fibril 4 of H170 SDFT at point 7 is visible. The data from point 7 (only frequencies 1 Hz and 10 Hz) can be included in the calculation again, even if the amplitude difference is not very large.
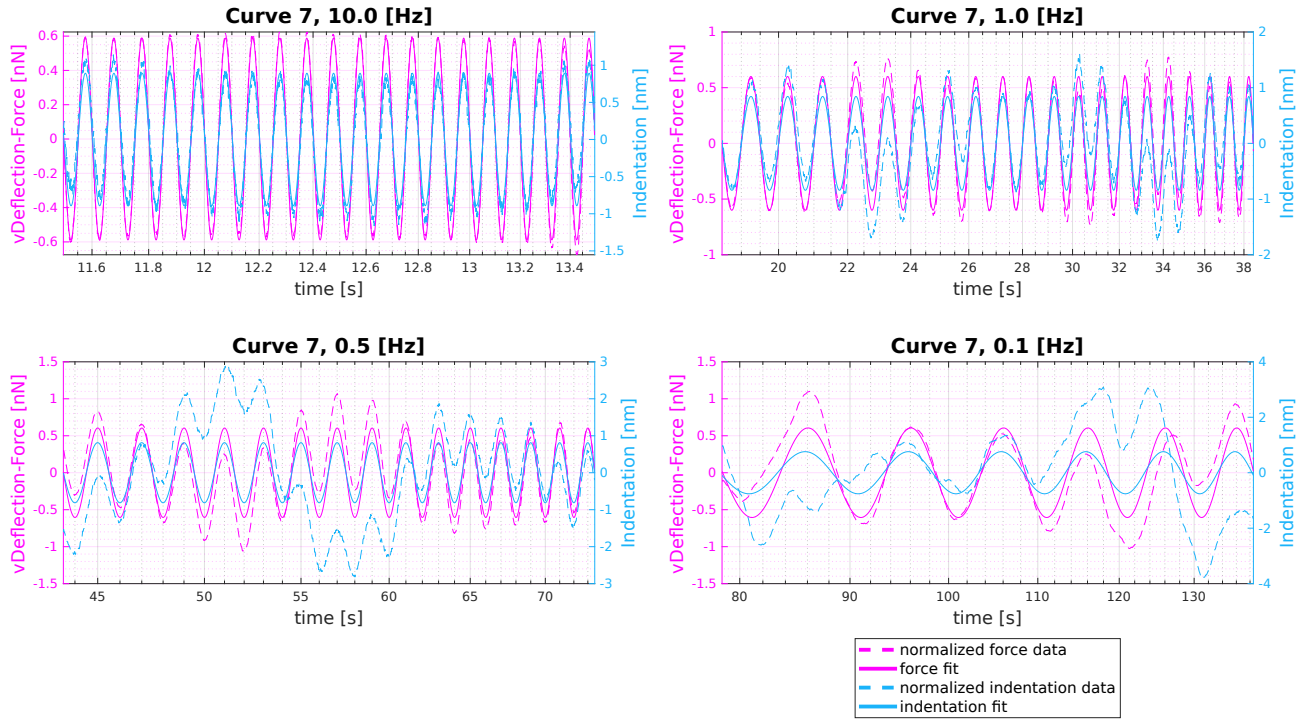
182

Figure 59: These four plots show the force and indentation signals over all measured frequencies with the respective sine fit of H170 SDFT fibril 4 curve 7.

H170 SDFT				
fibril 5 (apex 4)				
dynamic		D. approach slope	D. retraction slope	D. indentation depth (nm)
apex 4		0,716	0,779	11,52
frequency	0.1 Hz	0.5 Hz	1 Hz	10 Hz
amplitude force (nm)	0,586	0,597	0,59	0,6
amplitude indentation (nm)	0,93	0,85	0,89	0,82
phase shift ϕ (°)	26,57	0,63	-0,21	1,65
loss tangent	0,5	0,011	-0,0036	0,0288
storage modulus E' (MPa)	9,24	11,42	10,89	11,91
loss modulus E'' (MPa)	4,62	0,125	NaN	0,34

Table 43: In this table the material response of fibril 5 of H170 SDFT at point 4 is visible. Frequency 1 Hz shows a negative phase shift, that's why this frequency is excluded from the mean value calculation. It is noticeable that the values for the moduli are somewhat higher than for the other tested fibrils of H170 SDFT, which is why these will definitely lead to an upward shift in the mean value if these are taken into account.
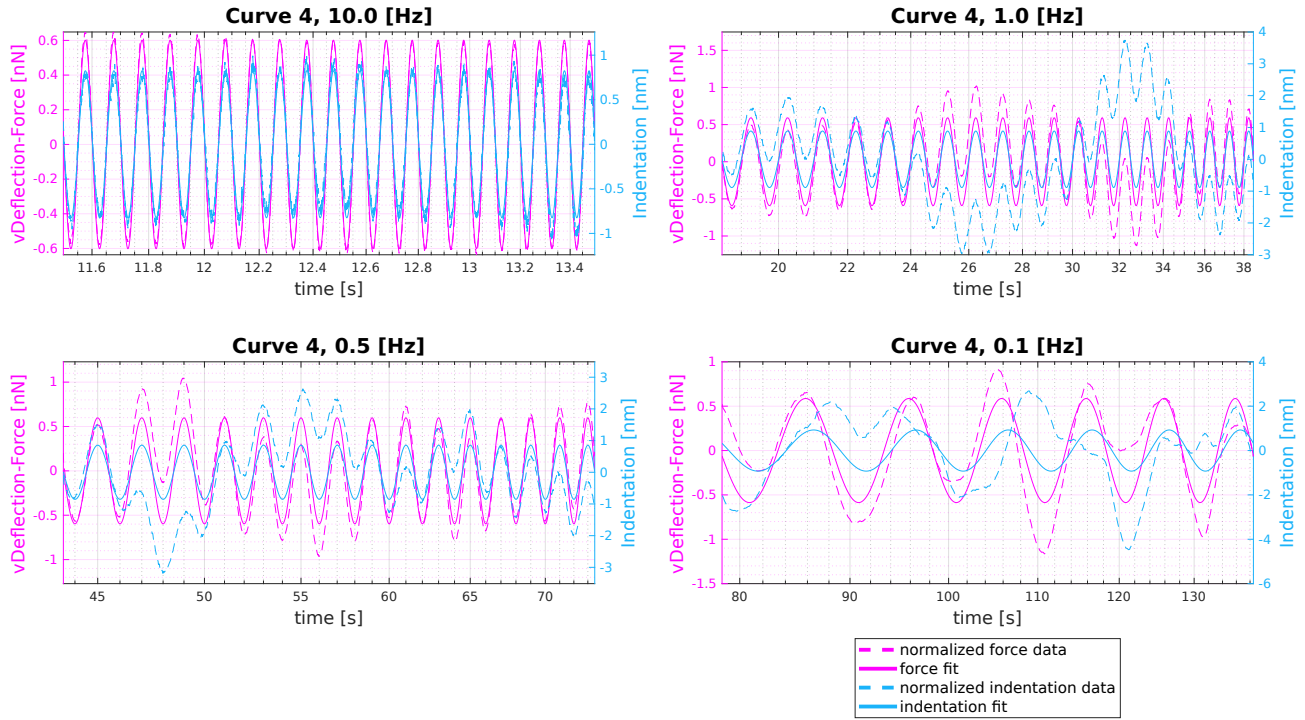
Figure 60: These four plots show the force and indentation signals over all measured frequencies with the respective sine fit of H170 SDFT fibril 5 curve 4.

Results from Experiment 2

The results are processed in the same way as for Experiment 1. After the quasi-static measurements, the four samples (H169 CDET, H169 CDET with MGO, H169 SDFT, H169 SDFT with MGO) are tested with a measurement protocol consisting of four frequencies.

Quasi-static

The quasi-static test procedure is the exact same as in Experiment 1: Approach, 10 seconds force controlled hold, retraction.

H169 CDET			
quasistatic test			
fibril	indentation modulus (MPa)	Q. approach slope	Q. retraction slope	Q. indentation depth (nm)
1	4.96	0.511	0.668	22.1
2	5.41	0.475	0.656	16.96
3	6.56	0.605	0.727	22.15
4	6.98	0.572	0.744	23.24

Table 44: In this table the results of quasistatic (stephold) experiments on 4 fibrils of H169 CDET are visible. Compared to the values of the first experiment, see table 9, they seem a bit higher but overall in a comparable range.

H169 CDET with MGO			
quasistatic test			
fibril	indentation modulus (MPa)	Q. approach slope	Q. retraction slope	Q. indentation depth (nm)
1	7.19	0.518	0.746	16.9
2	2.18	0.29	0.515	23.59
3	6	0.571	0.696	15.13
4	9.64	0.593	0.757	11.21

Table 45: In this table the results of quasistatic (stephold) experiments on 4 fibrils of H169 CDET with MGO are visible. The exact same 4 fibrils are measured again after the MGO treatment. Except for fibril 2 they show higher indentation moduli - this lower value should be excluded from mean value calculation.

H169 SDFT			
quasistatic test			
fibril	indentation modulus (MPa)	Q. approach slope	Q. retraction slope	Q. indentation depth (nm)
1	5.51	0.555	0.675	16.52
2	4.39	0.46	0.687	27.87
3	3.81	0.392	0.691	37.02
4	5.07	0.435	0.723	29.04

Table 46: In this table the results of quasistatic (stephold) experiments on 4 fibrils of H169 SDFT are visible. These indentation modulus values are slightly lower than in experiment 1 (table 11), but this can also simply be due to the scattering of the data.

H169 SDFT with MGO			
quasistatic test			
fibril	indentation modulus (MPa)	Q. approach slope	Q. retraction slope	Q. indentation depth (nm)
1	5.59	0.355	0.744	21.97
2	8.49	0.459	0.795	17.52
3	6.6	0.413	0.81	33.05
4	8.35	0.403	0.817	22.98

Table 47: In this table the results of quasistatic (stephold) experiments on 4 fibrils of H169 SDFT with MGO are visible. Indentation modulus values are significantly higher than before the MGO treatment (compare table 46).

H169 CDET

Before treatment with MGO, four fibrils of the sample were selected and tested with the defined frequency-dependent protocol. At first glance, the sinusoidal course of the deflection/force data was satisfactory, but an analysis of the data revealed that the course of the indentation data was very noisy. The slope of the approach and the retraction curve were around 1, which speaks against indentation into the material. At over 15 MPa, the values for the storage modulus are so high that none of the measurements can ultimately be accepted as valid.

H169 CDET with MGO

This sample is the only one of the four tested in Experiment 2 whose results from the dynamic measurement can be put into the larger context. However, the data situation was similar to that of the other samples: only a few points provided any data at all. The results at these points are checked for plausibility below.

H169 CDET with MGO				
fibril 1 (point 6)				
dynamic		D. approach slope	D. retraction slope	D. indentation depth (nm)
		0.61	0.769	36.48
frequency	0.5 Hz	1 Hz	5 Hz	10 Hz
amplitude force (nm)	0.57	0.586	0.597	0.61
amplitude indentation (nm)	1.01	0.94	0.89	0.83
phase shift ϕ (°)	5.25	2.66	5.02	5.7
loss tangent	0.0919	0.0465	0.0878	0.0998
storage modulus E′ (MPa)	4.79	5.3	5.7	6.24
loss modulus E″ (MPa)	0.44	0.25	0.5	0.623

Table 48: In this table the material response of fibril 1 of H169 CDET with MGO at point 6 is visible. The slope of the retraction curve and the force versus indentation amplitude ratios indicate possible testing of material at this point. The difference in the amplitudes is greatest at 0.5 Hz - the sine fit plot 61 shows that the indentation curve here is the smoothest of all frequencies. The fit also worked surprisingly well for this low frequency. However, the storage modulus values are lower than the indentation modulus values in the quasi-static experiment - see in table 45.
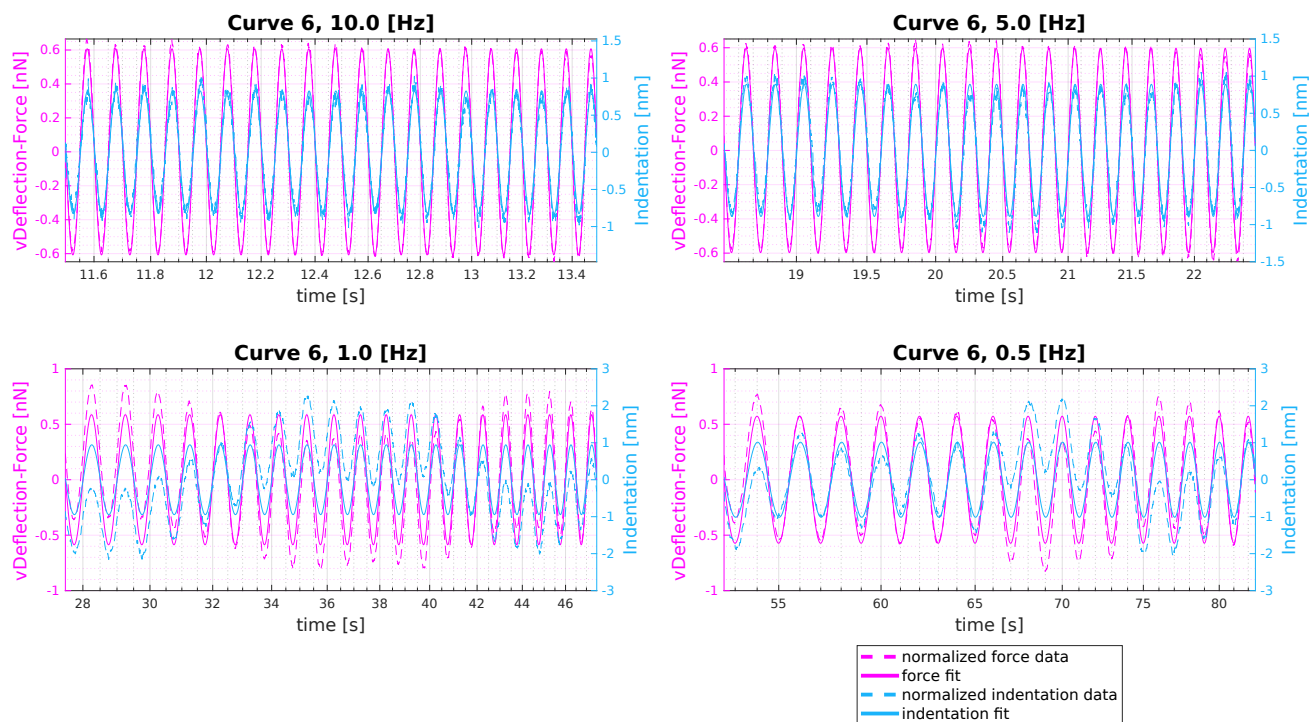
Figure 61: These four plots show the force and indentation signals over all measured frequencies with the respective sine fit of H169 CDET fibril 1 with MGO curve 6.

H169 CDET with MGO			
fibril 2 (point 2)			
dynamic		D. approach slope	D. retraction slope	D. indentation depth (nm)
		0.602	0.733	64.56
frequency	0.5 Hz	1 Hz	5 Hz	10 Hz
amplitude force (nm)	0.598	0.614	0.62	0.61
amplitude indentation (nm)	0.88	0.805	0.78	0.81
phase shift ϕ (°)	2.55	3.45	3.9	3.67
loss tangent	0.0446	0.0603	0.0681	0.0642
storage modulus E′ (MPa)	4.1	4.59	4.77	4.55
loss modulus E″ (MPa)	0.18	0.28	0.32	0.29

Table 49: In this table the material response of fibril 2 of H169 CDET with MGO at point 2 is visible. Here, too, the results for the storage modulus would be more likely to be assigned to a sample without MGO treatment.
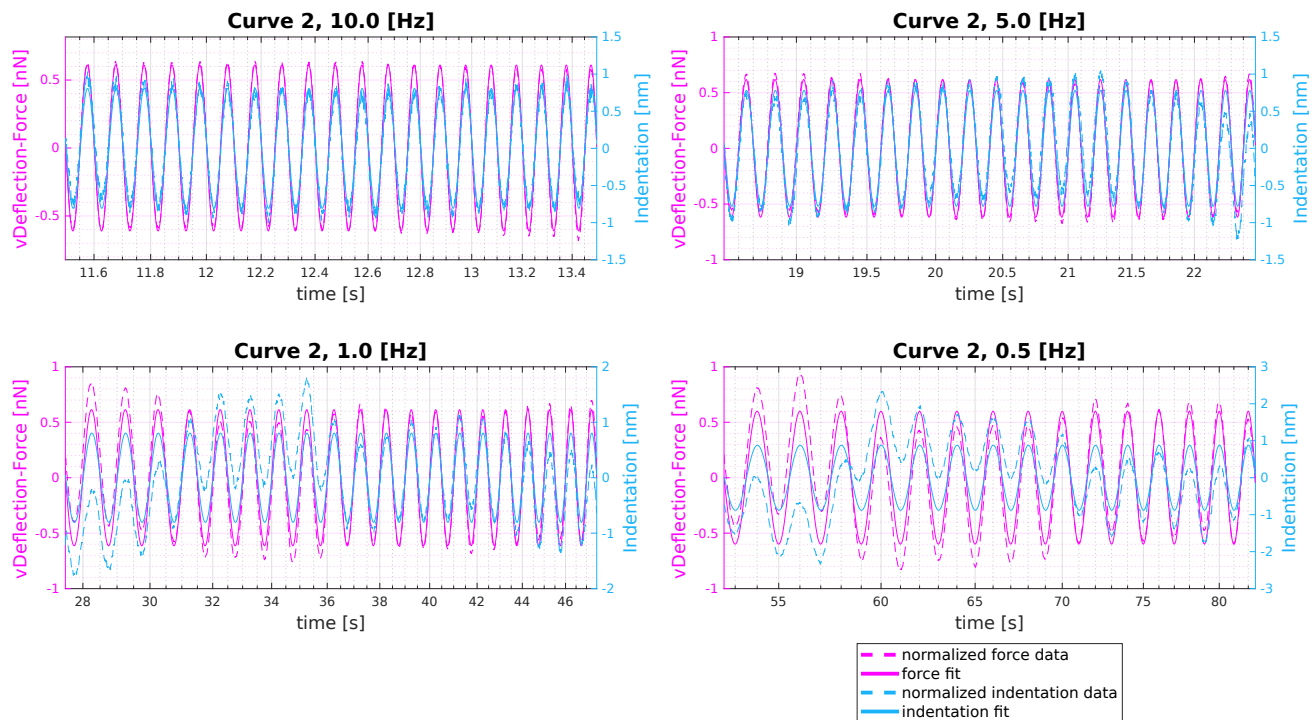
Figure 62: These four plots show the force and indentation signals over all measured frequencies with the respective sine fit of H169 CDET fibril 2 with MGO curve 2.

H169 CDET with MGO				
fibril 3 (point 6)				
dynamic		D. approach slope	D. retraction slope	D. indentation depth (nm)
		0.682	0.78	24.66
frequency	0.5 Hz	1 Hz	5 Hz	10 Hz
amplitude force (nm)	0.577	0.615	0.602	0.595
amplitude indentation (nm)	0.98	0.8	0.861	0.886
phase shift ϕ (°)	2.04	3.09	3.34	4.73
loss tangent	0.0356	0.054	0.0584	0.0828
storage modulus E' (MPa)	6.29	8.27	7.5	7.19
loss modulus E'' (MPa)	0.223	0.447	0.438	0.595

Table 50: In this table the material response of fibril 3 of H169 CDET with MGO at point 6 is visible. From the storage modulus values alone, this point on fibril 3 is the only one that provides similar values compared to the indentation modulus from the quasi-static measurements (see table 45).
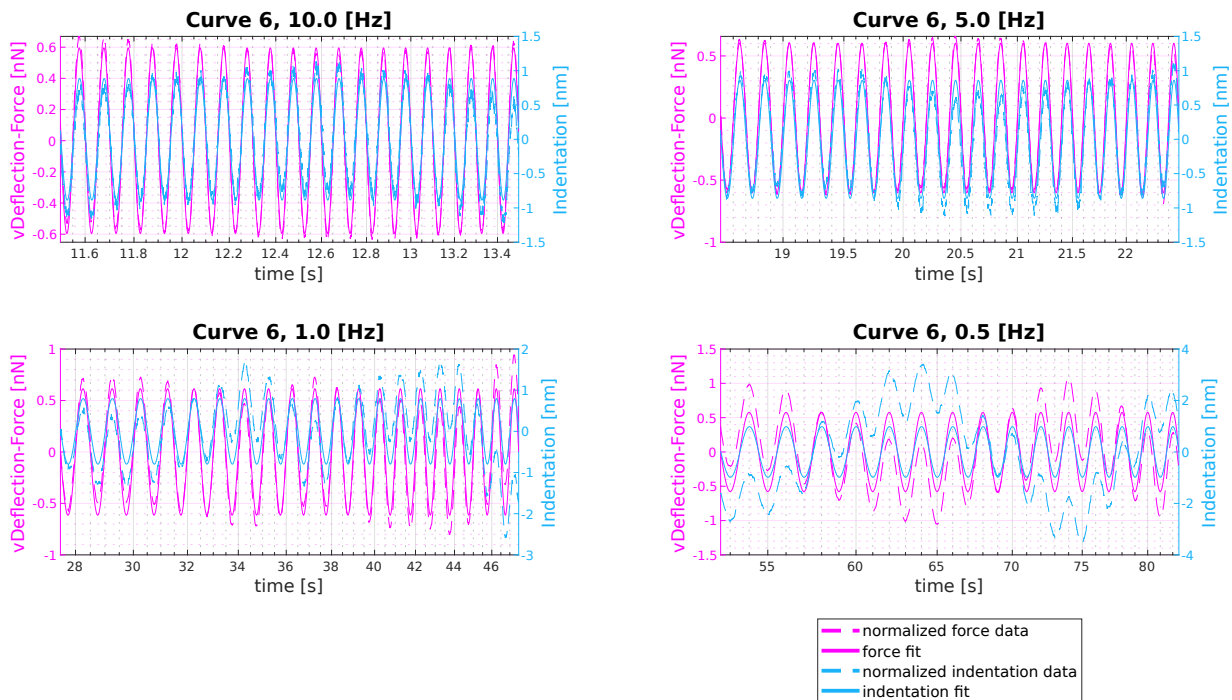
Figure 63: These four plots show the force and indentation signals over all measured frequencies with the respective sine fit of H169 CDET fibril 3 with MGO curve 6.

H169 CDET with MGO				
fibril 4 (point 2)				
dynamic		D. approach slope	D. retraction slope	D. indentation depth (nm)
		0.575	0.73	97.58
frequency	0.5 Hz	1 Hz	5 Hz	10 Hz
amplitude force (nm)	0.57	0.58	0.61	0.599
amplitude indentation (nm)	1.03	0.96	0.85	0.87
phase shift ϕ (°)	6.58	5.4	9.39	7.95
loss tangent	0.115	0.0946	0.165	0.1397
storage modulus E' (MPa)	2.49	2.76	3.21	3.1
loss modulus E'' (MPa)	0.29	0.26	0.53	0.43

Table 51: In this table the material response of fibril 4 of H169 CDET with MGO at point 2 is visible. The storage modulus values are so low that this selected point should be treated with caution. This results might be related to the really high indentation depth.
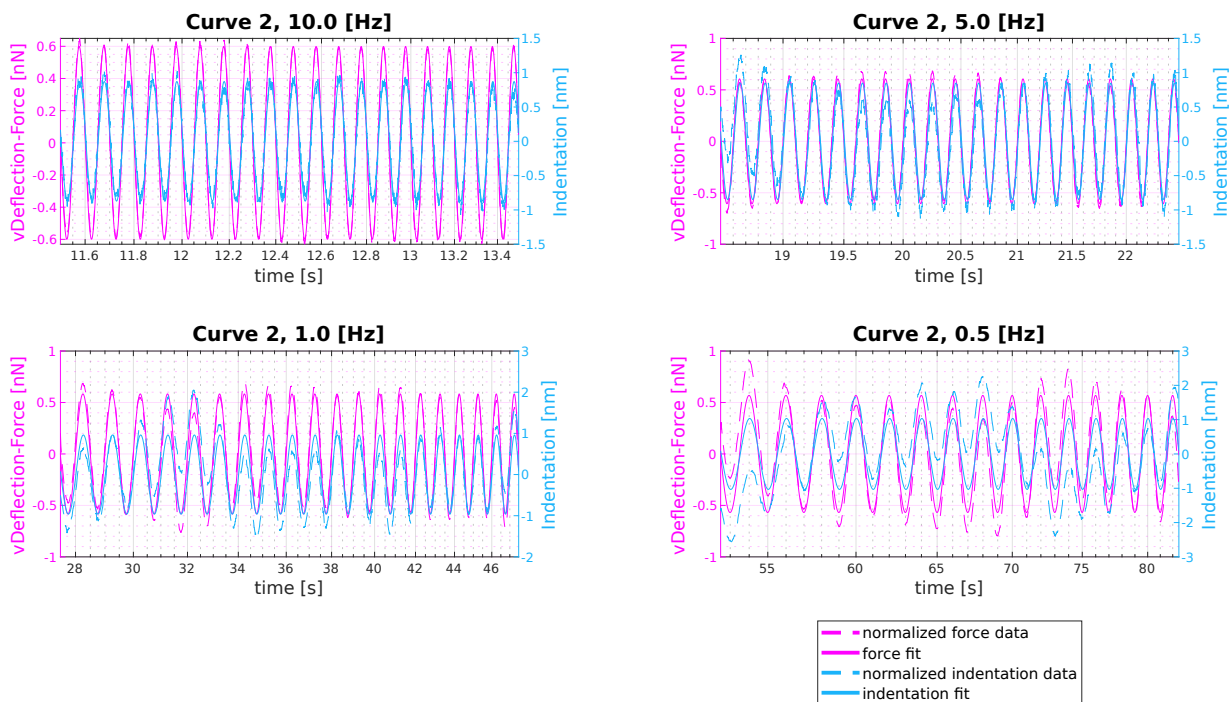
Figure 64: These four plots show the force and indentation signals over all measured frequencies with the respective sine fit of H169 CDET fibril 4 with MGO curve 2.

H169 SDFT

Although the previous quasi-static measurement of the first fibril gives an acceptable result (see table 46), this is not the case for the dynamic measurement: the slope of the retraction slope in each of the ten points is almost 1 and also the indentation amplitude is always smaller than the force amplitude. Unfortunately the same applies to fibrils 2, 3 and 4, leading to no meaningful results for this sample in experiment 2. Storage modulus values are then always over 15 MPa, which can be considered physically unrealistic. What is striking about the sine fit plots is that the deflection data looks good and can therefore also be approximated by a simple sine, but the indentation data on the other hand is very noisy (fig. 65), except when obviously glass is indented resulting in phase shifts of 180° (fig. 66).

Figure 65: These four plots show the force and indentation signals over all measured frequencies with the respective sine fit of H169 SDFT fibril 4 curve 1, which was identified as point on glass. The phase shift of 180° can be seen very easily in the plots.
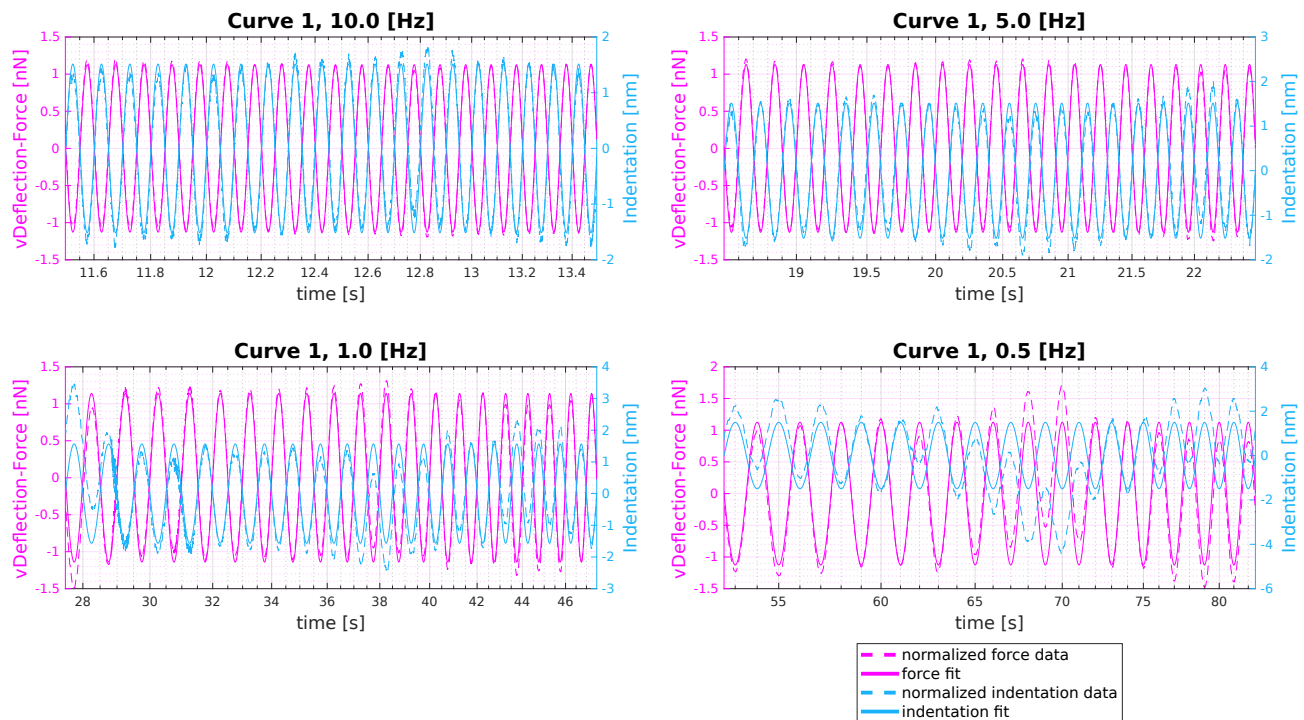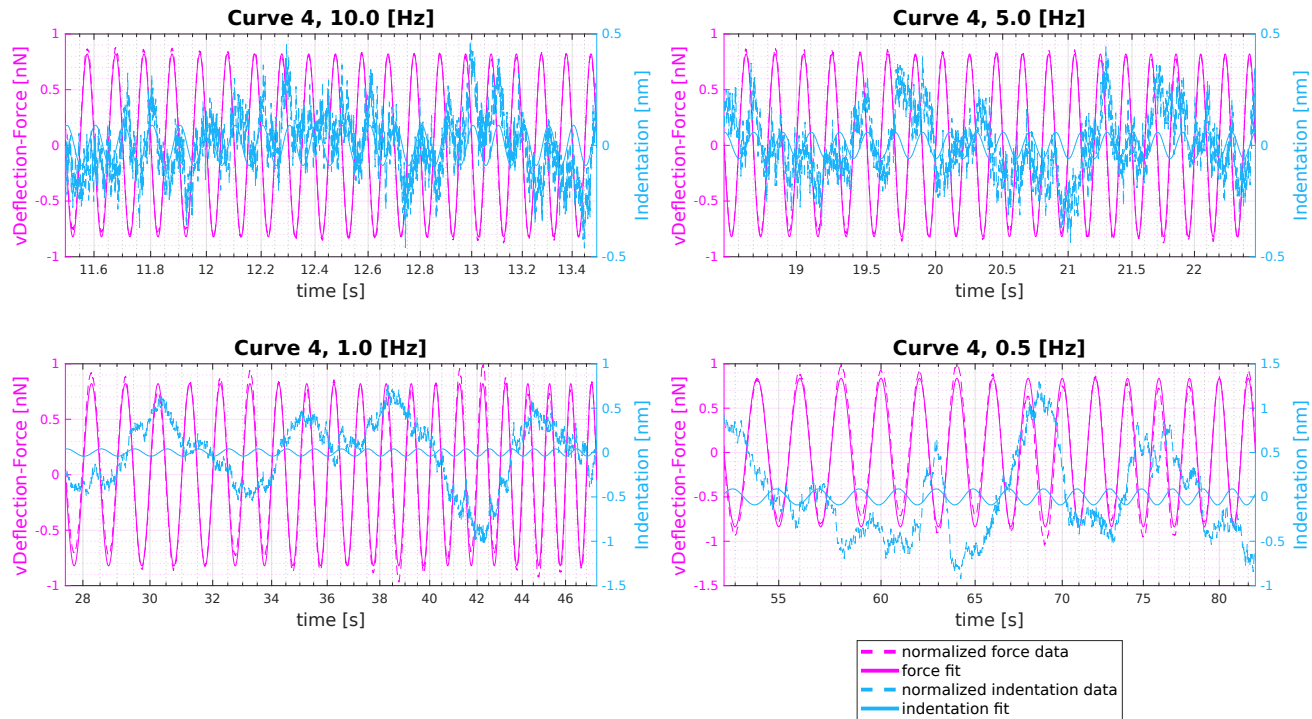
Figure 66: These four plots show the force and indentation signals over all measured frequencies with the respective sine fit of H169 SDFT fibril 4 curve 4, which shows a very noisy indentation signal. Within the ten measured points there is a clear separation into smooth but 180° out of phase curves and noisy signals. Possibly these points would lie on the fibril, but the proper measurement has obviously failed here. As a consequence, a sine fit is not possible.

H169 SDFT with MGO

Almost all measurements of the H169 SDFT sample after the MGO treatment do not provide any meaningful results. In the following, a point on fibril 4 is selected, but it should also be viewed with caution.

H169 SDFT with MGO				
fibril 4 (point 6)				
dynamic		D. approach slope	D. retraction slope	D. indentation depth (nm)
		0.465	1.043	113.37
frequency	0.5 Hz	1 Hz	5 Hz	10 Hz
amplitude force (nm)	0.55	0.47	0.5	0.61
amplitude indentation (nm)	0.86	1.3	1.14	0.51
phase shift ϕ (°)	15.08	8.7	11.6	20.9
loss tangent	0.27	0.153	0.205	0.382
storage modulus E' (MPa)	2.48	1.44	1.74	4.54
loss modulus E'' (MPa)	0.67	0.22	0.36	1.73

Table 52: In this table the material response of fibril 4 of H169 SDFT with MGO at point 6 is visible. The slope of the retraction curve is greater than 1 and the indentation depth is extremely large. Storage modulus values are expected to range between 6 and 9 MPa, however they turn out to be very low for the different frequencies at point 6. Only at 1 Hz and at 5 Hz the indentation amplitude is twice the force amplitude. The sine fit plots also show that the fit works best for the two middle frequencies (fig. 67).
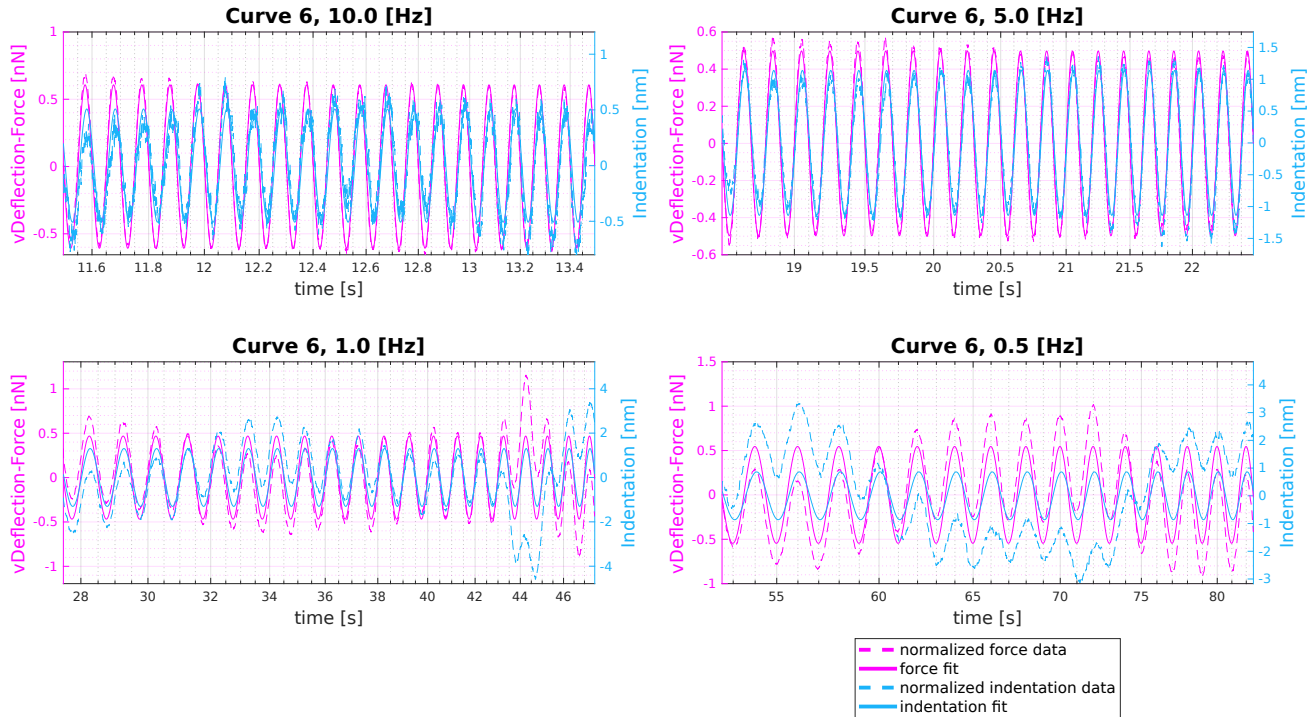
Figure 67: These four plots show the force and indentation signals over all measured frequencies with the respective sine fit of H169 SDFT fibril 4 with MGO curve 6. This point is to be most likely on the fibril. With increasing measurement, i.e. decreasing frequency, the indentation signal becomes smoother and smoother.

References

[1] Yuri M. Efremov, Takaharu Okajima, and Arvind Raman. "Measuring viscoelasticity of soft biological samples using atomic force microscopy". In: *Royal Society of Chemistry* 16.- (2020), pp. 64–81.

[2] Jordi Alcaraz et al. "Microrheology of Human Lung Epithelial Cells Measured by Atomic Force Microscopy". In: *Biophysical Journal* 84.- (2003), pp. 2071–2079.

[3] Jan Rother et al. "Atomic force microscopy-based microrheology reveals significant differences in the viscoelastic response between malign and benign cell lines". In: *Open Biol.* 4.5 (2014), p. 140046.

[4] Nelda Antonovaite et al. "Dynamic indentation reveals differential viscoelastic properties of white matter versus gray matter-derived astrocytes upon treatment with lipopolysaccharide". In: *Journal of the Mechanical Behavior of Biomedical Materials* (2020).

[5] Colin A. Grant and Peter C. Twigg. "Pseudostatic and Dynamic Nanomechanics of the Tunica Adventitia in Elastic Arteries Using Atomic Force Microscopy". In: *ACS Nano* 7.1 (2013), pp. 456–464.

[6] Orestis G. Andriotis et al. "Nanomechanical assessment of human and murine collagen fibrils via atomic force microscopy cantilever-based nanoindentation". In: *Journal of the Mechanical Behavior of Biomedical Materials* 39 (2014), pp. 9–26.

[7] Colin A. Grant et al. "Tuning the elastic modulus of hydrated collagen fibrils". In: *Biophysical journal* 97.11 (2009), pp. 2985–2992.

[8] Martin Stolz et al. "Dynamic elastic modulus of porcine articular cartilage determined at two different levels of tissue organization by indentation-type atomic force microscopy". In: *Biophysical journal* 86.5 (2004), pp. 3269–3283.

[9] Lukas Kain. "Structural and mechanical evaluation of collagen fibrils from equine tendon: The effect of age, tendon zone and type". MA thesis. Vienna University of Technology, 2017.

[10]   Colin A. Grant, Michael A. Phillips, and Neil H. Thomson. "Dynamic mechanical analysis of collagen fibrils at the nanoscale". In: *Journal of the Mechanical Behavior of Biomedical Materials* 5.1 (2012), pp. 165–170.

[11]   Helen L. Birch. "Tendon matrix composition and turnover in relation to functional requirements". In: *International Journal of experimental pathology* 88.4 (2007), pp. 241–248.

[12]   Chavaunne T. Thorpe et al. "Capacity for sliding between tendon fascicles decreases with ageing in injury prone equine tendons: a possible mechanism for age-related tendinopathy?" In: *European Cells and Materials* 25 (2013), pp. 48–60.

[13]   Chavaunne T. Thorpe et al. "The interfascicular matrix enables fascicle sliding and recovery in tendon, and behaves more elastically in energy storing tendons". In: *Journal of the Mechanical Behavior of Biomedical Materials* 52 (2015), pp. 85–94.

[14]   Masaru Sese et al. "Characteristics of collagen fibrils in the entire equine superficial digital flexor tendon". In: *Okajimas folia anatomica Japonica* 84.3 (2007), pp. 111–114.

[15]   Orestis G. Andriotis et al. "Hydration and nanomechanical changes in collagen fibrils bearing advanced glycation end-products". In: *Biomed. Opt. Express* 10.4 (2019), pp. 1841–1855.

[16]   Rene B. Svensson et al. "Effects of maturation and advanced glycation on tensile mechanics of collagen fibrils from rat tail and Achilles tendons". In: *Acta Biomaterialia* 70 (2018), pp. 270–280.

[17]   Michelle L. Oyen and Robert F. Cook. "A practical guide for analysis of nanoindentation data". In: *Journal of the mechanical behavior of biomedical materials* 2 (2008), pp. 396–407.

[18]   K. Gelse, E. Pöschl, and T. Aigner. "Collagens - structure, function, and biosynthesis". In: *Advanced Drug Delivery Reviews* 55.12 (2003), pp. 1531–1546.

[19]   Thomas E. Kruger, Andrew H. Miller, and Jinxi Wang. "Collagen Scaffolds in Bone Sialoprotein-Mediated Bone Regeneration". In: *The Scientifc World Journal* (2013), p. 6.

[20] John A. Petruska and Alan J. Hodge. "A SUBUNIT MODEL FOR THE TROPOCOLLAGEN MACROMOLECULE". In: *Proceedings of the National Academy of Sciences of the United States of America* 51.5 (1964), pp. 871–876.

[21] G. A. Di Lullo et al. "Mapping the Ligand-binding Sites and Disease-associated Mutations on the Most Abundant Protein in the Human, Type I Collagen". In: *The Journal of Biological Chemistry* 277.6 (2002), pp. 4223–4231.

[22] Jess G. Snedeker and Alfonso Gautieri. "The role of collagen crosslinks in ageing and diabetes - the good, the bad, and the ugly". In: *Muscles, Ligaments and Tendons Journal* 4.3 (2014), pp. 303–308.

[23] Gion Fessel, Christian Gerber, and Jess G. Snedeker. "Potential of collagen cross-linking therapies to mediate tendon mechanical properties". In: *Journal of shoulder and elbow surgery* 21.2 (2012), pp. 209–2017.

[24] Allen J. Bailey. "Molecular mechanisms of ageing in connective tissues". In: *Mechanisms of ageing and development* 122.7 (2001), pp. 735–755.

[25] Patrick Garnero. "The contribution of collagen crosslinks to bone strength". In: *BoneKEy reports* 1 (2012), p. 182.

[26] J. Kannus. "Structure of the tendon connective tissue". In: *Scandinavian Journal of medicine science in sports* 10.6 (2000), pp. 312–320.

[27] Yang Liu, H. S. Ramanath, and Dong-An Wang. "Tendon tissue engineering using scaffold enhancing strategies". In: *Trends in Biotechnology* 26.4 (2008), pp. 201–209.

[28] James H.-C. Wang. "Mechanobiology of tendon". In: *Journal of Biomechanics* 39.9 (2006), pp. 1563–1582.

[29] R. K. Smith et al. "The influence of ageing and exercise on tendon growth and degeneration—hypotheses for the initiation and prevention of strain-induced tendinopathies". In: *Comparative Biochemistry and Physiology Part A: Molecular Integrative Physiology* 133.4 (2002), pp. 1039–1050.

[30] Chavaunne T. Thorpe et al. "Specialization of tendon mechanical properties results from interfascicular differences". In: *Journal of the Royal Society Interface* 9 (2012), pp. 3108–3117.

[31] Henry Gray. *Anatomy of the Human Body*. Lea and Febiger, 1918.

[32] Claire O'Brien, Neil Marr, and Chavaunne Thorpe. "Microdamage in the equine superficial digital flexor tendon". In: *Equine Veterinary Journal* 53.3 (2021), pp. 417–430.

[33] Marta Godinho et al. "Elastin is Localised to the Interfascicular Matrix of Energy Storing Tendons and Becomes Increasingly Disorganised With Ageing". In: *Scientific Reports* 7.1 (2017), p. 9713.

[34] Ewa M. Spiesz et al. "Structure and collagen crimp patterns of functionally distinct equine tendons, revealed by quantitative polarised light microscopy (qPLM)". In: *Acta Biomaterialia* 70 (2018), pp. 281–292.

[35] Chavaunne T. Thorpe et al. "Fascicles and the interfascicular matrix show adaptation for fatigue resistance in energy storing tendons". In: *Acta Biomaterialia* 42 (2016), pp. 308–315.

[36] Chavaunne T. Thorpe et al. "Fascicles from energy-storing tendons show an age-specific response to cyclic fatigue loading". In: *Journal of The Royal Society Interface* 11.92 (2014), p. 20131058.

[37] S. V. Kontomaris and A. Stylianou. "Atomic force microscopy for university students: applications in biomaterials". In: *European Journal of Physics* -.- (2017), pp. -.

[38] G. Binnig and H. Rohrer. "Atomic force microscope". In: *Physical Review Letters* 56.9 (1986), pp. 930–933.

[39] G. Binnig, C. F. Quate, and Ch. Gerber. "Scanning tunneling microscopy". In: *Surface Science* 126 (1983), pp. 236–244.

[40] Andrea Alessandrini and Paolo Facci. "AFM: a versatile tool in biophysics". In: *Meas. Sci. Technol.* 16 (2005), R65–R92.

[41] Daniel Johnson, Nidal Hilal, and W. Richard Bowen. "Chapter 1 - Basic Principles of Atomic Force Microscopy". In: *Atomic Force Microscopy in Process Engineering*. Ed. by W. Richard Bowen and Nidal Hilal. Butterworth-Heinemann, 2009, pp. 1–30.

[42] Roberto Raiteri et al. "Micromechanical cantilever-based biosensors". In: *Sensors and Actuators B: Chemical* 79.2 (2001), pp. 115–126.

[43] John Elie Sader. "Susceptibility of atomic force microscope cantilevers to lateral forces". In: *Review of Scientific Instruments* 74.4 (2003), pp. 2438–2443.

[44] Jeffrey L. Hutter and John Bechhoefer. "Calibration of Atomic-Force Microscope Tips". In: *Review of Scientific Instruments* 64.7 (1993), pp. 1868–1873.

[45] Yongho Seo and Wonho Jhe. "Atomic force microscopy and spectroscopy". In: *Reports on progress in physics* 71.1 (2008), p. 016101.

[46] Bruker. "JPK MicroRheology module User Manual". In: (2020).

[47] G. M. Pharr, W. C. Oliver, and F. R. Brotzen. "On the generality of the relationship among contact stiffness, contact area, and elastic modulus during indentation". In: *Journal of Materials Research* 7.61 (1992), pp. 613–617.

[48] G. M. Pharr and W. C. Oliver. "Measurement of hardness and elastic modulus by instrumented indentation: Advances in understanding and refinements to methodology". In: *Journal of Materials Research* 19.3 (2004), pp. 3–20.

[49] E. G. Herbert, W. C. Oliver, and G. M. Pharr. "Nanoindentation and the dynamic characterization of viscoelastic solids". In: *Journal of Physics D: Applied Physics* 41.7 (2008), p. 074021.

[50] *Curve fitting to a sinusoidal function*. https://de.mathworks.com/matlabcentral/answers/121579-curve-fitting-to-a-sinusoidal-function. Accessed: 2022-07-14.

[51] *Zero-phase digital filtering*. https://de.mathworks.com/help/signal/ref/filtfilt.htmll. Accessed: 2022-07-14.

[52] *1-D digital filter*. https://de.mathworks.com/help/matlab/ref/filter.html. Accessed: 2022-07-14.

[53] Manuel Rufin. "Effect of glycation on surface charge and indentation stiffness of individual collagen fibrils". MA thesis. Vienna University of Technology, 2020.

[54] C. G. Schalkwijk and C. D. A. Stehouwer. "Methylglyoxal, a Highly Reactive Dicarbonyl Compound, in Diabetes, Its Vascular Complications, and Other Age-Related Diseases". In: *Physiological reviews* 100.1 (2019), pp. 407–461.

[55] Gion Fessel et al. "Advanced Glycation End-Products Reduce Collagen Molecular Sliding to Affect Collagen Fibril Damage Mechanisms but Not Stiffness". In: *PLoS ONE* 9.11 (2014).